Interactions between rod-like biopolymer solutions and saliva

By
Xinxin Li, BSc. MSc.

Thesis submitted to the University of Nottingham
For the degree of Doctor of Philosophy

Division of food science and dietetics
School of Biosciences
University of Nottingham
Loughborough
LE12 5RD

March 2021

Abstract

This thesis aims to evaluate underpinning mechanisms of oral processing of polysaccharide thickeners with a rod-like conformation. Xanthan gum (XG) and scleroglucan (SG) are identified as key research targets, with the view to identify the differences and similarities between XG and SG and to assess the potential of SG utilisation as XG analogue in specialised nutrition applications, such as in oropharyngeal dysphagia. Specifically, hydrodynamic properties of SG have been investigated, including hydrodynamic and thermodynamic non-ideality, as well as molecular weight distribution. Furthermore, rheological and lubrication properties have been studied to elucidate complex rheological behaviour of both polysaccharides, as well as to probe their interactions with human whole saliva and bovine submaxillary mucin, used as a saliva-mimicking model. The rheological behaviour was probed using a combination of the steady shear flow, small amplitude oscillatory shear, first normal stress difference and capillary break-up rheometry techniques, whilst lubrication and friction behaviour was examined using the soft-contact tribology method.

Sedimentation velocity in analytical ultracentrifuge (AUC) showed SG preparation was unimodal when concentration is higher than 0.75 mg/ml. However, it was resolved into two main components at lower concentrations with partial reversibility between two components. Sedimentation equilibrium experiments revealed that SG

exhibits partially reversible self-association behaviour. The molecular weight ranges from ~3×10^6 g/mol to ~5×10^6 g/mol after thermodynamic non-ideality correction. The results of SEC-MALS showed that the rod-shape structure of SG may transfer into a structure with more flexibility at higher masses. When XG solution or SG solution are mixed with mucin, sedimentation velocity experiment showed no apparent interactions at low concentrations.

At higher concentrations, XG and SG solutions of the same concentration have comparable steady shear flow profile and linear viscoelasticity spectra. At the same time, they show marked differences in the elongational flow behaviour, normal stress difference and lubrication behaviour. When XG and SG are dissolved in viscosified matrix (40% sucrose solution), the differences were minimised, confirming that chain relaxation dynamics at longer characteristic time is similar between XG and SG. The influence of saliva (or mucin) on complex rheological behaviour and lubrication of XG and SG was found to be minimal, which is consistent with the results of the sedimentation analysis showing no effect in low concentration solutions. The examined sets of rheological and tribological behaviour show new opportunities for the use of SG as a XG-replacing thickener in medical nutrition applications.

Acknowledgements

I would like to say thank you to those who supported me through my PhD study. I am extremely grateful to my supervisors Prof. Stephen Harding, Dr. Gleb Yakubov and Prof. Bettina Wolf, who inspired and taught me a lot towards my PhD research. Their deep insights gave me solid guidance at many stages of my research. I have gained many valuable suggestions and have learned much useful knowledge. I am also very grateful to them for their patience and understanding during my experiment and writing period, especially under this Covid-19 situation. It was such a wonderful experience for me to have this opportunity to work with all of you. My special thanks go to Dr. Gleb Yakubov, my thesis will be disaster without his careful and detailed guidance. He is also so kind to offer me a part time job during my writing period. A very special gratitude goes to the University of Nottingham for offering me the vice chancellor scholarship to finish my study.

My sincere thanks go to Prof. Tim Forster and Dr. Vincenzo Di Bari for offering me a part time job of working as a technical assistant during my PhD study. My grateful thanks also go to Nicole, Vlad, Yudong, Yangyi, Hui, Khat, Darrell and Gloria for teaching me many helpful skills for the experiment and doing analysis. My experiment will be messes without their help. My special thanks go to Thomas for helping me to proofread part of my thesis. I would like to thank Dr. Simon Balance and Hanne Zobel for helping me doing the SEC-MALS measurement. My sincere thanks go to all my friends in Food Science and NCMH: Chao, Katy, Yi, Tingting, Danni, Book, Juturat, May, Lucija and Izzi. Thank you very much for your encouragement and support. Many thanks go to other PhDs who also helped and guided me. My project would be slower without their help. It was great sharing lab with all of you.

My sincere thanks go to my friend Liling, for her encouragement and cheerful talk, which helped me a lot through my tough period. My grateful thanks also go to, but are not limited to my friends Ally Zhai, Kun Liu, Xinyu Liu, Ying Zhu, Qiong Zhong, Shiwei Chen, Dandan Qiu, Peipei Wang, Jiapeng Zong, Xingying Li, Nanxi Wang, Xuting Peng, Yang Hu, Yuechi Kuang, Yueran Ma, Yuetong Qiu, Jing Zhao, Weiran Jing, Daisi Wang, Yizheng Zhu, Mengjuan Ma and Tao Tian, for their patience, motivation, enthusiasm and for all the sacrifices you all made just for me. My special thanks go to my favourite bands Kanjani ∞ and Arashi. Their music and variety show cheered my up and helped me to go through all my bad times during the PhD.

My great thanks go to my boyfriend Shuo Feng, for his unconditional support. I would like to thank him for his encouragement and understanding to help me to finish this exciting but tough journey. He can always find my small accomplishment and be enthusiastic about them. He is a great listener and he always help me to go through all my negative emotions. He makes me feel more confident and positive. Thank you very much for being this person to me and for keeping me in your life. Loving you was one of the best decisions of my life.

Words cannot express my feelings for my parents for their continuous love. They are my eternal cheerleaders. I would not be here without their support and help. Please allow me to rewrite my thanks in Chinese here（亲爱的爸爸妈妈真的感谢你们为我做出的牺牲，感谢你们在我伤心疲惫的时候给我的鼓励和安慰，也感谢你们时常包容我的任性，我爱你们。）I would like to thank my grandma who always cooks great food to me and treat me like a small child when I am home. My great thanks go to my grandparents, aunts, uncles, and my little cousin (Xiayi Sheng) for their support and encouragement. I am also grateful to my other family members and friends who have supported me along the way. Thank you all very much!

List of Abbreviations and Symbols

List of abbreviations

a	MHKS power law viscosity coefficient
ANOVA	Analysis of variance
AUC	Analytical ultracentrifugation
b	MHKS power law sedimentation coefficient
BSM	Bovine submaxillary mucin
CaBER	Capillary break-up extensional rheometer
C_p	Power law model exponent
C_C	Cross model exponent
$c(r)$	Concentration at radius r
c^*	Critical overlap concentration
D(t)	Mid-point diameter of the filament as the function of time
D^0	Translational diffusion coefficient
f	Friction coefficient
F_f	Frictional force
G'	Storage modulus
G''	Loss modulus
G^*	Complex modulus
HWS	Human whole saliva
K_H	Huggins coefficient
K_K	Kraemer coefficient

L	Load (N)
L_{P}	Persistence length
LVE range	Linear-viscoelastic range
M_s	z-average molecular weight
M_{L}	Mass per unit length
M_w	Molecular weight
$M_{w,app}$	Apparent molecular weight
MHKS	Mark-Houwink-Kuhn-Sakurada
MTM2	Mini Traction Machine (2nd Edition)
N_1	The first normal stress difference
N_2	The second normal stress difference
NaCl	Sodium chloride
NaN_3	Sodium azide
PBS	Phosphate buffer saline
PDMS	Polydimethyl siloxane
r	Radius of the molecule from the centre of the rotation
R	Universal gas constant
RI	Refractive index
RS	Reconstituted saliva
R_g	Radius of gyration (nm)

RI	Refractive index
rpm	Revolutions per minute
RI	Refractive index
S	Svedberg unit
SAOS	Small angle oscillatory shear
SRR	Slide-to-roll ratio
s	Sedimentation coefficient
$s_{20,w}$	Sedimentation coefficient with the solvent of water at 20°C
$s^0_{20,w}$	$s_{20,w}$ extrapolated to "infinite dilution"
SE	Sedimentation equilibrium
SEC-MALS	Size exclusion chromatography coupled with multi angle light scattering
SV	Sedimentation velocity
$\bar{v}$	Partial specific volume (ml/g)
U	Entrainment speed

List of symbols

Υ	Shear strain
$\dot{\gamma}$	Shear rate
$\varepsilon^{\cdot}$	Extensional rate
η	Shear viscosity
η_0	Viscosity of the solvent

η^*	Complex viscosity
η_{inh}	Inherent viscosity
η_r	Relative viscosity
η_{red}	Reduced viscosity
η_E	Steady state extensional viscosity
$[\eta]$	Intrinsic viscosity
κ'	Mark-Houwink constant of intrinsic viscosity
κ_s	Mark-Houwink constant of sedimentation
λ	Relaxation time
μ	Friction coefficient (tribological term) Rate of movement per unit centrifugal field
ρ	Density
ρ_o	Density of the solvent
σ	Surface tension
τ	Shear stress
τ_E	Extensional stress
ω	Angular velocity (rad/s)

Table of Contents

Abstract I

Acknowledgements III

List of Abbreviations and Symbols VI

List of abbreviations VI

List of symbols VIII

Chapter 1 Introduction 1

1.1 Background 1

1.2 General aims 4

1.3 Structure of the thesis 5

1.4 Publications and presentations 8

Chapter 2 Literature review 9

2.1 Biopolymers 9

2.1.1 Xanthan Gum 10

2.1.2 Scleroglucan 25

2.2 Human whole saliva 36

2.2.1 Salivary glands, secretion, and collection 36

2.2.2 Saliva composition and function 41

2.2.3 Rheological properties of saliva 48

2.2.4 Saliva film and lubrication 51

2.2.5 Reconstituted saliva 54

Chapter 3 Techniques and Methods 56

3.1 Molecular characterisation of biopolymers 56

3.1.1 Intrinsic viscosity 56

3.1.2 Refractive index 60

3.1.2 Analytical ultracentrifugation 61

3.2 Flow behaviour 73

3.2.1 Viscosity 73

3.2.2 Viscoelasticity 77
3.2.3 Measuring system 83
3.2.4 Extensional rheology 86
3.3 Tribology study 91
3.3.1 From rheology to tribology 91
3.3.2 Friction 92
3.3.3 Lubrication 93
3.3.4 Soft contract tribology 96
Chapter 4 Characterisation of the molecular properties of scleroglucan as an alternative rigid rod molecule to xanthan gum for oropharyngeal dysphagia 99
Abstract 99
4.1 Introduction 100
4.2 Materials and methods 104
4.2.1 Materials 104
4.2.2 Sedimentation velocity in the analytical ultracentrifuge 105
4.2.3 Sedimentation equilibrium in the analytical ultracentrifuge 106
4.2.4 Capillary viscometry 107
4.2.5 Size exclusion chromatography coupled to multi-angle light scattering (SEC-MALS) and differential pressure viscometer 108
4.3 Results and discussion 110
4.3.1. Heterogeneity: Sedimentation coefficient and sedimentation coefficient distribution 110
4.3.2 Partially reversible self-association 114
4.3.3 Intrinsic viscosity 117
4.3.4 Conformation 118
4.3.5 Molecular weight distribution and comparison with xanthan 121
4.3.6 Sedimentation of mixtures of SG with bovine submaxillary mucin 123
4.4 Concluding remarks 125
Chapter 5 Complex rheological properties of xanthan gum and scleroglucan, and their mixtures with mucin and human whole saliva 127
Abstract 127

5.1 Introduction 128
5.2 Material and Methods 132
5.2.1 Biopolymers and biopolymer solution preparation 132
5.2.2 Saliva sample preparation 134
5.2.3 Reconstituted saliva composition and preparation 134
5.2.4 Biopolymer-saliva and reference mixture preparation 135
5.2.5 Steady shear and oscillatory shear rheological analysis 136
5.2.6 Normal stress analysis 137
5.2.7 Filament break-up and data analysis 137
5.3. Results and Discussion 139
5.3.1 Shear rheological analysis 139
5.3.2 Normal Stress analysis 143
5.3.3 Shear rheological analysis of mixing biopolymers with HWS and RS 145
5.3.4 Extensional Rheological analysis of control and saliva samples 149
5.4 Conclusions 155
Chapter 6 Probing interactions of xanthan gum and scleroglucan with bovine submaxillary mucin and human whole salivary surface films using soft-contact tribology 158
Abstract 158
6.1 Introduction 158
6.2 Materials and methods 162
6.2.1 Materials and solution preparation 162
6.2.2 Saliva/reconstituted saliva collection and mixture preparation 163
6.2.3 Stribeck tests 164
6.3 Results and discussions 167
6.3.1 Concentration dependence of the Stribeck behaviour of XG and SG 167
6.3.2 Effect of addition of RS and HWS on Stribeck behaviour 171
6.3.3 Kinetics of hydrocolloid/mucin interaction and comparison with whole human saliva 173
6.4 Conclusion 176
7. Conclusions and Future work 178

7.1 Molecular characterisation 178
7.2 Rheological study 180
7.3 Tribological study 182
7.4 Future directions 185
References 188
Appendix 211
Supplementary Table 211
Supplementary Figures 216

Chapter 1 Introduction

1.1 Background

Biopolymers are widely applied as thickening agents for consumers who suffer from oropharyngeal dysphagia to avoid aspiration (Newman et al., 2016, Manrique et al., 2014, Manrique et al., 2016). Oropharyngeal dysphagia is usually displayed by stroke patients (Martino et al., 2000). Although a wide range of biopolymers can be used as thickening additives to manipulate products' flow behaviour, the majority of thickeners are added at ~1 - 5% level, which greatly affects customers' experience due to the reduction in flavour release and diminished taste perception. In this context, biopolymers with "high thickening efficiency" become a preferred choice for food and medical nutrition products. Despite a substantial arsenal of food grade thickeners, only a small number bolster high thickening efficiency.

One of the key polysaccharides with high thickening efficiency is xanthan gum (XG). XG is a common choice in dysphagia formulations due to its unique shear-thinning properties (Song et al., 2006a, Song et al., 2006b). Compared to many biopolymers such as starch or pectin, only slight amount of XG is required to achieve the comparable thickening effect, alleviating the problem of reduced sensorial attributed in thickened foods (Baines and Morris, 1988, Baines and Morris, 1989, Preininger, 2016). In addition, XG is suggested to have limited suppression of flavour compared to many food industry polysaccharides such as guar gum (Cook et al., 2003), and the rod-like structure of XG can be the reason of the excellent flavour release ability (Preininger, 2016). Moreover, the V-VST (Volume-viscosity swallow test) combined with the videofluroscopic technique was used to study salivary swabs by Rofes et al. (2014), who found that there was no evidence of the increasing residues left in the oral cavity after using XG based thickeners on patients suffer from dysphagia. With the target of comparing rod like biopolymers, scleroglucan (SG) was chosen in this research. XG and SG are both microbial rod-like macromolecule with comparable molecular weight. SG is a neutral polysaccharide with a triple helix-based structure (Lecacheux et al., 1986, Yanaki and Norisuye, 1983, Rinaudo and Vincendon, 1982). XG and SG also have shear-thinning behaviour (see for example (Moresi et al., 2001, Whitcomb and Macosko, 1978)), which make them significant on affecting oral processing. SG was less investigated compared to XG, as such, the hydrodynamic properties and macromolecular structure could be further investigated.

Rheology plays a key role during bolus formation, during which the material experiences a mix of shear and elongational components of deformation (Stokes, 2012a). Rheological properties determine how the liquid film is squeezed out from the contact between oral surfaces. When liquid film separating oral surface and food is comparable with surface roughness, such aspects as lubrication and friction tend to dominate oral processing and become a factor in developing sensory attributes of texture. These properties can be explored using soft-contact tribology techniques, which utilise surfaces fabricated from compliant materials such as elastomers (Stokes et al., 2013, Stokes, 2012b, Chen and Stokes, 2012, Yakubov, 2014, Stachowiak and Batchelor, 2013). Saliva is another key factor in oral processing and swallowing (Qazi et al., 2017, Newman et al., 2016). Upon ingestion of thickening agent, the biophysical and biochemical characteristics of thickening agent can be altered due to dilutions and possible interactions with saliva (Boehm et al., 2020). It was previously reported that the filament break-up time of 0.5% XG solution mixed with human whole saliva (HWS) was prolonged compared with mixing with water (Choi et al., 2014). In this research, the rheological and tribological study of rod-like polysaccharide solutions and mixtures of XG/SG-saliva mixtures are studied. The insights gained in this research may also help to further explain observations on taste perception from rod-like versus random coil food thickeners.

Mucin glycoprotein is one of the main proteinaceous components in saliva. A number of unique physical properties of saliva such as viscoelastic, lubrication and interfacial behaviour are closely linked with the polymer properties of mucins (see for example, (Schipper et al., 2007)). Although mimicking saliva is very challenging (Yakubov, 2014), the bovine submaxillary mucin (BSM) was dissolved in inorganic buffer as a proxy for probing fundamental mechanisms of hydrocolloid – mucin interaction that can guide development of hypotheses to be subsequently tested *ex*/*in vivo*. Another advantage of using BSM is ability to minimise saliva variability and improve data reproducibility, which, in the case of saliva, can be rather significant due to deterioration of saliva properties which occurs almost as soon as a saliva sample is collected (Sarkar and Krop, 2019).It was further hypothesised that mucin solution can be used as the alternative of HWS when carrying out rheological or tribological measurement.

1.2 General aims

1. Characterise the hydrodynamic properties of scleroglucan:

In order to enable rational utilization of SG in medical formulations, it is important to characterize hydrodynamic properties. In particular, the heterogeneity and molecular weight distribution can be characterised using analytical ultracentrifugation (AUC) (sedimentation velocity and sedimentation equilibrium) and size-exlusion chromatography coupled to multi-angle light scattering and differential pressure viscometry (SEC-MALS). Moreover, with the target of investigating possible aggregations between rod-like biopolymer (XG and SG) solutions and mucin solutions, the sedimentation velocity technique was applied.

2. Study the differences between XG and SG, and interactions between human whole saliva and biopolymer solutions:

The biopolymer solutions during ingestion mainly experience the mixed flow fields of rheological and tribological deformation. It is therefore significant to investigate the rheological and lubrication behaviour of XG and SG solutions, and the mixtures of XG/SG solutions with human whole saliva. In order to evaluate different aspects of complex rheological behaviour, four different techniques were used: rotational rheometry (steady shear and first normal stress differences tests), small amplitude oscillatory shear rheometry (amplitude sweep and frequency sweep tests), capillary breakup extensional rheometry and soft contact tribology.

3. Study the feasibility of replacing human whole saliva with reconstituted saliva: As saliva can deteriorate quick upon collection, the reconstituted saliva was applied in this research as the proxy of human whole saliva in rheological or tribological *ex-vivo* studies. It was prepared by dissolving BSM in inorganic buffers. The interactions of XG and SG with human whole saliva (HWS) or reconstituted saliva (RS) were also investigated and compared by using the above-mentioned techniques.

1.3 Structure of the thesis

Chapter 2 provides a literature review of macromolecular and hydrodynamic properties of XG and SG (Chapter 2.1) and gives the background study of human whole saliva, including the secretion, components, function, rheological and lubrication properties (Chapter 2.2).

Chapter 3 describes the techniques and research methods of this thesis, which are divided into three categories: (a) the macromolecular characterisation techniques; (b) the rheological techniques; (c) the tribological techniques. The macromolecular characterisation techniques explained in detailed in this chapter are intrinsic viscosity characterisation, refractive index measurement and analytical ultracentrifugation analysis. The rheological methods described in this chapter are steady shear tests, small amplitude oscillation tests, first normal stress difference measurements and elongational flow measurements. The equipment used to perform these measurements and test is also reviewed. The description of soft-contact tribological instrumentation and tribological methods such as Stribeck curve analysis and dynamic tribology protocol (Fan et al., 2021) are also provided in this chapter.

Chapter 4, 5 and 6 are results chapters. Chapter 4 focuses on the characterisation of macromolecular properties of SG using analytical ultracentrifugation (AUC) technique. Sedimentation velocity tests show SG may have two components with partially reversible concentrations between the components. Moreover, sedimentation equilibrium tests show SG has partial self-association behaviour with the molecular weight of SG ~ $(2.8 \pm 0.3) \times 10^6$ Da.

Chapter 5 investigates rheological behaviour of XG and SG solution and their mixtures with human whole saliva or reconstituted saliva. XG and SG have comparable behaviour in steady shear and small amplitude oscillatory rheological tests. By contrast, the first normal stress difference and elongation flow tests show a marked difference between XG and SG solutions. When mixed with HWS or RS with biopolymer solutions, the elongation test is the key method to detect the differences between salivary mixture samples and control samples. Last but not least, RS can be the proxy of HWS in the rheological analysis.

Chapter 6 discusses the lubrication properties of XG and SG, and their interactions with HWS or RS. First, SG solutions have higher friction coefficients than XG solutions under conditions of the Stribeck test between two hydrophobic PDMS surfaces. When mixed with HWS or RS, the Stribeck curves of hydrocolloid-HWS and hydrocolloid-RS mixtures are comparable. However, in the kinetic, film-formation tests the hydrocolloid-RS and hydrocolloid-HWS yield different values of the friction coefficient and show a marked difference in the responsiveness of the adsorbed RS or HWS films to the presences of polysaccharide hydrocolloids. These results confirm that mucin does not mimic lubrication properties of HWS, nor it captures the responsive nature of the adsorbed salivary films.

Chapter 7 is the conclusion chapter, which summarises the results and provides future recommendations.

1.4 Publications and presentations

Publications

Li, X., Lu, Y., Adams, G. G., Zobel, H., Ballance, S., Wolf, B., & Harding, S. E. (2020). Characterisation of the molecular properties of scleroglucan as an alternative rigid rod molecule to xanthan gum for oropharyngeal dysphagia. Food Hydrocolloids, 105446.

Poster presentations

- Li, X., Harding, S.E. & Wolf, B. Interactions between rigid rod polysaccharides and saliva, *3rd UK Hydrocolloids Symposium*, Loughborough, the UK, 2017.

- Li, X., Harding, S.E. & Wolf, B. Interactions between rigid rod polysaccharides and saliva, *British Society of Rheology Mid-Winter Meeting*, Bristol, the UK, 2017.

Oral presentations (speaker underlined)

- <u>Li, X.</u>, Harding, S.E. & Wolf, B. Interactions between rigid rod polysaccharide solutions and saliva, *Anural European Society of Rheology*, Sorrento, Italy, 2018.

- <u>Li, X.</u>, Lu, Y., Adams, G. G., Zobel, H., Ballance, S., Wolf, B., & Harding, S. E. Characterisation of the molecular properties of scleroglucan for food & medicinal nutrition application, *20th Gums and Stabilizers for the Food Industry*, San Sebastian, Spain, 2019.

Chapter 2 Literature review

2.1 Biopolymers

XG has a unique place in food industrial applications; the key property of xanthan gum is high thickening effectiveness, meaning it can thicken at low mass concentrations, and the marked shear thinning and apparent yield stress behaviour, associated with weak aggregation of XG polymer chains. Due to low mass concentration of XG in the thickened food, XG has low influence on the diffusion and partitioning coefficient of solutes such as tastants (salt, sugar) and aroma molecules. This makes XG-thickened foods superior in terms of flavour profile to the analogues manufactured using other common thickeners such as pectins or galactomannans (guar gum, LBG). Previous researchers found that xanthan gum has no obvious flavour suppression when it is dissolved into 10% sucrose solution with a concentration lower than 1% (Baines and Morris, 1988, Baines and Morris, 1989, Preininger, 2016). It was hypothesized that the high thickening ability originates from its rod-like molecular conformation, which, in solutions, renders the XG "phase" to occupy a large packing volume, analogous to suspensions of rod-shaped particles (Morris, 1993). The similarity of the molecular conformation served the basis for comparing XG with another rod-like polysaccharide, scleroglucan (SG). XG and SG have comparable molecular weight (Li et al., 2020). XG and SG are both microbial gums with shear-thinning rheological behaviour (see for example (Choi et al., 2014, Survase, 2007, Zhang et al., 2013, Phillips and Williams, 2009)).

2.1.1 Xanthan Gum

2.1.1.1 Macromolecular properties

Xanthan gum (XG) is an extracellular polysaccharide produced by the fermentation of corn starch or sucrose by the bacterium *Xanthomonas Campestris*. It was first discovered in the 1950s in the United States (García-Ochoa et al., 2000, Kang and Pettitt, 1993). Lyophilised or drum dried, XG is nearly odourless, cream-coloured powder, readily soluble in water (García-Ochoa et al., 2000).

The primary structure refers to the monosaccharide and linkage composition, as well as to specific motifs of monosaccharide/linkages distribution. XG is a branched polysaccharide with the linear backbone comprised of β-1, 4 linked glucose (G) units, rendering its classification amongst other polysaccharides as glucan. The C-3 carbon of every second glucose unit of the backbone is decorated with a negatively charged tri-saccharide side chain (Figure 2.1). The side chain consists of two residues of mannose (M) and one residue of glucuronic acid (GluA) arranged in a sequence (M $\beta(1\rightarrow4)$ – GluA $\beta(1\rightarrow2)$ – M $\alpha(1\rightarrow3)$ – $G_{backbone}$), (see for example, (Song et al., 2006b, Phillips and Williams, 2009, Abbaszadeh et al., 2015)). Many previous studies suggested that the side chain can impact the stability of XG structure. However, Millane et al. (1990) observed that elimination of terminal mannose has little impact on the stability of the ordered structure in XG solution. The result of X-ray scattering show that XG and XG without terminal mannose (also known as polytetramer) have comparable conformation (Millane and Narasaiah, 1990). The inner mannose residue can be acetylated while the terminal side mannose can be pyruvated (Phillips and Williams, 2009, Cadmus et al., 1976, Muller et al., 1986). Recently, Kool et al. (2013) reported that the terminal mannose can also have substitutions of acetyl groups, which may amount to ~11% of total acetyl groups on XG. Different XG products can have different percentage of pyruvate and acetate substitutes on mannose units (Rochefort and Middleman, 1987, Cadmus et al., 1976). The presence of acetyl group on the inner mannose unit can facilitate XG adopting a rod-like conformation in solution (Morris and Harding, 2009). Several studies suggested that the higher acetyl content is associated with lower flexibility of XG chains that can also facilitate and stabilise XG's secondary and tertiary structure (see for example (Kool et al., 2013, Morrison et al., 2004, Shatwell et al., 1990)). Further, the viscosity can also be impacted by the amount of acetyl and pyruvyl groups present in XG solutions, which will be explained in Chapter 2.1.1.2.

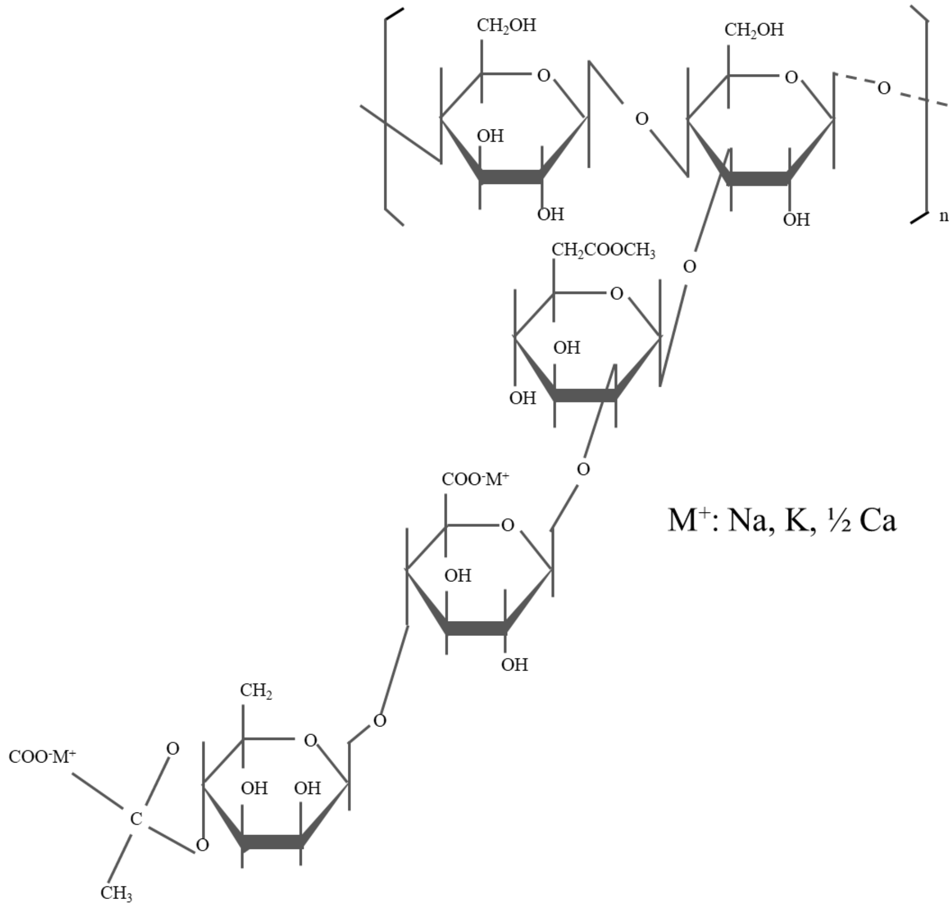

Figure 2.1 Primary structure of xanthan gum indicating the backbone and the tri-saccharide side chain

The repeat unit of XG is a cellobiose unit decorated with a tri-saccharide sidechain. The axial translation cellobiose unit is around 0.94nm (Okuyama et al., 1980, Stokke et al., 1989). The expected mass per unit length (M_L) of XG is around 900 g/(mol·nm), based on the monosaccharide composition of the decorated cellobiose unit. The M_L of single helix model XG determined by using X-ray fibre diffraction is ~ 996 g/(mol·nm) (McNeely and Kang, 1973, Andrew, 1977). Similar result (~ 950 g/(mol·nm)) was later reported by other researchers using the same technique (Sato et al., 1984, Okuyama et al., 1980). For the double stranded xanthan assemblies the reported mass per unit length ranges from 1700 to 2200 g/(mol·nm) as determined by using electron microscopy (EM) (Stokke et al., 1989). These values are consistent with the X-ray diffraction data obtained for the single stranded xanthan chains.

The secondary structure of XG is still under discussion. Morris et al. (1977) suggested that XG is a single helix. By contrast, Holzwarth and Prestridge (1977) suggested that XG can have multi-stranded helical structure (Morris, 2019). Holzwarth (1978) also reported that M_L of ordered native XG is twice as high as single helix model of XG. The specific details of XG helical structure have been reported by several researchers, who proposed, based on X-ray fibre diffraction, XG has a five-fold helix, with the pitch of ~4.7nm for both single and double helices models (see for example (Lapasin and Pricl, 1995, Moorhouse et al., 1977, Okuyama et al., 1980)). In a single helical model, the side chains are suggested to be folded back rendering the backbone to be highly rigid, to an extent that rigidity of a single and double stranded XG configurations are not too dissimilar (Rochefort and Middleman, 1987, García-Ochoa et al., 2000). Some researchers also suggest that the secondary structure of XG solution may be dependent on the treatment (purification) method after fermentation, the type of sample and corresponding solvent (Rochefort and Middleman, 1987). Morris (2019) proposed that single helix or double helix can co-exist, though the double helix model is reported to be enthalpically more favourable (Moffat et al., 2016) due to the presence of physical, non-covalent interactions (Morris, 2019). However, the double helical structure of XG is not a unique molecular configuration. It is suggested that double helixes can be coaxial or antiparallel. Further, they can have different level of multi-chain assembly and the level of structure imperfection. Gulrez et al. (2012) suggested that re-assembly of XG double helices after dissociation step can result in the formation of less ordered double helical structures with higher chain flexibility compared with the natural double helix, which is characterised by the higher degree of molecular order. The wide range of assemblies and the physical nature of intermolecular interaction of XG offers unique opportunity to create different structures with different rheological and diffusive properties through using various processing techniques. Gulrez et al. (2012) and earlier Norton et al. (1984) proposed the model of XG structural transformations from a coil to single helix to double helix, with different configuration and levels of intramolecular association. Specifically, such processing methods as high-pressure homogenisation, ultra-sound treatment, extrusion (Foster and Mitchell, 2012) and radiation can be used to treat XG samples in order to modify the structure of molecular assemblies and modulate the thickening and gelling functionality of XG.

Due to high level of backbone decoration and propensity to form helical structures, the XG chain has a rod like conformation with limited flexibility (Harding et al., 2017). The reported values of the persistence length (L_P) range from 100 to 150 nm, although there might be big variations depending on specific solvent conditions, temperature and secondary structure. The molecular weight of XG ranges from 2×10^6 to 5×10^7 Da, depending on the fermentation method (see for example, (García-Ochoa et al., 2000, Muller et al., 1986)). In this work, the Keltrol-T XG was used. The choice was due to high levels of polydispersity and clarity. Dhami et al. (1995) used a similar grade Keltrol-RD xanthan gum (larger particle size) with a molecular weight of ~ 6×10^7 Da, with low level of polydispersity as evident from the distribution of the sedimentation coefficient (*s*) which appears as a narrow single peak with the average $s = 12.97 \pm 0.26$ S (Dhami et al., 1995).

The self-association behaviour of XG strongly depends on the structure of the side chains (acetylation, pyruvation, counterions) and their distribution (blockiness). The structure of side chain could be impacted by the effect of heat, acid, alkaline and enzymes (Lapasin and Pricl, 1995, Sworn, 2009a). The helix-coil transition of the secondary structure of XG in solution is influenced by pH, temperature, the content of pyruvate/acetate and electrolytes (Rochefort and Middleman, 1987, Abbaszadeh et al., 2015, Lecourtier et al., 1986). Furthermore, it is found when added cadoxen to XG solution, the helical structure could convert to disordered random coil (Sato et al., 1984). The process of helix-coil transition proposed by Morris (2019) is a two-step process: (a) first, coil converts to single helix; (b) second, the single helix undergoes dimerization to form a double helix (Morris, 2019). Like many polysaccharides, the helix-coil transition of XG is associated with the formation and dissociation of hydrogen bonds and, hence, is thermally reversible. And the helix-coil transition temperature can increase with the concentration of salt (Sworn, 2009a)

XG can disperse in both hot and cold water while it cannot be dissolved in non-polar organic solvents. The intrinsic viscosity ([η]) of XG is around 7534 ± 2700 ml/g (Dhami et al., 1995). Other intrinsic viscosity values were found in different XG product samples with different solvent (see for example (Lecourtier et al., 1986)). The critical overlap concentration (c*) defined by Launay equation is around 0.5 mg/ml (Dhami et al., 1995). Further, Wyatt and Liberatore (2009) claimed that XG solution (salt free solvent) can have three critical concentrations, which are critical overlap concentration (c^*) with the value of 0.07 mg/ml, entanglement concentration (c_e) with the value of 0.4 mg/ml with the value of and final critical electrostatic blob overlap concentration (c_D) with the value of with the value of 2 mg/ml. However, when XG is dissolved into 0.05 M NaCl solution, only two critical concentrations were found, which are c^* with the value of 0.2 mg/ml and c_e with the value of 0.8 mg/ml (Wyatt and Liberatore, 2009).

XG solutions at room temperature are highly extended because of the electrostatic repulsions among side chains. When electrolytes are added to XG solution at room temperature, the side chains could fold back to the backbone due to electrostatic effect, and the structure of XG becomes stabilized and ordered (Rochefort and Middleman, 1987, Norton et al., 1984). Therefore, the structure of XG can be more flexible under low ionic strength (Xu et al., 2012). Although XG can dissolve in water easily, when the concentration of electrolytes are high, the dissolving time can be comparatively long (Jindal and Singh Khattar, 2018).

Table 2.1 Macromolecular and hydrodynamic properties of xanthan gum

	XG		
		Measuring methods	References
Mass per unit length (g/(mol·nm))	1700 to 2200	EM (electron microscopy)	(Stokke et al., 1989)
	950	X-ray fibre diffraction	(Okuyama et al., 1980, Sato et al., 1984)
	996	X-ray fibre diffraction	(Andrew, 1977, McNeely and Kang, 1973)
	1900	X-ray scattering	(Holzwarth, 1978)
Persistence length (nm)	100 to 150	X-ray fibre diffraction / AFM (Atomic force microscopy)	(Harding et al., 2017)

Molecular weight (Da)	2×10^6 to 5×10^7	Chromatix KMX6 photometer	(García-Ochoa et al., 2000, Muller et al., 1986)
	6×10^7	AUC (Analytical ultracentrifugation)	Product type: Keltro RD (Dhami et al., 1995)
Critical overlap concentration (mg/ml)	0.5	Launay equation: c~3.3/[η]	(Dhami et al., 1995)
	0.07	TA Instruments AR-G2 stress-controlled rheometer	(Wyatt and Liberatore, 2009)
Intrinsic viscosity (ml/g)	7534 ± 2700	Capillary (Ostwald) viscometer	Water as the solvent (Dhami et al., 1995)

2.1.1.2 Rheological and tribological properties

XG solutions have shear-thinning rheological behaviour, which can depend on the concentration of the solution. Like most of polysaccharides, dilute XG solutions can have Newtonian-like rheological behaviour (see for example (Zhang et al., 2013, de

Moura and Moreno, 2019)). With the increase of concentrations, the shear thinning behaviour can be more pronounced (see for example (Bais et al., 2005, Lapasin and Pricl, 1995)). It was previously reported that the stiffness of rod like polysaccharide can also impact the rheological behaviour (Lapasin and Pricl, 1995). It is suggested that polysaccharides with stronger stiffness chains can have more pronounced shear-thinning behaviour. The viscosity of XG solution can have plateaus when the shear rate is extremely low and extremely high (Song et al., 2006b, McClements, 2007, Sworn, 2009b). It is suggested that when the concentration of XG solution is higher than 5 mg/ml, it may have weak gel properties (see for example (Carnali, 1991)). Further, XG solution with concentration higher than 10 mg/ml can have a transient gel-like structure at rest state (Sworn, 2009a).

The viscosity of XG solutions can be stable in a wide pH range from 4 to 10 (Sworn, 2009b, García-Ochoa and Casas, 1994). The viscosity of XG solution can be decreased when the pH is reduced to 3 while it shows reversibility when pH comes back to neutral condition. Further, Kang and Pettitt (1993) suggested that when pH is higher than 9, XG can experience deacetylation. However, it has little influence on viscosity. The structure of XG solution can be stable within a big temperature range. It is suggested that the viscosity of XG solution can be reversible when heated up XG solution until 100 °C cools down the solution to 20 °C (Sworn, 2009b, Sworn, 2009a).

The rheological behaviour of XG solution can be influenced by the concentration of salt in the solution (Norton et al., 1984, Rochefort and Middleman, 1987, Bewersdorff and Singh, 1988). Zatz and Knapp (1984) found when the concentration of XG is lower than 3 mg/ml, the viscosity of XG may decrease when adding salt with the concentration of 10^{-4} mol/L. On the contrary, when the concentration is higher than 3 mg/ml, the viscosity may increase with the addition of electrolytes. Muller et al. (1986) found the structure of XG to have a dramatic change when the salt concentration is increased to around 0.01 M NaCl. Therefore, XG may have completely ordered structure when the concentration is higher or equal to 0.01 M NaCl, which means when concentration of salt goes higher than 0.01 M NaCl, it is suggested that salt has little influence on viscosity of ordered XG solution (Rochefort and Middleman, 1987). Further, when XG in semi-dilute regime, the addition of salt can lower the viscoelastic moduli (Pelletier et al., 2001). The strength of XG gel can be enhanced by different cations, and among commonly used cations, Ca^{2+} shows the highest strengthen ability (Ross-Murphy et al., 1983). The acetyl and pyruvyl groups can also impact the rheological behaviour of XG solutions. It is reported that higher acetyl XG have lower viscosity compared with XG have less acetylate counterparts. By contrast, pyruvyl groups on terminal mannose tend to increase the viscosity of XG solution (Cheetham and Nik Norma, 1989).

XG can have apparent yield stress behaviour at high concentrations due to strong intermolecular association in concentrated condition (see for example, (Hannote et al., 1991, García-Ochoa and Casas, 1994, Marcotte et al., 2001)). It is suggested that low concentrations of XG solutions can have undetectable yield stresses (Ewoldt et al., 2010, Parker et al., 1995). Carnali (1991) reported that the yield stress detectable concentration can be around 8 mg/ml with the yield stress of ~0.3 Pa while Yaseen et al. (2005) reported that XG solution with the concentration of 5 mg/ml is ~ 2 Pa. The yield stress of XG can be influenced by temperature, which is suggested that higher temperature can lead to lower yield stress values (Song et al., 2006a). The Heinz-Casson model, Hershel-Bulkley model and Mizrahi-Berk model can be used to determine the yield stress of XG solution (Marcotte et al., 2001, Whitcomb and Macosko, 1978, Song et al., 2006a).

Morris (2019) and Pelletier et al. (2001) stated that unlike other entangled coil polysaccharides (Cox and Merz, 1958), the complex viscosity (η*) of concentrated XG solution is higher than shear viscosity due to viscoelastic gel structure. Similar conclusions were also reported by Ross-Murphy et al. (1983) and Richardson and Ross-Murphy (1987), who reported that the complex viscosity of semi-dilute XG solution is also slightly higher than shear viscosity, and this correspond to findings in this research (Chapter 5). However, this may due to different test conditions or different samples, Tam and Tiu (1989) stated that XG solutions may only obey Cox-Merz rule when the frequency and shear rate is in low range. It is overall suggested that XG may not obey Cox-Merz rules under most rheological conditions.

By analysing normal force data using FENE-P dumbbell model, Stokes et al. (2011) found that XG has longer characteristic relaxation time compared with the majority of common food grade polysaccharides such as locust bean gum or pectin. The tribological studies of XG are mainly done by de Vicente et al. (2005) and Stokes et al. (2011), who reported that XG can adsorb to PDMS surface. The tribological behaviour of XG solution were also studied in this research (Chapter 6).

2.1.1.3 Application in industry

The key properties that make XG widely applied in industry are: (a) viscosifying capacity across a broad range of pH from acidic to alkaline (pH 4-10, in the presence of salt, under low salt conditions the range can be narrower) (Sworn, 2009a); (b) XG is stable against most of the common enzymes present in foods, incl. of bacterial origin (such as lactobacilli); (c) XG has unique shear-thinning behaviour, with an apparent yield stress-like behaviour at low shear rates (García-Ochoa et al., 2000); (d) many XG products can be characterised by the dissolution in cold water, making processing simple and efficient (Phillips and Williams, 2009).

Another advantage of XG is its safety with low levels of allergenicity or intolerance, as well as a long-standing record of the history of use. As a food grade polysaccharide, XG was approved by FDA in the United States in 1969 and later was approved by Europe in 1974 (Jindal and Singh Khattar, 2018). Booth et al. (1963) observed that when applied XG on rats, there was no growth inhibition. Furthermore, later research done by Woodard et al. (1973) found after feeding dogs and rats XG for 2 years, no tumours were detected and no significant negative impact was found on blood and organ condition. It has been further proven that does not cause skin rashes or eye irritations (Sworn, 2009a, Sworn, 2009b).

In addition to foods, XG has also been applied in other industrial applications, such as oil drilling, agricultural products, pharmaceutical and cosmetics area (García-Ochoa et al., 2000). It also used in shampoos or moisturisers due to its effect as a stabiliser. It can also be employed in toothpaste as it has high yield stress and high shear-thinning behaviour (Morris and Harding, 2009). XG can also be utilized as cross-linker for many polysaccharides, such as locust bean gum or guar gum (Harding et al., 2017). When added guar or locust bean gum to XG solution, the synergistic interaction may make the gel stronger (Morris and Harding, 2009).

XG in food application and beyond can be used in emulsions, suspensions and foam formulations where XG acts as a stabiliser against creaming. This phenomenon is necessary for consumers' acceptability and shelf-life of products. When XG is applied in an emulsion or foam, it can slows creaming by reducing the rates of coalescence and Ostwald ripening (McClements, 2007, García-Ochoa et al., 2000, Sworn, 2009a, Phillips and Williams, 2009, Petri, 2015). The mechanism of stabilisation against creaming deserves further scrutiny. Initially, it was proposed that creaming is prevented by the apparent yield stress of XG, which at low shear rates arrests droplet motion (rising). However, this hypothesis was disproven by Parker et al. (1995) who demonstrated that firstly XG does not have a true yield stress, but creaming stabilisation occurs due to XG-induced formation of the flocs of the oil droplets. Parker et al. (1995) posit that repulsive interactions between XG and oil droplets result in depletion flocculation. The formation of the flocs increases the effective phase volume of the oil phase resulting in the emergence of the true yield stress behaviour that stabilises emulsion against creaming.

XG can also be used as the packaging material of food or medicine (Harding et al., 2017). Like many polysaccharides with β-glucan backbone, XG can be applied widely in industry due to its film formation, fat replacement and gelling properties (Viñarta et al., 2013). It is also suggested that viscoelastic properties of XG may be effectively mimic some aspects of saliva rheology, making XG to be a functional component of several saliva substitute formulations (van der Reijden et al., 1994). Mystkowska et al. (2013) found 3.5 mg/ml XG solution with SDS solution have comparable fiction coefficient as human whole saliva as measured using pin-on-disc tester (Mystkowska et al., 2013).

2.1.2 Scleroglucan

2.1.2.1 Macromolecular properties

Like XG, scleroglucan (SG) is an extracellular polysaccharide derived from fungus genus *Sclerotium sp*. *Sclerotium glucanicum* and *Sclerotium rolfsii* (see for example (Phillips and Williams, 2009, McNeil and Harvey, 1993)). Figure 2.2 show the primary structure of SG: it has a curdlan backbone consists of β-D-1, 3-glucopyranosyl units (Bluhm et al., 1982), with every third unit linked by a 1-6 glycosidic bonds with a single β-D-glucose side-chain. It should be noted that an analogous polysaccharide schizophyllan (SPG) has the same linkage composition and molecular structure, however, compared to SG it is markedly less soluble in water. In this thesis, several preliminary experiments were conducted using SPG. However, due to limited solubility the work was not pursued further. Unlike XG, SG is a neutral polysaccharide, with the mass per unit length (M_L) estimated to be 2300 - 2860 g/(mol·nm), with the lower bound determined from the small angle X-ray scattering (SAXS) and the upper bound corroborated based on the AFM (Stokke et al., 2001, Gawronski et al., 1999).

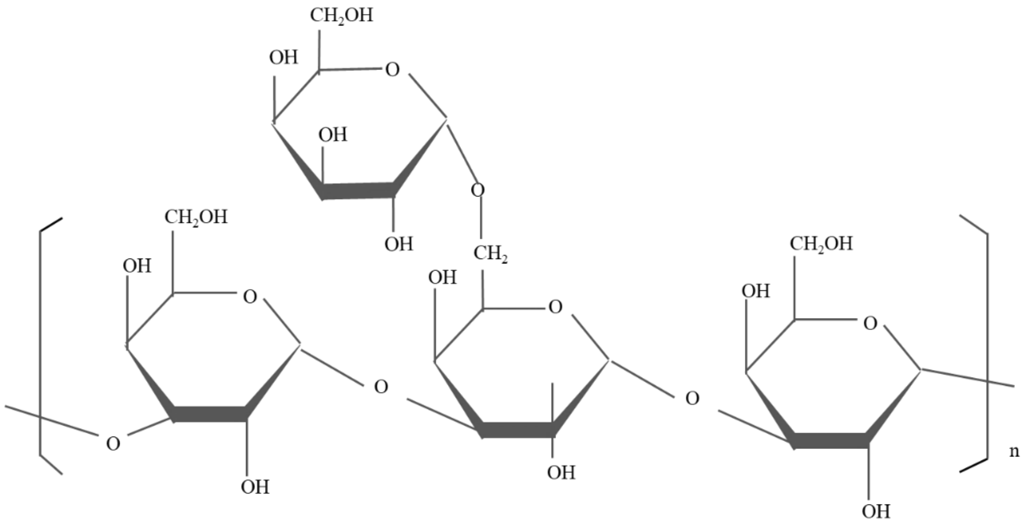

Figure 2.2 The primary structure of SG

In solution, SG is postulated to adopt a triple helical structure (Yanaki et al., 1981, Vuppu et al., 1997, Stokke et al., 2001) stabilised by hydrogen bonds (Gawronski et al., 1999). The diameter of the central cavity in the helical structure is reported to be ~ 0.35 nm (Okobira et al., 2008, Gidley and Nishinari, 2009) and the triple helical assembly is ~ 1.65 nm (Okobira et al., 2008). Okobira et al. (2008) also reported that the pitch of SG in crystalline state is ~ 1.94 nm.

The persistence length (L_P) of SG measured by AFM (Stokke et al., 2001) and calculated by wormlike cylindrical model (Noïk and Lecourtier, 1993, Yamakawa and Fujii, 1974) ranges from 140 to 200 nm. SPG has comparable persistence to SG, which is ~ 180 nm by using light scattering photometer (Kashiwagi et al., 1981, Harding et al., 2017). When comparing SG with XG, it has longer persistence than XG, which means it has more rigid structure (Table 2.1). Noïk and Lecourtier (1993) also observed that temperature can influence the persistence length of SG, as L_P becomes shorter with increasing temperature, which can imply that the structure of SG becomes more flexible at high temperatures.

It is reported that the average molecular weight of SG ranges from 1.3×10^5 to 6.0×10^6 Da depending on different measuring techniques (including light scattering (Yanaki et al., 1981), SEC-LALLS (Lecacheux et al., 1986), GPC-MALLS technique (Gawronski et al., 1999). The molecular weight was also characterized in this PhD project (Chapter 4) by using analytical ultracentrifugation (AUC), which is ~ $(2.8 \pm 0.3) \times 10^6$ g/mol (Li et al., 2020). The molecular weight of SPG has comparable molecular weight as SG, which is ~ 2.6×10^6 Da (Fang et al., 2004). Lecacheux et al. (1986) also suggested that the molecular weight of 1,3-β-D-glucan polysaccharides (including SG) may not be dependent on production cultivation condition. The SG molecules can be broken down into smaller pieces under sonication. When sonicating SG for 10 min with the 20kHz frequency and 30% amplitude, the molecular weight can reduces to half (Ansari et al., 2012).

SG is suggested to have self-association behaviour (Bluhm et al., 1982), which is also confirmed by experiment done using Analytical Ultracentrifugation (AUC) (details in Chapter 4) (Li et al., 2020). It is also observed that SG may have intermolecular association between side chains (β-D-glucose unit) (Bluhm et al., 1982). The intrinsic viscosity [η] of SG is ~ (2190 ± 110) ml/g by using the Ostwald viscometer, which can be found in Chapter 4 (Li et al., 2020). An estimation of critical overlap concentration (*c**) was done by Japper-Jaafar et al. (2009), who extrapolated zero-shear viscosity back to zero concentration and found c* is around 0.54 mg/ml. In Chapter 4, similar c* was also estimated by sedimentation velocity analysis using AUC, which ranges from 0.4 to 0.75 mg/ml (Li et al., 2020, Cuvelier and Launay, 1986). It is further suggested that SG and Keltrol RD Xanthan gum have comparable critical overlap concentration (Dhami et al., 1995, Japper-Jaafar et al., 2009, Li et al., 2020).

Unlike curdlan, the β-D-glucopyranosyl unit side chain can increase the solubility and decrease the gelling ability of SG (Stokke et al., 2001, Yanaki et al., 1980, Brigand, 1993, Phillips and Williams, 2009, Survase, 2007). When preparing aqueous solution, it is suggested to dispense SG powder slowly to prevent lumping. It is reported that when dissolving SG in DMSO, the molecular weight of SG decreases to 1/3, which is suggested to be because DMSO can break down the triple helical structure to single helices (Yanaki and Norisuye, 1983, Bluhm et al., 1982). In this thesis we observed that solubility of SG in DMSO is lower compared with research by Yanaki and Norisuye (1983), which may be caused by different SG products used in Yanaki's research and this project as Lecacheux et al. (1986) suggested that different fermentation methods or fermented fungus can lead to markedly different solubility of SG products.

Table 2.2 Macromolecular and hydrodynamic properties of scleroglucan

	SG		
		Measuring methods	References
Mass per unit length (g/(mol·nm))	2600 ± 260	AFM (Atomic force microscopy)	(Stokke et al., 2001)
	2300	SAXS (Small angle X-Ray scattering)	(Gawronski et al., 1999)
Persistence length (nm)	140 to 200 nm	AFM (Atomic force microscopy)	(Stokke et al., 2001, Yanaki et al., 1981, Bluhm et al., 1982, Biver et al., 1986, Noïk and Lecourtier, 1993)
Molecular weight (Da)	1.3×10^5 to 6.0×10^6	GPC/PCD (Multidetector gel permeation	(Phillips and Williams, 2009, Gawronski et al.,

		chromatography coupled with post column delivery)	1999, Lecacheux et al., 1986, Fariña et al., 2001)
	(2.8 ± 0.3) $\times 10^6$	AUC (Analytical ultracentrifugation)	(Li et al., 2020)
Critical overlap concentration (mg/ml)	0.54	TA-instruments Rheolyst AR 1000N controlled-stress rheometer	(Japper-Jaafar et al., 2009)
	0.45 to 0.7	Launay equation: c~2.9/[η]	(Cuvelier and Launay, 1986, Li et al., 2020)
Intrinsic viscosity (ml/g)	2190 ± 110	Capillary (Ostwald) viscometer	Water as the solvent (Li et al., 2020)

2.1.2.2 Rheological and tribological properties

Like XG, SG solutions have shear-thinning behaviour, and it can be more pronounced in concentrated solutions (see for example (Moresi et al., 2001)). On the other hand, it is reported that very dilute SG solution can have Newtonian-like behaviour (see for example (Finnerty, 2000, Phillips and Williams, 2009, Fariña et al., 2001). The rheological behaviour of SG solutions was measured and compared with XG solutions at different concentrations in this thesis (details in Chapter 5), and the results are in good agreement with previous research (Japper-Jaafar et al., 2009, Lafforgue et al., 2018).

It is suggested that the viscosity of SG solution can be stable within a wide pH range from 1 to 12. When pH goes higher than 12.5, SG may lose its shear-thinning behaviour due to the partially dissociation of helical structure (Baba Hamed and Belhadri, 2009, Brigand, 1993, Yanaki and Norisuye, 1983). Further, several publications also suggested that the triple helical structure can be destroyed when pH goes higher than 13 (Fariña et al., 2001, Stipanovic and Giammatteo, 1989), so that the viscosity of SG solution can decrease dramatically when pH goes higher than 13 (Fariña et al., 2001). Other publications also observed that when pH of SG solution is around 14, SG solution may have Newtonian behaviour as the helical structure may be completely destroyed (Mazzuca et al., 2017). On the contrary, Fariña et al. (2001) also stated that lowering the pH (even goes down to 0) does not impact apparent viscosity. Like XG, the viscosity of SG shows high reversibility within a big temperature range from 20 °C to 100 °C (Fariña et al., 2001). Further, Brigand (1993) also reported that when the pH of SG solution remains between 4 to 10, the viscosity can barely vary even heated up to 121 °C for 20 h. Unlike XG, the rheological behaviour of SG is not sensitive to inorganic salt (Fariña et al., 2001, Brigand, 1993). However, Finnerty (2000) suggested SG solution can become to gel when the salt concentration is very high as the quality of solvent is reduced, which may increase the opportunities of macromolecules interaction (Rau et al., 1990).

Like XG, SG solution also has an apparent yield stress behaviour. Benna-Zayani et al. (2008) reported that the yield stress of 6 mg/ml SG is ~ 0.85 Pa. For entangled solutions, when compared SG with XG under the same concentration, it is found that XG have a slightly higher yield stress than SG (Benna-Zayani et al., 2008, Yaseen et al., 2005). Further, like XG, it is reported that SG also does not obey Cox-Merz rule (Gidley and Nishinari, 2009). It is suggested that the difference between complex viscosity and steady shear viscosity becomes larger with the increasing concentration. Gidley and Nishinari (2009) also suggested that Cox-Merz rule may not obeyed by most (1,3)-β-glucans with rod like structures. Japper-Jaafar et al. (2009) suggested 5 mg/ml SG solution can have gel-like structure. Further, like XG, 10 mg/ml SG has a weak gel structure at rest state (Gidley and Nishinari, 2009). It is observed that the 5 mg/ml SG has a higher tanδ (tanδ=G”/G’) value compared with solutions with higher concentrations. However, when concentrations of SG solutions reach 40 mg/ml, the tanδ value will remain stable (François et al., 2003).

The Trouton ratio of SG solution is much higher than 3. Japper-Jaafar et al. (2009) suggested that the Trouton ratio of SG solution may decrease dramatically over the increasing concentration, especially in the range of 3 mg/ml to 5 mg/ml. However, Trouton remains stable with the value around 340 when the concentration ranges between 1 mg/ml to 3 mg/ml (Japper-Jaafar et al., 2009).

When adding crosslinker (such as borax) to SG solution, it can transform to gel (Coviello et al., 2010). The strength of SG-borax gel is comparatively high due to the strong linkages (partially covalent bonds) between SG helixes and borate ions (Gidley and Nishinari, 2009). Bais et al. (2005) reported when adding non-ionic surfactants (such as dimethicone copolyol) to SG solutions, the connection between helices can be destroyed, which lead to lower viscosity and lower storage moduli.

There are few research focusing on the tribological study of SG. Previous research found that like many polysaccharides, the friction coefficient of SG solution decreases with the increasing concentration at 1mm/s entrainment speed (Garrec and Norton, 2012). Moreover, it is also suggested that SG may not adsorb to PDMS surface during tribological tests.

2.1.2.3 Application in industry

SG have similar key properties as XG and SPG that means SG can also be widely applied in industry, which are: (a) SG can be stable within a wide pH range between 1 to 12; (b) SG solution has highly shear-thinning behaviour with apparent yield behaviour and the viscosity of SG solution can be stable under high salinity condition

(Baba Hamed and Belhadri, 2009); (c) SG can be resistant to hydrolysis (Coviello et al., 2005); d) The structure of SG solution can still be stable even with the presence of ethanol and glycol (Moresi et al., 2001).

SG is proven to be non-toxic at levels required for technological function in foods (Finnerty, 2000, Sworn, 2009b). It is found that SG will not cause irritation when in contact with eyes or skin (Bais et al., 2005, Brigand, 1993). Even though SG has not been approved by EU for use as food grade biopolymers, several Japanese patents suggest that SG can be used for producing instant drinks (Fujiwara and Ohashi, 1982e), Japanese rice crackers (Fujiwara and Ohashi, 1982c), steamed foods (Fujiwara and Ohashi, 1982d), cakes (Fujiwara and Ohashi, 1982b) and confectionery dough of bakery (Fujiwara and Ohashi, 1982a). Viñarta et al. (2013) also suggested that SG may be applied in dairy industry due to its thickening ability. It is also suggested that SG can be used as a suspending agent, which reported 1 mg/ml to 2 mg/ml SG solution can usually stabilize 5 % to 10 % suspensions of powders (for example, zinc oxide) (Phillips and Williams, 2009, Finnerty, 2000, Brigand, 1993). As mentioned in Chapter 2.1.1.3, it is found that yield stress is not the main reason to explain the stabilizing impact of XG. There are few publications to investigate the mechanism of stabilizing effect of SG, which can be emphasized in the next phase research. Overall, it is suggested that SG can be used as stabilizing agent, thickening agent or gelling agent in food industry (Survase, 2007).

van der Reijden et al. (1994) claimed that SG can be a saliva proxy for ex-vivo study since SG is stable within a big pH range, and not sensitive to inorganic salt. It is found that 0.1 mg/ml XG and SG have comparable viscoelastic behaviour as saliva (van der Reijden et al., 1994). However, these biopolymer solutions have different tribological behaviour and non-linear viscoelasticity as human whole saliva (see Chapter 6), which suggests that XG and SG may not be comprehensive proxies of saliva.

Like XG, SG can be used in the oil industry for drilling, oil recovery and thickening (Baba Hamed and Belhadri, 2009, Fariña et al., 2001). Davison and Mentzer (1982) reported that SG can still maintain 90% of its viscosity in 90 °C sea water condition for more than 500 days, indicating that SG is a promising agent applied in oil drilling industry. SG can also be used in cosmetic products, such as creams, shampoos or moistures as stabilizing agent (Coviello et al., 2005, Brigand, 1993). Like some other β-glucans, SG can also be applied in pharmaceutical area due to its antitumor and antiviral activity (Kurachi et al., 1990, Singh et al., 1974, Kitamura et al., 1994, Brigand, 1993). Coviello et al. (2005) also suggested that SG also has the function of anti-inflammatory. Further, previous research conducted on chicks and dogs show that SG can reduce the cholesterol level when ingesting SG together with feed (Halleck, 1970, Griminger and Fisher, 1966).

SG have several unique advantages compared to XG and can be promising alternative in industrial application: (a) SG has high resistance to electrolytes or hydrolysis, showing a higher stability than XG due to the structure (Phillips and Williams, 2009, Baba Hamed and Belhadri, 2009); (b) It is less sensitive to temperature and pH than XG (Stokke et al., 1992). However, the yield of SG is still much lower than XG, which leads to much higher price (McNeil and Harvey, 1993). Furthermore, SG still has not been approved to be used as food-grade biopolymer. Therefore, XG is still more widely accepted because of its higher commercial availability (Phillips and Williams, 2009).

2.2 Human whole saliva

2.2.1 Salivary glands, secretion, and collection

Saliva is the liquid in mouth secreted by salivary glands, and the secretion of saliva is controlled by the autonomic nervous system (ANS) (Pereira, 2012). The secretion of saliva is mainly triggered by the flavour and chewing activity (Chaudhari and Roper, 2010, Carpenter, 2012, Garrett et al., 1999). Carpenter (2012) supplemented that smell can also stimulate saliva at some extent. Saliva secretion can be influenced by many factors, such as the circadian rhythm, the type of the salivary gland, diet, age, gender, blood type, collection method etc. (Schipper et al., 2007).

It is found that 90% of human saliva is secreted by three main salivary glands, which are parotid, submandibular, and sublingual glands (see for example (Pereira, 2012, Llena, 2006)). Recently, a new study observed that there can be a fourth main salivary gland, which is named as the tubarial salivary gland (Valstar et al., 2020). Figure 2.3 displays the location of salivary glands in the oral cavity. Parotid glands are the largest salivary gland, which is located in the retromandibular fossa anterior to the ear and sternocleidomastoid muscle (at both sides of the face) (Pereira, 2012), which can contribute to around 60% of salivary flow (Carpenter, 2012). α-amylase is mainly produced by the acinar cells in parotid gland (Llena, 2006). The sublingual gland is located between the muscles of the oral cavity floor (under the tongue) and the submandibular gland is in the posterior portion of the submandibular triangle (at the bottom of the mouth) (Pereira, 2012). Sublingual gland saliva and submandibular gland saliva contain high concentrations of mucin (Carpenter, 2012). Sublingual gland plays an important role on preventing dryness within the oral cavity due to high elasticity and viscosity (Silletti et al., 2008). The main function of submandibular saliva can be formation of bolus and promoting oral lubrication during swallowing or speaking (Silletti et al., 2008). Figure 2.3.b displays the schematic region of tubarial gland, which is located in the posterolateral wall of human nasopharynx (Valstar et al., 2020). Unlike other main salivary glands, tubarial gland does not have a capsule (Valstar et al., 2020). There were few serous acini found in tubarial gland, which may indicate that this gland cannot produce amylase. Valstar et al. (2020) also reported possible difficulties can be faced when collecting saliva from tubarial gland alone due to its location. Some minor salivary glands (essentially mucous) located in our cheek, lip, palate and tongue can also provide around 10% of saliva (Schipper et al., 2007, Pereira, 2012, Humphrey and Williamson, 2001, Llena, 2006). Although the limited contribution, saliva secreted from these minor salivary glands contains high concentration of mucin and Immunoglobulin proteins, which helps maintaining the mucin-rich layer on the oral mucosa (Carpenter, 2012).

(a) (b)

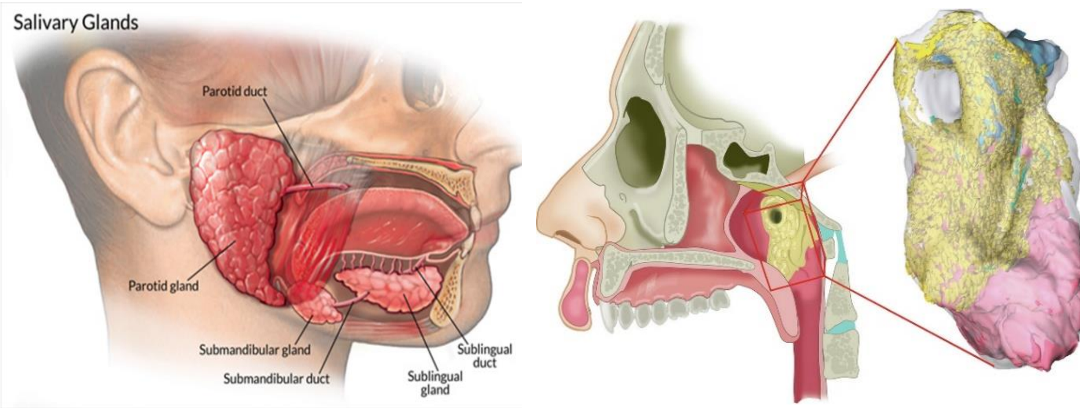

Figure 2.3 (a) Salivary glands in oral cavity (WebMD UK Limited., 2017); (b) Schematic figure of tubarial gland that newly discovered (Valstar et al., 2020)

The cells found in salivary glands are mainly acinar cells, myoepithelial cells and duct cells (Humphrey and Williamson, 2001, Pereira, 2012). Among those cells, acinar cells are responsible for saliva secretion, which are wrapped by the long myoepithelial cells (Humphrey and Williamson, 2001, Pereira, 2012). Saliva is plasma-like fluid after secretion by acinar cells (Dodds et al., 2005, Carpenter, 2012), which can be transferred to oral cavity by different gland ducts. During the transfer process, the concentrations of different inorganic compounds can be regulated by striated duct cells and excretory duct cells (Humphrey and Williamson, 2001, Pereira, 2012). The volume of saliva that a healthy adult can secrete ranges from 500 ml to 1500 ml per day (Schipper et al., 2007, Llena, 2006, Humphrey and Williamson, 2001, Aps and Martens, 2005). Salivary glands usually produce greatest volume of saliva before or after meals, and the production peak can be reached at noon, and decreases during sleep period (Llena, 2006). Moreover, when under anxiety or stress, the saliva secretion is also lower than the normal level because the nerve traffic from the brain to the salivary glands can be impaired (Carpenter, 2012).

The type of saliva (stimulated or non-stimulated) secretion also varies in different salivary glands. Stimulated saliva accounts for around 80 % to 90% of the amount of saliva secretion (Humphrey and Williamson, 2001). For the stimulated saliva, parotid glands contribute more than other two major glands, which is around 50% to 60% of the total volume (Silletti et al., 2008, Humphrey and Williamson, 2001). The unstimulated saliva can be mainly produced by the submandibular glands, which accounts for ~ 65% (Llena, 2006, Humphrey and Williamson, 2001, Silletti et al., 2008). Parotid glands contribute to around 20% of unstimulated saliva secretion and some minor glands produce less than 10% of the total unstimulated saliva (Humphrey and Williamson, 2001).

Different methods of saliva collection were studied and discussed by Navazesh (1993), who suggested that swab method and suction method are not suitable for unstimulated whole saliva collection as they both can trigger saliva stimulation at some degree. For the unstimulated saliva collection, the draining and spitting method are more accurate and reproducible. Further, Navazesh (1993) suggested that spitting method is also suitable for stimulated saliva collection, and the spitting method can be the most widely applicable method. For the stimulated saliva, the stimuli can be either mechanical or acid and the composition can be varied when using different collection methods (Proctor, 2016). Previous research found that when collecting acid-stimulated saliva, it has higher mucin content compared with mechanically stimulated saliva (see for example (Stokes and Davies, 2007b)). However, Mohamed et al. (2012) reported that the saliva stimulated by acid has lower protein concentrations, particularly in the concentrations of IgE (Immunoglobulin E) and myoglobin. Mechanically stimulated saliva was used in this research and the collection method can be found in Chapter 5.2.

For the in-vitro research involving saliva, it is important to inhibit the metabolism in saliva. It is suggested that stimulated saliva is more stable at room temperature compared with non-stimulated saliva (Rantonen and Meurman, 1998). Precautionary methods should be taken during saliva collection, such as adding protease inhibitor or collecting saliva under cold condition (recommended at 4 °C) (Veerman et al., 1989). Further, with the objective of minimizing the bacterial action in saliva, the saliva should be centrifuged before storage (Schipper et al., 2007). It is suggested to store saliva under -80 °C (Henson and Wong, 2010), and the properties of saliva samples do not have obvious changes for 6 weeks under this temperature (Schipper et al., 2007).

2.2.2 Saliva composition and function

Saliva have several functions that can help preserve and maintain oral health, i.e., lubrication, cleansing, anti-microbial activity, buffering activity, tasting activity and teeth preservation (remineralization) (see for example, (Humphrey and Williamson, 2001, Stokes and Davies, 2007b)). Carpenter (2012) also suggested that different surfaces (teeth or mucosa) in oral cavity may require different functions from saliva, for example teeth can require the mineralisation function from saliva to prevent teeth cavities. For healthy oral cavity, the pH of saliva varies from 6.2 to 7.5 over the day to help with the mineralisation (van der Reijden et al., 1994, Aps and Martens, 2005, Schipper et al., 2007).

With a content as high as 99.5%, water is the main component of saliva. Water in saliva mainly has the function of cleaning (Lynge Pedersen and Belstrøm, 2019). Saliva also contains of 0.2% inorganic compounds and 0.3% protein (Schipper et al., 2007, Humphrey and Williamson, 2001, Sarkar and Singh, 2012). The inorganic compounds in saliva are different types of electrolytes under different concentrations, which include calcium, sodium, potassium, magnesium, phosphate and bicarbonate ions etc. (Schipper et al., 2007, Humphrey and Williamson, 2001). The proteins in saliva contain enzymes (α-amylase, etc.), mucins, peptides and immunoglobulins etc. (Schipper et al., 2007, Humphrey and Williamson, 2001). Further, it is suggested that the saliva composition may not be the same during in-vitro and in-vivo study (Schipper et al., 2007).

The inorganic compounds in saliva have the function of preserving the mucosa integrity, buffering action and maintain the perfection of teeth (remineralization) (Llena, 2006, Humphrey and Williamson, 2001). It is found that calcium ion can impact the structure of saliva. Further, Raynal et al. (2003) reported that the intrinsic viscosity and the average molecular weight of saliva increases significantly with the addition of calcium ion to saliva. The phosphate ions, bicarbonate ions and urea have the functions of buffering as well as adjusting the pH of saliva (Dodds et al., 2005, Humphrey and Williamson, 2001). Dodds et al. (2005) also reported that the inorganic compounds and pH in saliva may also impact the organic compounds.

Proteins in saliva have some significances in terms of maintaining oral health (microbial balance), lubrication and digestion (Hu et al., 2007). Further, it is observed that some types of proteins in saliva (such as PRPs, cystatins, mucins) may contribute to the formation of enamel pellicle and mucosa pellicle (Lynge Pedersen and Belstrøm, 2019, Hu et al., 2007). Moreover, Hu et al. (2007) reported some glycosylated salivary proteins can be beneficial for sustaining mucosal barriers. There are different types of proteins in saliva, including enzymes (such as α-amylase, lysozyme), antimicrobial proteins, mucins, immunoglobulins, peptides (such as cystatins, histatins) and proteins with high content of proline (Sarkar and Singh, 2012, Humphrey and Williamson, 2001, Hu et al., 2007, van Nieuw Amerongen et al., 2004, Dodds et al., 2005, Jensen et al., 1992).

For the enzymes in saliva, α-amylase plays an important role on preliminary hydrolysis of foods containing starch , during which, starch can be broken down to maltose (Sarkar and Singh, 2012). Lysozyme is known as the enzyme with the antimicrobial functionality and is secreted by parotid gland (van Nieuw Amerongen et al., 2004). Further, it was previously reported that lysozyme can still have antimicrobial activity after heating treatment (van Nieuw Amerongen et al., 2004, Humphrey and Williamson, 2001).

The proteins with high proline content are also named proline-rich proteins (PRPs), which account for 35% to 40% of total protein in saliva (Dodds et al., 2005, Carpenter, 2012, Matsuo and Morimoto, 1994). Matsuo and Morimoto (1994) reported that PRPs are the main protein type in submandibular and parotid glands saliva, which have the function of binding and precipitating tannins. PRPs can be divided into three categories, i.e. acidic, basic and glycosylated PRPs (Matsuo and Morimoto, 1994).

PRPs can precipitate easily during centrifugation, and at least 10% of PRPs can be removed after centrifugation (Campese et al., 2009). PRPs have effective film formation ability, which can adsorb on both hydrophobic and hydrophilic surfaces (Hahn Berg et al., 2004). Further, it is observed that even though PRPs do not play a role in lubrication, they can improve the wear resistance ability (Yakubov et al., 2015).

Statherin can be found in saliva secreted from submandibular and parotid glands, with the molecular weight of ~ 5400 Da (Yakubov et al., 2014). Statherin can carry calcium to prevent teeth erosion (Carpenter, 2012, Hay and Schlesinger, 1977), and it also has the function of aggregating microorganisms (Lynge Pedersen and Belstrøm, 2019). The C-terminal of statherin is not charged and the N-terminal of statherin is negatively charged, which lead to the surfactant functionality of statherin (Proctor et al., 2005). The charged N-terminal can bind with hydroxyapatite, which may increase the lubrication ability (Harvey et al., 2011a). Proctor et al. (2005) suggested that the surface-active property of statherin may be the reason of the wettability of saliva.

Cystatins are phosphoproteins containing cysteine, which can inhibit proteinase and has the function of antifungal, antiviral and antibacterial ability (Lynge Pedersen and Belstrøm, 2019, Shomers et al., 1982). The main proteoforms of cystatins can be found in human whole saliva are cystatin A, cystatin B, cystatin D, cystatin S, cystatin SA and cystatin SN (Henskens et al., 1994, Lynge Pedersen and Belstrøm, 2019). It is found that cystatin SA level in saliva could correspond to the periodontal disease and kidney function (Techatanawat et al., 2019). Previous research also suggested that the level of albumin and cystatin may correspond to the health of periodontium (Henskens et al., 1993). Henskens et al. (1993) also suggested that the concentrations of cystatin of periodontitis patients are remarkably higher than healthy people. Further research also found that the concentrations of basic cystatin C in healthy people is low while for patients with gingivitis or periodontitis, the concentrations are significantly higher (Henskens et al., 1994).

Histatins are known as histidine-rich proteins in saliva with the molecular weight ranging from 3000 to 5000 Dalton (Dodds et al., 2005, Yakubov et al., 2014). Previous research found that histatin can only be found in saliva of humans or some primates (Padovan et al., 2010, Yakubov et al., 2014). For human saliva, Campese et al. (2009) reported that parotid saliva has the highest concentration of histatin. There are three types of histatins in human saliva, namely histatin 1, histatin 3 and histatin 5. Histatin 5 is the hydrolysis product of histatin 3 (Yakubov et al., 2014). The recent research also observed histatin 1 can be the biomarker of children's oral health as it can be related with the buffering capacity in oral cavities (Shimomura-Kuroki et al., 2020). Further, histatin can also bind tannins, and among three types of histatins, histatin 5 can bind tannin most effectively at neutral pH (Perry et al., 2007).

Mucins may account for around 20% to 30% of total proteins in saliva (Thornton et al., 1999). For stimulated saliva, mucin accounts for around 16% of total proteins (Rayment et al., 2000). Mucins in saliva are mainly secreted by the submandibular and sublingual glands (Pereira, 2012, Llena, 2006, Dodds et al., 2005). Mucins in saliva contain around 25% amino acids and 75% carbohydrates. Mucins are negatively charged as it contain sulphate groups, sialic acid and other amino acids (Silletti et al., 2008). Mucin has semi flexible random coil structure containing a glycosylated protein backbone with oligosaccharide sidechain (Harding, 1989, Bansil et al., 1995, Bansil and Turner, 2006). The conformation of mucins can be impacted by the pH and ionic strength (Bansil and Turner, 2006). With the addition of bicarbonate ion in saliva, the bicarbonate ion can reduce the amount of calcium ions bound to mucins, which may reduce the cross-linking properties of mucins so that the structure of mucin can become more flexible (Löfgren et al., 2016). Mucin also exhibits adhesive properties due to hydrogen bonds or hydrophobicity (Bansil and Turner, 2006). Mucin populations in saliva contain two types, i.e., MG1 and MG2 (Humphrey and Williamson, 2001, Thomsson et al., 2002, Wickström et al., 2000). It is found that MG1 has oligomeric structure with 15% protein and MG2 has monomeric structure with 30% protein (Wickström et al., 2000, Thomsson et al., 2002). It is suggested that MG1 is converted by gene MUC5B and MG2 is converted by gene MUC7 (Wickström et al., 1998, Bobek et al., 1993). The molecular weight of MG1 is around 2000 kDa and the molecular weight of MG2 ranges from 100 to 300 kDa (Thornton et al., 1999, Yakubov et al., 2014). From the rheological point of view, it is also suggested that mucin in human whole saliva can be divided into three categories, i.e., sol MUC5B, gel MUC5B and MUC7 (Wickström et al., 2009). Among different types of mucins, MUC5B is the dominant mucin and has the highest molecular weight, ranging from 2 to 40 million Da (Löfgren et al., 2016, Sonesson et al., 2008, Rayment et al., 2000). In sol MUC5B, the charged mucin has higher sialic acid concentration compared with other mucins (Yakubov et al., 2014). Raynal et al. (2002) also reported that MUC7 and several other salivary proteins can also bind with MUC5B, which may give saliva its certain rheological or tribological behaviour. It is suggested that most of the proteins are bound with mucins under hydrogen bonds or electrostatic interactions while a small number of proteins could bind mucins with covalent bonds or hydrophobic interactions (Radicioni et al., 2016, Meldrum et al., 2018). The calcium ion can help to build the mucin and non-mucin protein network, which may be responsible for the specific viscoelastic behaviour of saliva (Raynal et al., 2002). Further, it is reported that for the new-born, the MUC5B content in its whole saliva will increase in the first 12 months while the MUC7 will decrease during this period (Ruhl et al., 2005). However, Sonesson et al. (2008) observed that the content level of MUC7 secreted by labial gland increases again with age. It is also reported that old people tend to have less mucin content in their whole saliva compared with young adults (Denny et al., 1991, Navazesh et al., 1992).

2.2.3 Rheological properties of saliva

Saliva has weak shear-thinning behaviour, and its viscosity can be impacted by many factors, such as the measurement methods, collection time or the saliva donation protocol (Schipper et al., 2007, Stokes, 2012a). Rantonen and Meurman (1998) reported that the viscosity of unstimulated saliva is highly dependent on the collection time in the day. However, no such obvious changes were found in stimulated saliva (Rantonen and Meurman, 1998). The viscosity of saliva from each individual also varies, however, Rantonen and Meurman (1998) observed that the viscosity of saliva does not depend on the sexes. The viscosity of saliva can decrease with the decrease of pH due to the proteolysis of mucins (Schipper et al., 2007). When collecting saliva without precaution methods, the viscosity of saliva samples can reduce during storage (Kusy and Schafer, 1995). It is suggested that saliva does not have apparent yield stress behaviour (Stokes, 2012a). Further, saliva has a comparatively high first normal stress difference value and high elastic properties (Stokes and Davies, 2007b). The oscillatory tests of saliva samples also indicate that saliva (individual sample) have a series of relaxation time (Yakubov et al., 2014). For the saliva after centrifugation, it is suggested that the Trouton ratio is ~120 (Haward et al., 2011).

It is found that saliva secreted by different glands have distinct rheological behaviour. The parotid saliva has shear-thinning behaviour and is slightly more viscous than water (Silletti et al., 2008, Schipper et al., 2007, van der Reijden et al., 1993).

Sublingual saliva has most pronounced shear-thinning behaviour among saliva secreted by different glands (Schipper et al., 2007). Unlike parotid and sublingual saliva, submandibular saliva and saliva secreted by minor salivary glands have Newtonian-like rheological behaviour (Silletti et al., 2008). It is reported that the parotid saliva shows the lowest viscosity while the sublingual saliva shows the highest viscosity among saliva secreted by different glands (van der Reijden et al., 1993). The whole saliva and submandibular saliva have comparable viscosities, which are slightly lower than the viscosity of sublingual saliva. Zussman et al. (2007) reported that the relaxation time of parotid gland saliva is the lowest, and the relaxation time of sublingual and submandibular saliva are ten times higher than parotid gland saliva. It is suggested these differences can be caused by different concentrations of mucins (van der Reijden et al., 1993, Silletti et al., 2008, Schipper et al., 2007, Zussman et al., 2007).

It is suggested that the collection methods of stimulated saliva have little influence on the flow rate of saliva (Stokes, 2012a, Stokes and Davies, 2007b). For unstimulated saliva, the flow rate ranges from 0.3 to 0.4 ml/min (Proctor, 2016, Sreebny and Vissink, 2010). It is found that the flow rate of elderly people is also higher than younger people, which can be related to a higher concentration of protein of older people’s saliva (Zussman et al., 2007, Nagler and Hershkovich, 2005).

Waterman et al. (1988) reported the rheological measurement of saliva can be inaccurate when rheological measurements are conducted without considering the effects of interfacial elasticity that come into play when a proteinaceous film forms at the air interface at the edge of the measuring geometry. As such, the measured stress is heavily skewed by the presence of the elastic interfacial film, rendering determination of bulk viscosity inaccurate. Statherin and mucin linkages can be the main reason of the fault measurement (Yakubov et al., 2014, Proctor et al., 2005). Therefore, it is recommended to add a small amount of surfactant for saliva measurement (such as sodium dodecyl sulphate solution) on the edge of the geometry to decrease the impact caused by the protein adsorption and to minimize the surface artefacts (Stokes, 2012a).

Löfgren et al. (2016) reported that the storage modulus of unstimulated saliva ranges from 0.15 to 2.1 Pa. The phase angle of unstimulated saliva tends to be lower than 30° indicating its high elasticity. It is reported that the viscosity of mechanically stimulated saliva and unstimulated saliva have comparable viscosity. However, mechanically stimulate saliva shows a higher first normal stress difference. Stokes and Davies (2007b) also observed the shear thinning rheological properties of stimulated saliva triggered by citric acid is more pronounced than mechanically stimulated saliva. The viscoelastic behaviour of saliva can be defined by the ratio of first normal stress difference N_1 and shear stress σ. For acid stimulated whole human saliva, the value of the N_1/σ ratio is around 100, while for the mechanically stimulated saliva, the value of the ratio ranges from 10 to 100, indicating acid stimulated saliva is more elastic (Stokes and Davies, 2007b). The high value of N_1/σ can be caused by the larger amount of the sol MUC5B, which has the weak gel structure built by non-covalent interaction (Taylor et al., 2003). Overall, the viscoelasticity of saliva is dependent on the collection and stimulation methods (Stokes, 2012a).

2.2.4 Saliva film and lubrication

In oral cavity, a thin film of saliva is covered on the teeth and oral mucosa. The oral cavity surface is hydrophobic, however, with the adsorption of secreted saliva, the surface become hydrophilic (Lindh et al., 2001). It is reported that the thin salivary film in oral cavity can contain five layers, i.e., the outer layer (air-saliva interface), the liquid layer, the hydrated mucin layer, the protein layer (bounded tightly) and the precursor layer (Löfgren et al., 2016, Veeregowda et al., 2012, Lundin et al., 2009, Yakubov et al., 2014, Yakubov et al., 2015). It is also observed that salivary film in oral cavity may also include food residuals or proteins from bacteria (Yakubov et al., 2014). Further, Yakubov et al. (2015) suggested that the functional layers for saliva adsorption can be: (a) layer formed with proteins with low molecular weight which may not be lubricious; (b) hydrated mucin layer offering lubrication function. Further, it is reported that saliva film on different parts of oral cavity have different composition, structure and function (Yakubov et al., 2014). For the enamel pellicle, it can help to maintain the health of teeth as it has the function of lubrication and the steady state between remineralization and demineralization (Lynge Pedersen and Belstrøm, 2019). For the saliva film on oral mucosa, it is reported that it does not contain statherin or PRPs, and it may have hydrophobic behaviour to the surface of epithelial cells (Gibbins et al., 2014a, Gibbins et al., 2014b, Hannig et al., 2017). Hannig et al. (2017) also observed that the mucosa pellicle has a hydrogel-like structure in which the water can be preserved by glycoproteins in mucosa pellicle. The mucosa pellicle has the lubrication and antimicrobial function.

Saliva has comparatively high normal stress ratio indicating that saliva is able to separate surfaces even under thin layer film, which may further contribute to oral lubrication (Löfgren et al., 2016, Stokes and Davies, 2007b). The thickness of saliva film can vary significantly from each individual (Larsen et al., 1999). Collins and Dawes (1987) calculated the average thickness of salivary film by determining the surface area, and the thickness of unstimulated saliva ranges from 70 to 100 μm. The other research compared the saliva thickness of health adults and dry mouth patients by using micro-moisture meter found that the film thickness of healthy adults varies from 17 to 58 μm. For the patients with dry-mouth, the thickness ranges from 9 to 26 μm (Lee et al., 2002). The friction coefficient of saliva is dependent on the collection methods, for example, the acid-stimulated may have lower friction coefficient (Harvey et al., 2011b). The friction coefficient of saliva is around 0.03 under 1N load with 50%

SRR and 5 mm/s entrainment speed under smooth hydrophobic PDMS surfaces (Yakubov et al., 2015).

It is known that mucins, proline-rich glycoproteins, acidic proline-rich proteins, peptides (such as statherin) and amylase can contribute to the lubrication properties of saliva (Schipper et al., 2007, Boze et al., 2010, Bongaerts et al., 2007b, Cárdenas et al., 2007). Saliva can be the lubricant between different oral surfaces, for example, tongue, palate, or teeth. Since most surfaces in oral cavity are soft, the soft contact tribology becomes more significant in oral lubrication study (Yakubov, 2014, Yakubov et al., 2014). During food digestion, the interactions between the saliva and the food product or ingredients can be significant. At the first stage of food ingestion, the salivary film is thick, the bulk rheological properties are the dominant factor in this stage. However, with the process of eating, the salivary film becomes thinner, the interfacial rheological behaviour is more significant. With further mastication, food bolus is in contact with proteins in oral substrate, people can feel resistance at this boundary lubrication stage (Chen and Stokes, 2012, Yakubov et al., 2014).

Since salivary film and food components may have interactions during food ingestion, people can have astringency feel indicating the increase of friction coefficient. One reason of the increasing friction coefficient can be the aggregation of salivary proteins due to the presence of foods in oral cavity (Rossetti et al., 2009, Bongaerts et al., 2007b, Stokes and Davies, 2007b), while the other reason can be the ionic strength modification (Pradal and Stokes, 2016, Macakova et al., 2011). Many chemical compounds can result in the astringent sensation, for example, organic acids, ethanol, chitosan or polyphenols. Polyphenols are one of the most important compounds widely applied in food industry, which can bind with PRPs in salivary film and lead to astringency sensation (Yakubov et al., 2015).

2.2.5 Reconstituted saliva

Saliva can deteriorate quickly after collection, which may cause inconveniences to further experimentation. Therefore, reconstituted saliva (RS) was prepared and suggested as a proxy of saliva in this research. As mentioned in section 2.2, mucin is the main protein in saliva and mucin is one of the main proteins in saliva responsible for the function of lubrication and viscoelastic behaviour in the oral cavity (Dodds et al., 2005, van der Reijden et al., 1993). Löfgren et al. (2016) also suggested that MUC5B could be responsible for the rheological and tribological properties of saliva. It was therefore hypothesized that reconstituted saliva prepared by mucin can be used to mimic the rheological and tribological behaviour of saliva. In this research, animal mucins were used to prepare the reconstituted saliva. It is reported that bovine submaxillary mucin (BSM) and porcine gastric mucin (PGM) share some similarities with MUC5B (Park et al., 2007, Sarkar and Krop, 2019). It is found that BSM is more sensitive to the changes of pH because it is abundant in negatively side chains compared to PGM (Madsen et al., 2016). Further, BSM has better lubricity and more elastic film than PGM (Sarkar and Krop, 2019). BSM also has a better ability on anchoring to the hydrophobic PDMS surface than PGM (Madsen et al., 2016), and has a remarkably higher content of sialic acid, which make BSM more similar to sol MUC5B in human saliva (Wickström et al., 2000) . It is suggested that BSM may mimic the human salivary mucin better than PGM, which also corresponds to conclusion had by Sarkar et al. (2019).

Reconstituted saliva (RS) was prepared by dissolving bovine submaxillary mucin (BSM) (Type I-S, M3895, Sigma-Aldrich, Gillingham, UK) in an aqueous solution of the composition detailed in Table 5.1 (Chapter 5). The molecular weight of BSM ranges from $1.6*10^6$ to $4.1*10^6$ Da (Bettelheim and Dey, 1965). These inorganic components and their concentrations are representative of HWS. The inorganic buffer was prepared according to the protocol published by Sarkar et al. (2009) (details in Chapter 5.2.3).

Chapter 3 Techniques and Methods

3.1 Molecular characterisation of biopolymers

The molecular properties of the rod like biopolymer SG were characterized in this research for the first time and compared to those of xanthan gum. The detailed description of techniques used to characterize the molecular properties of both scleroglucan and xanthan gum is given below:

3.1.1 Intrinsic viscosity

Intrinsic viscosity ($[\eta]$) is related to the hydrodynamic volume occupied by the macromolecule in a dilute solution (Lapasin and Pricl, 1995). For a macromolecule, the intrinsic viscosity depends on chain flexibility, the degree of water binding, and the overall molecular shape. For non-globular macromolecules, the molecular weight of the molecule will also impact on the intrinsic viscosity (Harding, 1997, Harding, 2013).

The intrinsic viscosity measurement of the scleroglucan solution was carried out in U-tube capillary viscometer. First, the relative viscosity (η_r) was determined. This is the ratio of solution's viscosity to that of the solvent, and was evaluated using Eq 3.1., where t is the flow time of the solution between two fixed points, t_0 is the flow time of pure solvent, ρ is the density of the solution, and ρ_0 is the density of the solvent.

$$\eta_r = \frac{\eta}{\eta_o} = \frac{t}{t_o} \cdot \frac{\rho}{\rho_o} \tag{3.1}$$

Then, the reduced viscosity (η_{red}) can be calculated using Eq. 3.2., where c is the mass concentration of the macromolecule in solution.

$$\eta_{red} = \frac{\eta_r - 1}{c} \tag{3.2}$$

The reduced viscosity and the inherent viscosity ($\ln\eta_r/c$) were then plotted as a function of concentration. A linear fit of each of these data sets give the Huggins (Eq. 3.3) and Kraemer equations (Eq. 3.4), respectively. The fitting lines in accordance with Huggins and Kraemer equations were extrapolated to $c \rightarrow 0$ to obtain the values of intrinsic viscosity (Huggins, 1942, Kraemer, 1938), whilst the values of the slope were used to evaluate the Huggins (K_H) and Kraemer constants (K_K), which provide the first-order estimation of non-ideality effects.

$$\eta_{red} = [\eta] \cdot (1 + K_H \cdot c) \tag{3.3}$$

$$\frac{\ln \eta_r}{c} = [\eta] \cdot (1 - K_K \cdot [\eta] \cdot c) \tag{3.4}$$

The relative viscosity data can also be fitted using the Solomon-Ciuta model (Eq. 3.5), which provides an approximate evaluation of intrinsic viscosity without the need for extrapolation of concentration to zero (Solomon and Ciută, 1962). All three equations share the same principle but differ in the method of extrapolation to obtain the value of [η].

$$[\eta]_{SC} \sim \left(\frac{1}{c}\right) \cdot [2 \cdot (\eta_r - 1) - 2 \cdot \ln(\eta_r)]^{1/2} \tag{3.5}$$

When the concentration is high, the distorted flow may impact the neighbouring macromolecule (Serdyuk et al., 2007). Therefore, at high concentrations, the viscosity and concentration may have a non-linear relationship. The concentrations used to calculate the intrinsic viscosity should be lower than the coil overlapping concentration, as demonstrated by Harding (1997).

The relationship of the intrinsic viscosity, molecular weight and shape is summarized in the Mark-Houwink-Kuhn-Sakurada equation (Eq. 3.6), *a* is the MHKS power law viscosity coefficient (see for example, (Harding et al., 2017)) and references cited therein), *κ'* and *a* are dependent on the rigidness and conformation of the macromolecule (Lapasin and Pricl, 1995). Similar equations can also be used to study the hydrodynamic macromolecular relationship between molecular weight and sedimentation coefficient *s*, the radius of gyration R_g or the translational diffusion coefficient D^o. The macromolecule is spherical when $a = 0$. The shape of the macromolecule is random coil when a range from 0.5 to 0.8. The macromolecule has a rigid rod conformation when a = 1.8 (Harding et al., 2017).

$$[\eta] = \kappa' \cdot M^{a} \tag{3.6}$$

Several types of viscometers could be used to measure the intrinsic viscosity [η], such as capillary (Ostwald) viscometer, rotational viscometer, rolling ball viscometer or differential pressure viscometer (Serdyuk et al., 2007). In this work, the Oswald U-tube capillary viscometer (Schott-Geräte, Mainz, Germany) is used to evaluate the value of intrinsic viscosity. The Oswald viscometer is one of the best techniques to determine intrinsic viscosity as the viscometer can be calibrated easily (Serdyuk et al., 2007). Viscosity is sensitive to temperature. Thus, the experiment was carried out in (20.00 ± 0.01 °C) water bath which contains a cooler (Haake, Thermo Fisher Scientific, MA, USA) and a heater (Schott AG, Germany). 2mL of biopolymer solution was injected to the reservoir. Then the solution was pumped until the meniscus lay above the upper mark indicated in Figure 3.1. The flow time was recorded as the solution was allowed to flow under gravity through the capillary tube until the meniscus passed the lower mark (Figure 3.1). The flow time of the fluid is proportional to the relative viscosity of the fluid. A series of concentrations (0.01 mg/mL, 0.02 mg/mL, 0.03 mg/mL, 0.04 mg/mL and 0.05 mg/mL) of biopolymer solutions were selected for the triplicate measurements.

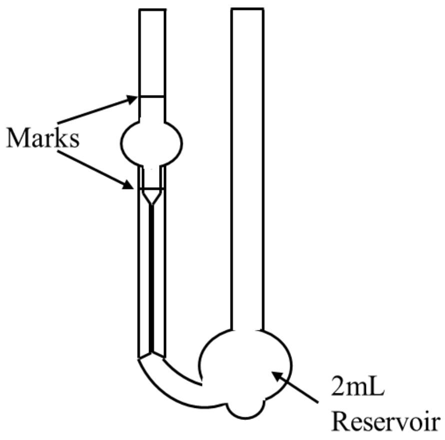

Figure 3.1 Ostwald capillary viscometer

3.1.2 Refractive index

There are several methods to determine the concentration of a solution, such as the refractive index method or UV absorbance. However, the UV absorbance method is not suitable for polysaccharide concentration measurement, as polysaccharides do not exhibit strong absorption of light within the near-UV spectrum. Therefore, the concentrations of the biopolymer solutions were measured using differential refractometry before performing the macromolecular characterization. When a ray of light enters a biopolymer solution, the ray will be bent by the solute macromolecules. The refractive index represents the degree of bending of the light through the biopolymer solution. There will be greater bending at higher concentrations. The refractive index increment *dn*/*dc* represents the degree of bending per unit of concentration for a given polymer in solution. In this work, the refractive index was measured using the DD-7 Atago refractometer (Tokyo, Japan). 2 ml of solvent was injected into the sample and reference channels of the Atago refractometer to calibrate the instrument. Then the samples were injected to measure the concentration in Brix% (w/v). The concentration of the biopolymer solution can be converted using Eq. 3.7. to give the concentration in mg/mL.

$$Concentration = Brix\% \cdot \left(\frac{(\frac{dn}{dc})_{biolymer}}{(\frac{dn}{dc})_{sucrose}}\right) \cdot 10 \qquad (3.7)$$

3.1.2 Analytical ultracentrifugation

Polysaccharides can be challenging to characterise due to their swelling and polydispersity (Harding, 2005b). Analytical ultracentrifugation (AUC) is the main technique used in this work to characterise the macromolecular properties of scleroglucan, and the interactions between biopolymer solutions and mucin solutions (details can be found in Chapter 4). Unlike chromatography or field flow fractionation, AUC does not require filtration matrix or membrane. Furthermore, AUC is more resolving than dynamic light scattering. Moreover, AUC can be used to characterise molecules in a large molecular weight range, i.e., 10^2 to 10^8 Da (Demeler, 2010, Harding et al., 2018), as well as under different solvent conditions such as pH, ionic strength and within a relatively broad range of solution conditions. In this present study, the AUC experiments were carried out using the Beckman Optima XL-I analytical ultracentrifuge (AUC) (Beckman Instruments, Palo Alto, USA). The AUC is equipped with an optical system to monitor the sedimentation process of macromolecules over time (Scott and Schuck, 2005).

Figure 3.2.a shows a rotor and a cell for the AUC. An 8-hole rotor (Beckman-Coulter An-50Ti) was used to perform each experiment. One hole of the rotor is used to insert a counterbalance while the other seven holes are for samples. The counterbalance is used as a reference to calibrate radial distance. There were two types of cells used in AUC experiments. For the sedimentation velocity analyses, the 12 mm optical path length double sector aluminium epoxy cells with sapphire windows were used (Beckman-Coulter, Indianapolis, USA). For the sedimentation equilibrium analyses, 20 mm long optical path length double-sector cells with sapphire windows were used (Nanolytics, Potsdam, Germany). Each cell contains two sectors, one for the reference solvent and one for the sample, in this case biopolymer solutions (Figure 3.2.b). During the AUC run, the laser shines through each sector of each cell as it rotates. The detector captures the light and sends the data to the computer. Several optical methods can be applied in AUC to identify the molecular properties of macromolecules, such as the absorbance optical system, and Rayleigh interference optical system. However, the absorbance optical system is more suitable for protein or nucleic acid analysis as these molecules contain benzoyl chromophores that can be detected using the UV light absorption. For polysaccharides, which do not have such a chromophore, the Rayleigh interference optical system is more suitable (Harding, 2005a) and is therefore used in

the current work. The rotor of an analytical ultracentrifuge is capable of rotating at speeds up to 60,000 rpm. With the target of minimizing heating caused by the friction and other non-ideality, the rotor should be spun in an evacuated chamber (Ralston, 1993).

There are two main types of analysis used in AUC, namely sedimentation velocity and sedimentation equilibrium. The principles and details of these two analyses will be explained below.

(a) (b)

Figure 3.2 An 8 hole rotor (a) and cell (b) of an AUC

3.1.2.1 Sedimentation velocity

Sedimentation velocity depends on the molar mass and the molecular shape and size. It can be used to quantify the conformation and conformation flexibility, and the state of aggregation state of samples (Demeler et al., 2014, Ralston, 1993, Harding et al., 2018). The centrifugation speed is comparatively high for the SV (sedimentation velocity) analysis, which is anywhere between 30,000 to 60,000 rpm, which produces a depletion of solute near the meniscus and the formation of the sharp boundary between the depleted region and the uniform concentration of sedimenting solute (the plateau) (Figure 3.3.a). With the increase of the centrifugation time, the boundary moves to the cell base. The rate of the movement of the boundary can be captured by the optical system. The high centrifugal forces can lead to relatively rapid sedimentation of solute towards the cell base and leave the clear solvent near the meniscus (Figure 3.3.b). During the sedimentation velocity process, the macromolecules can display hydrodynamic non-ideality. The hydrodynamic non-ideality can be caused by the back-flow viscosity and exclusion volume effects between the macromolecules (Harding and Johnson, 1985b, Harding and Johnson, 1985a, Laue and Stafford, 1999). With the increase of hydrodynamic non-ideality, the sedimentation coefficient decreases (Laue and Stafford, 1999, Ralston, 1993). These effects can be minimised by working at low concentration, and eliminated by extrapolation of the sedimentation coefficient to infinite dilution (concentration $c = 0$).

(a) (b)

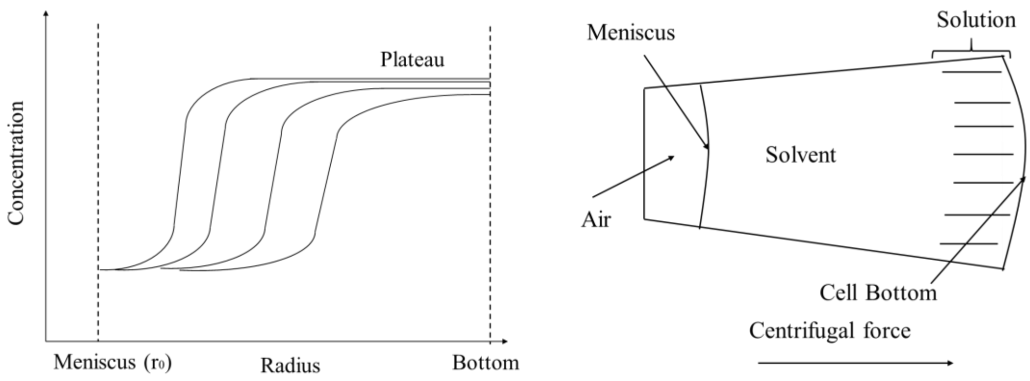

Figure 3.3 Sedimentation velocity: (a) the movement of boundary in sedimentation velocity analysis; (b) the top view of sample sector of the centrifuge cell

The Svedberg equation (Equation 3.8) can be used to determine the sedimentation coefficient, *s,* in Svedbergs (S), or 10^{-13} seconds. The sedimentation coefficient can be used to estimate the molecular weight if the shape contribution is known since sedimentation coefficient is dependent on size and shape of the macromolecule. Factors which influence molecular friction coefficient, such as size and shape of the macromolecule will have an impact on the sedimentation coefficient. For example, for a rod-like macromolecule or a random coil macromolecule will have a lower sedimentation coefficient than a spherical molecule if they all have the same molecular weight (Van Holde, 1985).

$$s = \frac{u}{\omega^2 r} = \frac{M(1-\bar{v}\rho_0)}{N_A f} \qquad (3.8)$$

where u is the rate of movement per unit centrifugal field, ω (rad/s) is the angular velocity, r is the radius of the particle from the centre of the rotation (thus $\omega^2 r$ is the angular acceleration or known as the centrifugal field), M is the molecular weight of the solute, N_A is the Avogadro's number, f is the friction coefficient, ρ_0 is the density of the solvent, $\bar{v}$ is the partial specific volume (ml/g). Partial specific volume defines the change volume of the solution when adding a small amount of solute (Cammack et al., 2006). For polysaccharides, the partial specific volume is ~ 0.61 mL/g (Zaccai et al., 2017).

The sedimentation coefficient depends on temperature, as well as density and viscosity of the solvent. The sedimentation coefficient s is usually corrected to the standard solvent conditions, namely the density and viscosity of water at 20.0 °C (Eq. 3.9) to give $s_{20,w}$:.

$$s_{20,w} = s_{T,b} \cdot \left(\frac{1-\bar{v}\rho_{20,w}}{1-\bar{v}\rho_{T,b}}\right) \cdot \left(\frac{\eta_{T,b}}{\eta_{20,w}}\right) \qquad (3.9)$$

where, $\rho_{T,b}$ and $\eta_{T,b}$ are the density and viscosity of the buffer, respectively, for a given temperature. The computer software SEDNTERP was used to calculate the $s_{20,w}$ (Hayes et al., 1995).

Similar to intrinsic viscosity, sedimentation coefficient depends on the concentration of the solution due to non-ideality effects. After the 'apparent' sedimentation coefficients have been measured for different concentrations, a plot of apparent sedimentation coefficient versus concentration is made, followed by an extrapolation back to zero concentration to take account the non-ideality effect (see, for example, (Dhami et al., 1995)). The intercept gives the 'infinite dilution' sedimentation coefficient, $s^{0}_{20,w}$ (Eq. 3.10).

$$\frac{1}{s_{20,\,w}} = \frac{1}{s^{0}_{20,w}} \cdot (1 + k_s \cdot c) \tag{3.10}$$

Where k_s (mL/g) is the sedimentation concentration regression coefficient, or 'Gralen' coefficient.

The SEDFIT software can be used to analyse the data of sedimentation velocity, which is based on the Lamm equation (Eq. 3.11) (Dam and Schuck, 2004, Lamm, 1929). It can transform the boundary movement profiles into the distribution of sedimentation coefficients.

$$\frac{dC}{dt} = \frac{1}{r}\frac{d}{dr}\left[rD\frac{dC}{dr} - s\omega^2 r^2 C \right] \tag{3.11}$$

Where D is the translational diffusion coefficient.

There are two types of analysis procedure, namely the least square Gaussian distribution g(s) and diffusion corrected distribution c(s). The ls-g*(s) model can be used to identify the heterogeneity of the sample (Cole et al., 2008, Harding, 2005a, Harding, 2005b). It is also a suitable model for large macromolecules (such as polysaccharides) with, comparatively, small diffusion coefficients (Harding, 2005a, Harding, 2005b, Schuck and Rossmanith, 2000). For the c(*s*) model, one of the major advantages compared to g(*s*) is that it takes diffusion effect into consideration, and this can lead to sharper peaks, as compared to the g*(*s*) model (Cole et al., 2008, Dam and Schuck, 2004).

Sedimentation coefficients are used to estimate the molecular weight of macromolecules. One method of determining the molecular weight is by knowing the diffusion coefficient D^0 (Eq. 3.12) (Van Holde, 1985). By combining equation 3.8 and 3.12, the molecular weight is calculated using Eq. 3.13 (Harding, 2005a).

$$D^0 = \frac{RT}{Nf_0} \tag{3.12}$$

$$M = \frac{s^0 RT}{D^0(1-\bar{v}\rho_0)} \tag{3.13}$$

The *Extended Fujita* method (Harding et al., 2011) can also be used as a method to estimate the molecular weight distribution. It is an extension of the Fujita method (Fujita, 1962) (Eq. 3.14), which transforms the sedimentation coefficient distribution g(*s*) at low concentration to a molecular weight distribution *f(M)* vs *M*, based on the assumption that molecules adopt a random coil conformation.

$$f(M) = g(s)\cdot(ds/dM) \tag{3.14}$$

The *Extended approach* is used for all conformations and utilises the power-law relationship between the sedimentation coefficient and molecular weight, analogous to the MHKS equation for viscosity (Eq. 3.6) (Harding et al., 1991, Smidsrød and Andresen, 1979, Tsvetkov et al., 1971):

$$s = \kappa_s \cdot M_w{}^b \tag{3.15}$$

where *s* and *b* are characteristic coefficients related to conformation. If s and b are known, then the molecular weight distribution can be calculated.

$$\frac{ds}{dM} = b \cdot \kappa_s^{1/b} \cdot s^{(b-1)/b} \tag{3.16}$$

3.1.2.2 Sedimentation equilibrium

Sedimentation equilibrium is one of the most rigorous methods to determine the molecular weight of the biopolymer. This technique can also determine the molecular weight of polydisperse and non-ideal systems (for example, polysaccharides) (Morris et al., 2014). In this type of analysis, the sedimentation is balanced by the diffusion force, which acts to disperse analyte molecules across the volume, meaning that the diffusion force counteracts sedimentation (Figure 3.4.a). The choice of the centrifugation speed depends on the range of macromolecular weights being investigated. A very high molecular weight macromolecular assembly may only need as low as 2000 rpm centrifugation speed. However, for a very low molecular weight molecule, the centrifugation speed can be as high as 60,000 rpm (Mächtle and Börger, 2006). Unlike sedimentation velocity, sedimentation equilibrium depends only on the molecular weight of the macromolecules as frictional/conformational effects do not implicate the analysis (see for example, (Van Holde and Baldwin, 1958)).

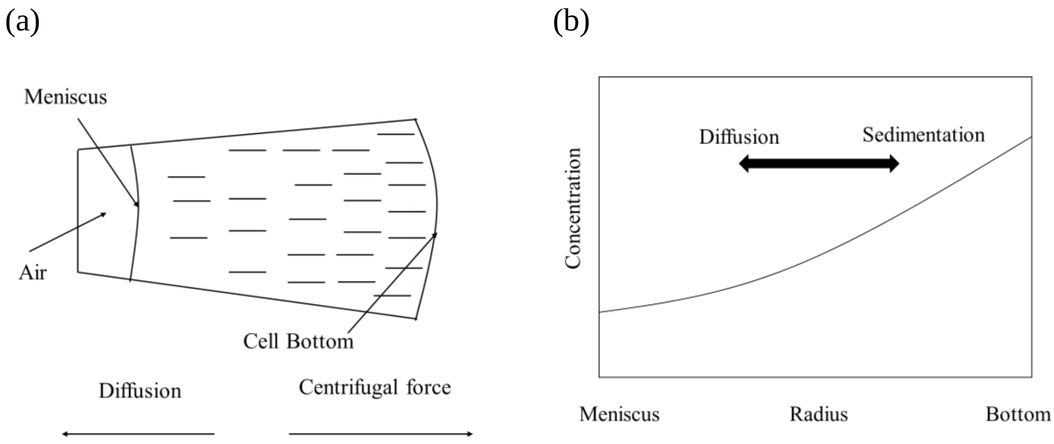

Figure 3.4 Sedimentation equilibrium: (a) The top view of sample sector of the centrifuge cell of sedimentation equilibrium analysis; (b) The schematic figure of concentration vs radius in the cell

The column length of the cell used in sedimentation equilibrium is shorter than for sedimentation velocity, to reduce the time needed to reach the equilibrium, which depends on the square of the column length of the cell. At the same time, care has to be taken to avoid making columns too short as it may lead to loss of accuracy (Laue and Stafford, 1999). However, in this work, the cells used in sedimentation equilibrium analysis are longer than the cells used in sedimentation velocity analysis as scleroglucan has comparatively high molecular weight. The resolution of the sedimentation curve can be more accurate when carried out the sedimentation equilibrium analysis in longer cells.

The concentration of the solute increases exponentially from the meniscus towards the bottom of the cell (see (Cole et al., 2008)) (Figure 3.4.b). Eq. 3.17 describes the concentration distribution of monodisperse solute in an ideal condition (Van Holde, 1985).

$$c(r) = c_0 \exp\left(\frac{M_{w,\,app}(1-\bar{v}\rho_0)\omega^2(r^2 - r_0^2)}{2RT} \right) \tag{3.17}$$

c(r) is the concentration of the macromolecule at the radius of r, c_0 is the concentration at the meniscus. R is the gas constant and T is temperature. $M_{w,app}$ is the molecular weight at the radius of r.

For the sedimentation equilibrium analysis, the thermodynamic non-ideality should be taken into consideration, which can make the characteristic process time shorter than the ideal case (Laue and Stafford, 1999). Therefore, with the target of determining molecular weight, the MSTAR algorithm was developed by Creeth and Harding (Creeth and Harding, 1982b). It is particularly suitable for heterogeneous systems, as it avoids problems of concentration extrapolations to the cell base. This algorithm is implemented in the SEDFIT-MSTAR software package (Schuck et al., 2014). The $M^*(r)$ function of MSTAR is given below (Eq. 3.18).

$$M^{*}(r)=\frac{(c(r)-c(a))}{kc(a)(r^{2}-a^{2})+2k\int_{a}^{r}r\left[c(r)-c(a)dr\right]} \quad (3.18)$$

c(a) is the concentration at the meniscus and *k* can be calculated by the following equation 3.19:

$$k=\frac{(1-\bar{v}\rho)\omega^{2}}{2RT} \quad (3.19)$$

The (apparent) weight average molecular weight $M_{w,app}$ over the whole distribution can be obtained from the identity below (Creeth and Harding, 1982b):

$M_{w,app} = M^*$ $\quad (r = b)$

i.e. by extrapolating *M*(r)* to the cell base r = b.

The point (apparent) weight average molecular weights $M_{w,app}(r)$ were also estimated from local slopes of the ln$c(r)$ vs r^2 plots. This provides another estimate of the molecular weight over the whole distribution $M_{w,app}$, since at the "hinge point" the concentration at the radial position $r = hinge$ in the ultracentrifuge cell, $c(r{=}hinge)$, is the same as the initial loading concentration, c, then $M_{w,app}$ (r = hinge) = $M_{w,app}$. For a non-associating macromolecule, $M_{w,app}$ can be corrected to the ideal molecular weight M_w by extrapolating the apparent molecular weight measured at a series of concentrations to c = 0 (Tanford, 1961):

$$M_w = M_{w,\,app}\cdot(1+2BM_wc) \quad (3.20)$$

This relation is valid in dilute solutions, where B is the second thermodynamic virial coefficient which has the unit of ml·mol/g^2.

3.2 Flow behaviour

Rheology is the science of the studies on materials' deformation and flow behaviours (see for examples, (Lapasin and Pricl, 1995, Mezger, 2014)). It is also the study of the structural changes in microscopic levels of materials. Rheology is widely used in food industry, as it can characterise solid, semi-solid and liquid food products. Moreover, with the development of the food industry, oral rheology receiving increasing attentions. During the first stage of digestion, food experiences mastication and interacts with stimulated saliva in the oral cavity (Stokes, 2012b, Stokes, 2012a). Therefore, it is more important to understand the rheological behaviour of biopolymer solutions and the mixtures of biopolymer solutions and saliva.

3.2.1 Viscosity

The two-plate-model (Figure 3.5) is usually used to demonstrate the principle of shear rheology. The plates are parallel, and the bottom plate is at a fixed position. It is assumed that the fluid between two plates adhere to both plate, which means it does not show wall slip (Mezger, 2014). Shear stress (τ) is the shear force F applied on the upper plate per unit area. The shear rate ($\dot{\gamma}$) is the velocity (v) of the upper plate (highest velocity in this model) divided by the distance between the plates (h). The molecules in solution have relative motions between each other. Thus, the flow liquid can experience internal friction force, and this flow resistance can be interpreted in the term of viscosity (η) (Malkin and Isayev, 2012a, Mezger, 2014). Eq. 3.21 shows the relation of the shear stress, shear rate and shear viscosity.

$$\tau = \dot{\gamma} \cdot \eta \tag{3.21}$$

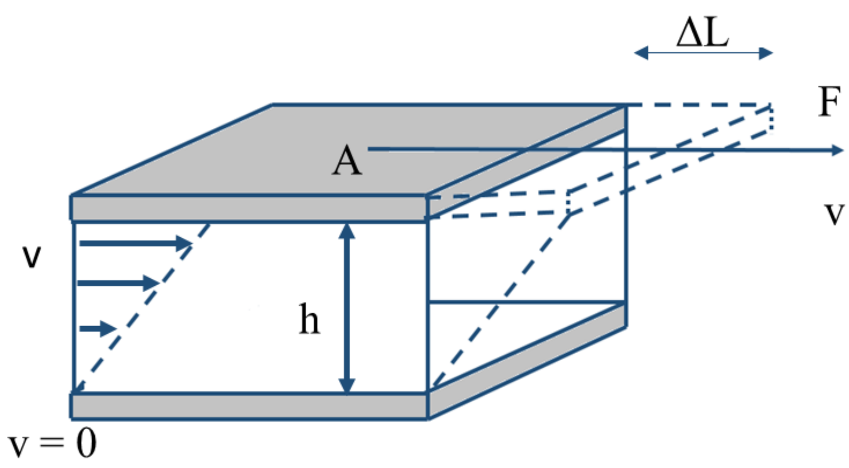

Figure 3.5 Two-plate-model to induce shear flows: A indicates the area of the plate (m²), v indicates the velocity of the upper plate (m/s), *h* indicates the gap between the two plates (m), *F* indicates the force that applied (N) and ΔL indicates the distance that the upper plate moved

For the Newtonian fluid at a fixed temperature, the viscosity is constant, and the shear stress and shear rate have a linear relationship (Mezger, 2014, Malkin and Isayev, 2012a). For the non-Newtonian fluid, the viscosity is shear rate dependent. Most of the food systems have non-Newtonian flow behaviour, and most of non-Newtonian fluids have shear thinning rheological behaviour (apparent viscosity decreases with the increase of shear rate) (Shewan and Stokes, 2020, Stokes, 2012a). On the contrary, the viscosity of shear thickening fluid increases with the shear rate. One food product example of shear thickening fluid is 50% potato starch slurry (Lapasin and Pricl, 1995). At the molecular level, the viscosity can be explained by the frictional force between molecules. For the Newtonian liquid, the collision among molecules can happen in an extreme short time. Therefore, the force is linear with the rate under different shear rate, which explains the viscosity of Newtonian fluid is not dependent on the shear rate (Doolittle, 1952). Viscosity can also play an important role in the liquid food lubrication properties, which can help to build the of safe-to-eat oral rheology (Stokes, 2012a).

The experimental data of viscosity can be fitted in different rheological models depending on the flow behaviour of samples. Several models that are commonly used in food industry are explained in the following section.

3.2.1.1 Ostwald de Waele (Power law)

The Eq. 3.22 explains the relationship of the power law model. C_p is the power law model exponent. When the sample fluid is shear thinning, the power law index $n < 1$. On the contrary, $n > 1$ when the fluid is shear thickening. A sample has Newtonian behaviour when n = 1.

$$\tau = C_p \dot{\gamma}^n \tag{3.22}$$

Viscosity data in the low shear and high shear range cannot be accurately modelled by the power law model for polymer solutions (see e.g., (Lapasin and Pricl, 1995, Mezger, 2014)). Therefore, this model is suggested to be applied in modelling the viscosity in medium range shear rate in industry.

3.2.1.2 Cross model

In order to extend the modelled shear rate range, more parameters have to be included in the equation. The Cross model uses four parameters and can be used to model zero shear viscosity η_0 and infinite shear viscosity η_∞. n is the power law index and corresponds to the power law model (Lapasin and Pricl, 1995). C_C is the Cross model exponent. For concentrated polymer solutions, the η_∞ can be neglected since the value could be dramatically low compared to η_0 (Mezger, 2014).

$$\eta = \eta_\infty + \frac{\eta_0 - \eta_\infty}{1 + (C_c \cdot \dot{\gamma})^{1-n}} \tag{3.23}$$

3.2.1.3 Carreau-Yasuda model

The Carreau model and the Cross model are comparable, but the Carreau model can be further modified in several ways, for example the Carreau-Gahleitner model. The Carreau-Yasuda model is suggested to be more accurate than the Cross model, and it can also model the relaxation time, λ. n_1 is the Yasuda exponent (Mezger, 2014).

$$\eta = \eta_\infty + \frac{(\eta_0 - \eta_\infty)}{\left[1 + (\lambda \cdot \dot{\gamma})^{n_1}\right]^{(1-n)/n_1}} \tag{3.24}$$

3.2.2 Viscoelasticity

Non-Newtonian fluids can be divided into two categories: non-Newtonian purely viscous fluid and viscoelastic fluid (Malkin and Isayev, 2012a). When the external stress is applied on the non-Newtonian purely viscous fluid, the deformation gradually disappears (Malkin and Isayev, 2012a). On the other hand, the viscoelastic fluid has delayed response to the external stress or strain, as part of the deformation is stored as elastic energy in the fluid, and the deformation is released as elastic deformation (Malkin and Isayev, 2012a, Mezger, 2014), and the deformation of viscoelastic fluid is not reversible (Mezger, 2014). The viscoelastic properties of polysaccharide solutions in this research were characterized by using oscillatory tests, normal stress tests and extensional rheological tests (Mezger, 2014, Stokes, 2012a).

3.2.2.1 Oscillatory test

Oscillatory tests mainly focuses on characterising the dynamic structure changes rather than the liquid flow behaviour (Mezger, 2014). For the steady shear rheological tests and normal stress analysis, measurements are taken of large shear deformation within a big shear rate range. However, for the oscillatory test, the amplitude is small.

The two-plates-model can be used to explain the principle of the oscillatory test, which is shown in Figure 3.6. It is assumed that the fluid between two plates adhere to either plate, i.e., does not show wall slip. The samples also do not have plastic behaviour, which means it deforms homogenously (Mezger, 2014).

(a) **(b)**

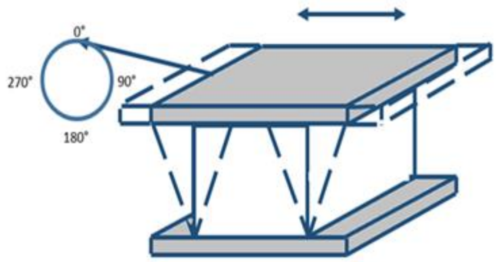

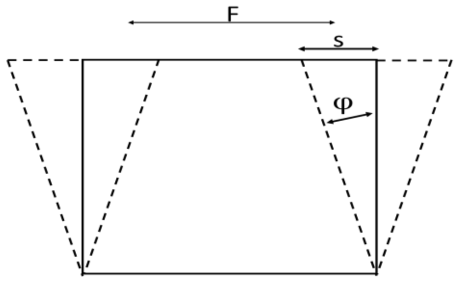

Figure 3.6 Two-plates-model of the oscillatory test (a) schematic figure; (b) sectional view

The bottom plate of the model is fixed. The top plate is controlled by the wheel. When the wheel is rotating, the upper plate is moved back and forth with the constant force F (Figure 3.6b). From this movement, the deflection path s and the deflection angle ϕ can be obtained and studied. Eq. 3.25 explains the relationship of the shear strain and the deflection angle.

$$\pm\gamma = \frac{\pm s}{h} = \tan\varphi \tag{3.25}$$

When the angle is at 0° and 180°, the upper plate is at zero position. The velocity is at the maximum value, and *s* (deflection path) and ϕ (deflection angle) are zero. Thus, Υ (shear strain) and τ (shear stress) equal to zero. When the upper plate is at 90° and 270° angle position, the velocity equals to zero, and *s* and ϕ are at the maximum value. Therefore, $\Upsilon = \pm \Upsilon_{max}$ and $\tau = \pm \tau_{max}$, respectively. The relation between time *t* and the shear strain can be explained in Eq. 3.26. γ_0 is the amplitude and ω is the angular frequency of the oscillation.

$$\gamma(t) = \gamma_0 \cdot \sin \omega t \tag{3.26}$$

For the viscoelastic material, the viscous phase may respond slower. There can be a loss angle δ between the stress and external strain. δ is 0° when the material has full elastic behaviour. On the other hand, when the sample is viscous material, δ equals to 90°.

$$\tau(t) = \tau_0 \cdot \sin(\omega t + \delta) \tag{3.27}$$

The stress can be divided into two components: the storage modulus (*G'*) and the loss modulus (*G"*). *G'* indicates the elastic behaviour of the material and *G"* indicates the viscous behaviour of the material (Mezger, 2014). The storage and loss moduli are not dependent on the strain amplitude. The damping factor tanδ can be used to define the viscoelasticity of the material (Eq. 3.28). When the material has elastic dominant behaviour, the value of tanδ is lower than 1.

$$\tan\delta = \frac{G''}{G'} \tag{3.28}$$

The vector sum of *G'* and *G''* is complex modulus *G** (Eq. 3.29). *G** is the product of the complex viscosity η* and the angular frequency ω.

$$|G^*| = \sqrt{(G')^2 + (G'')^2} = \eta^* \cdot \omega \tag{3.29}$$

In this research, the strain sweep test and frequency sweep test were carried out to analyse the biopolymer solutions and their mixture with human whole saliva or reconstituted saliva.

Amplitude sweep test

For the amplitude sweep test, the frequency is kept as constant, and the strain is controlled. During the low strain range, *G'* and *G''* can be constant (the values are different mostly), and this range is known as the linear viscoelastic range (LVE range). When *G'* is higher than *G*" within the LVE range, the material has a gel-like structure. With the increase of the shear strain, many materials will have very low viscosity and have liquid behaviour. Therefore, *G'* will decrease and *G''* will increase. These materials can only be stated to have gel-like structure under low shear strain range (Mezger, 2014). When *G'* and *G*" are equal in the LVE range, it is often stated that the material is at the transition line of the gel and the liquid behaviour of the material.

When the loss modulus is higher than the storage modulus during the LVE range, the material has a liquid-like structure (Mezger, 2014).

Frequency sweep test

The strain is at constant value for frequency sweep test. The fixed strain value should be determined from the LVE range (Hyun et al., 2002). Therefore, the amplitude sweep test should always be done before the frequency sweep test (Mezger, 2014). For the stable gel or solid, *G'* is larger than *G*" in the whole frequency range. Further, *G'* and *G*" tend to level off with a small angle. Further, the complex viscosity η* may not be useful to interpret the result as the sample is not flowable. When *G*" is larger than *G'*, the sample is suggested to be viscoelastic liquid at rest state.

3.2.2.2 Normal stress differences

When viscoelastic materials deform, they deform in three dimensions, which can be explained clearly in Cauchy system (Mezger, 2014) (Figure 3.7). For the linear viscoelastic tests, the deformation is comparatively small, and the properties of materials may not change under linear viscoelastic test (Lapasin and Pricl, 1995). By contrast, for the non-linear viscoelastic analysis, the relationship of the input and the output are not proportional (Malkin and Isayev, 2012b). The deformation of non-linear viscoelastic tests can be comparatively large, which may change the properties of the material.

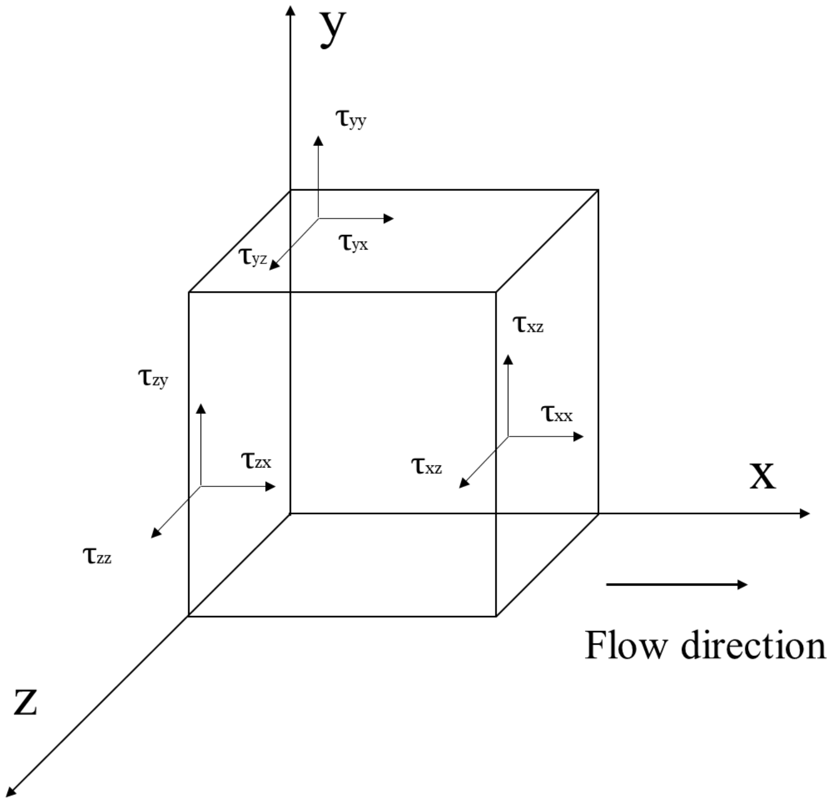

Figure 3.7 Cauchy system of the stress tensor

With the target of understanding the nonlinear viscoelasticity of biopolymer solutions, the normal stress differences can be measured. There are two rheological normal stress differences, which are the first normal differences (N_1) and the second normal stress differences (N_2) (Eq. 3.30 and Eq. 3.31). The first normal stress difference test was carried in this research. The normal stress differences are zero for Newtonian fluid (Dealy and Wang, 2013).

$$N_1 = \tau_{xx} - \tau_{yy} \tag{3.30}$$

$$N_2 = \tau_{yy} - \tau_{zz} \tag{3.31}$$

When the shear rate is comparatively low, the normal stress is usually smaller than the shear stress. The normal stress increases faster than shear stress with the increase of shear rate (Malkin and Isayev, 2012b). For the viscoelastic fluid, the normal stress is comparable with Newtonian fluid at low shear rate range (Dealy and Wang, 2013). It is also found that N_1 is proportional to the square of shear stress. N_2 is negative and N_1 is always significantly higher than the absolute value of N_2 (Dealy and Wang, 2013, Malkin and Isayev, 2012a).

When measuring N_1, the highest shear rate should increase to 10^5 s^{-1}, and this shear rate can be easily achieved by the parallel plate geometry under narrow gaps. On the contrary, other commonly used geometries like cone and plate can be difficult in reaching this shear rate (Kravchuk and Stokes, 2013). Further, when carrying out experiment under narrow gaps, there can be gap error. In this research, the gap error was corrected by using the protocol published by Davies and Stokes (2005, 2008). The final gap set in this research is 50 μm.

3.2.3 Measuring system

3.2.3.1 Cone and Plate

Figure 3.8 shows the schematic figure of cone and plate geometry. R is the radius and α is the angle between the cone and the bottom plate. The radius of the cone can vary from 10 mm to 100 mm. The cone with small radius may not have enough sensitivity to detect the low shear stress and torque value (Mezger, 2014). The ISO standard states the cone angle should be smaller than 4° (Mezger, 2014). CP 50-2 geometry was used in this research, which indicates the diameter of the geometry is 50 mm and the angle is 2°.

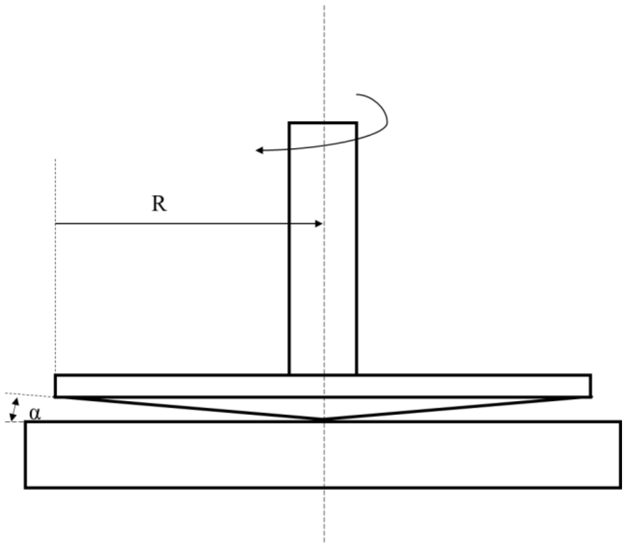

Figure 3.8 Schematic figure of cone and plate geometry (adjusted from Mezger (2014))

One advantage of cone and plate geometry is that the shear rate is constant between the upper geometry and the bottom plate (see e.g., (Mezger, 2014, Lapasin and Pricl, 1995, Shewan and Stokes, 2020)). The constant shear rate is important for non-Newtonian fluids as they are shear rate dependent (Shewan and Stokes, 2020). Further, the volume of sample required for cone and plate geometry is also comparatively less compared to some other geometries. However, the limitation of the particle size is the disadvantage of the cone and plate geometry as the gap may be blocked by these particles during the test (Mezger, 2014, Stokes, 2012a).

3.2.3.2 Parallel plate

Figure 3.9 shows the schematic figure of parallel plate geometry. *R* is the radius and *H* is the gap between the geometer and the bottom plate. The gap *H* can influence the result of the rheological test. When the gap is comparatively high, the result of the shear rheological test can be influenced more than the oscillation tests (in particular under LVE range). For example, the low viscosity fluid samples under parallel geometry may have turbulent flow in the gap under steady shear rheological test. Moreover, the viscoelastic material may also experience edge failure due to the elasticity of samples (Mezger, 2014). The diameter of the parallel plate ranges from 20 mm to 50 mm. The geometry used in this research is PP50 (50 mm diameter).

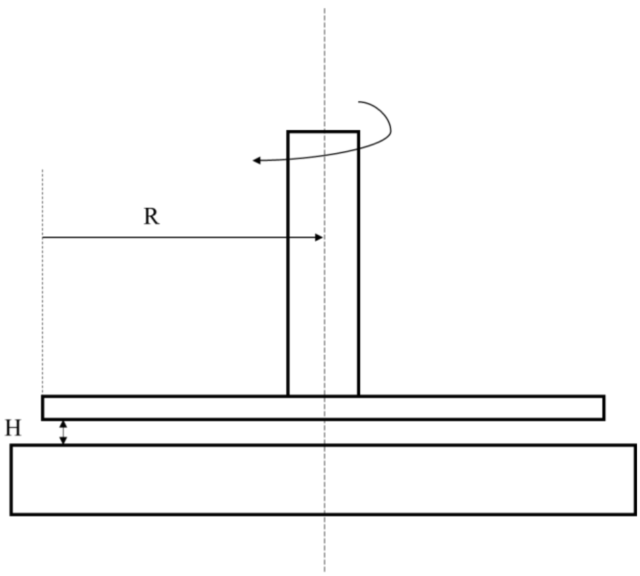

Figure 3.9 Schematic figure of parallel plate geometry (adjusted from Mezger

(2014))

The parallel geometry is capable of characterising the rheological behaviour of large size particles, i.e., larger than 5 μm (Mezger, 2014, Shewan and Stokes, 2020). Unlike cone and plate geometry, the shear rate in the gap is dependent on the position in the gap (Shewan and Stokes, 2020, Stokes, 2012a). The shear rate is zero at the centre of the plate and reaches the maximal value at the edge. The parallel plate geometry is also suitable for the narrow gap analysis with the sample volume less than 100 μL (Stokes, 2012a).

3.2.4 Extensional rheology

3.2.4.1 Extensional flow

Extensional flow is also known as elongation flow, stretching flow or shear-free flow. The extensional flow can be found in many circumstances, such as the break-up of droplets or spraying etc. (Barnes, 2000). The relationship of the extensional stress τ_E and extensional rate $\dot{\varepsilon}$ is shown below in Eq. 3.32:

$$\tau_E = \eta_E \cdot \dot{\varepsilon} \qquad (\eta_E \neq \eta) \tag{3.32}$$

The extensional flow can be described by using the Eq. 3.33. In this equation, $\dot{\varepsilon}(t)$ indicates the extensional rate and $\dot{\Upsilon}$ indicates the rate-of-deformation tensor. v_{xx}, v_{yy} and v_{zz} can describe the direction of the extensional flow (Lapasin and Pricl, 1995, Petrie, 2006). There are three types of extensional flow: simple elongational flow (also named as uniaxial extensional flow), biaxial extensional flow and planar elongational flow (also named as pure shear flow) (Lapasin and Pricl, 1995). When the extensional flow is uniaxial, v_{xx} = 2, v_{yy} = -1 and v_{zz} = -1. For the biaxial extensional flows, v_{xx} = 1, v_{yy} = 1 and v_{zz} = -2. For the planar flows, along the third axis, the material does not deform due to the constrain, so v_{xx} = 1, v_{yy} = 0 and v_{zz} = -1.

$$\dot{\gamma} = \begin{pmatrix} v_{xx} & 0 & 0 \\ 0 & v_{yy} & 0 \\ 0 & 0 & v_{zz} \end{pmatrix} \cdot \dot{\varepsilon}(t) \qquad (\dot{\varepsilon}(t) > 0) \tag{3.33}$$

Although most rheological studies investigated shear flow behaviours, the majority of real flows are present as extensional flows. In extensional flow, the extensional flow is much more sensitive to the molecular structure of the material than the shear flow (Lapasin and Pricl, 1995, Barnes, 2000). For polysaccharide solution, the elongation flow behaviour can be impacted by the molecular structure the molecular weight (Stelter et al., 2002). McKinley (2005) suggested that fluids with larger molecular weight can postpone the elasto-capillary breakup. The extensional viscosity of the fluid is usually higher than the shear viscosity. Trouton's law stated that when the fluid is Newtonian, the extensional viscosity is three times of the shear viscosity, see Eq. 3.34.

$$\eta_E = 3\eta_S \tag{3.34}$$

3.2.4.2 Filament break-up test

Four types of extensional rheometers are mainly used in current scientific research, i.e. Rheotens Fiber Spinning Rheometer, CaBER (Capillary Break-up Elongational Rheometer), SER (Sentmanat extensional rheometer) and FSR (Filament Stretching Extensional Rheometer) (te Nijenhuis et al., 2007, McKinley and Sridhar, 2002). Among these rheometers, Rheotens is mainly designed for polymer melts and fibre spinning while CaBER is designed for less concentrated fluids with lower viscosity (te Nijenhuis et al., 2007).

In this research, a capillary break-up extensional rheometer (CaBER-1, Thermofisher Haake, Kalsruhe, Germany) was used to quantify the extensional rheological behaviour of the rigid rod polysaccharide solution. Previous studies using CaBER mainly focus on the research of synthetic polymers (see for example, (Miller et al., 2009)). It is suggested that the Capillary break-up rheometer has the measuring viscosity range of 0.01 to 100 Pa·s (Anna and McKinley, 2001, Miller et al., 2009). Unlike SER, CaBER cannot be set with a filament break-up rate on sample, the filament break-up rate mainly depends on the type of the material.

Figure 3.10 shows the schematic diagram of the capillary break-up experiment. For the capillary break-up experiment, 790 μL of the sample is placed between the fixed plate and the moving plate (6 mm diameter). The initial gap was set at 3mm. Then the moving plate is lifted rapidly to a specified height at a constant extensional rate. After the fluid sample is stretched to the final gap, the laser measures the diameter changes the middle point of the fluid filament with time (te Nijenhuis et al., 2007, Miller et al., 2009). Finally, the capillary filament breaks, mainly due to the surface tension, elasticity and viscosity. The relationship of the time and the diameter changes can be plotted. The final gap of the fluid is suggested to follow this formula $3 \leq L_f / R_0 \leq 15$ (L_f indicates the length of the final gap and the R_0 indicates the radius of the plate) (Miller et al., 2009). The Haake CaBER handbook also recommends that the final gap of the fluid samples should normally be set within 10 to 20 mm (ThermoElectron, 2009).

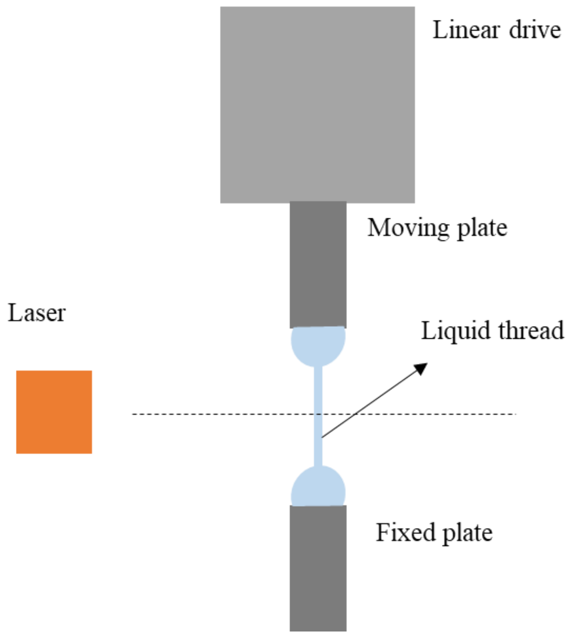

Fig 3.10 Schematic diagram of the capillary break-up extensional experiment

For the Newtonian fluid, the filament middle point diameter decreases linearly with the time. On the other hand, for most polysaccharide solutions, the mid-point diameter experiences an exponential decrease with time. The relationship between the mid-point diameter and time has two regions, which are the exponential and the linear region. The relaxation time (λ) and the apparent steady state extensional viscosity (η_E) can be calculated respectively by these two regions (Anna and McKinley, 2001, Kheirandish et al., 2008, McKinley, 2005, Stelter et al., 2000, Stelter et al., 2002). The relaxation time is the time that the disturbed system returns to equilibrium.

Eq. 3.35 indicates the relationship between the mid-point diameter and the time in the exponential region (Stelter et al., 2002). D_0 (mm) is the mid-point diameter when time is zero and λ (s) is the relaxation time.

$$D(t) = D_0 \exp(-\frac{t}{3\lambda}) \tag{3.35}$$

Eq. 3.36 shows the decay of filament in the linear region. The filament has Newtonian-like behaviour. The mid-point diameter is proportional to the surface tension in this region and is inversely proportional to the steady state extensional viscosity(Stelter et al., 2002). σ (mN/m) indicates the surface tension of fluid. In this thesis, the surface tension is assumed as the same as the water surface tension, which is 72 mN/m. η_E (Pa.s) indicates the steady state extensional viscosity.

$$\eta_E = -\frac{\sigma}{dD(t)/dt} \tag{3.36}$$

3.3 Tribology study

3.3.1 From rheology to tribology

Tribology studies the friction, lubrication and wear among the interacting surfaces in relative motion (Chen and Stokes, 2012, Sarkar and Krop, 2019, Stokes, 2012b, Stachowiak and Batchelor, 2013). The term tribology comes from the Greek word ‘tribos’ meaning “I rub” (Stachowiak and Batchelor, 2013). In recent years, tribology has been widely applied in food industry, especially in the area oral tribology, which is related to the tribological study of the surface interaction between the food bolus and oral surfaces with saliva coating (Sarkar and Krop, 2019). As mentioned in previous section, when processed food is in the oral cavity, the rheological behaviour analysis of food systems is more applicable in the first stage of oral processing. However, as mastication progresses, tribological analysis starts to play a more important role as food is processed into smaller particles in micrometre scale (Chen and Stokes, 2012, Stokes, 2012b, Stokes et al., 2013). Chen and Stokes (2012) reported that rheological tests also have the limitation of detecting texture properties for fluid or semi-fluid food. Further, rheological tests cannot determine sensory properties (such as astringency), while tribological tests can. For example, tribology can differentiate between low-fat and full-fat mayonnaise (Stokes, 2012b). It was found that astringency may be caused by the salivary film lubrication loss, and the interfacial rheological interactions loss (Rossetti et al., 2009).

3.3.2 Friction

The friction coefficient (μ) is the main parameter defining the tribological properties of products, which is dependent on the interactive surface properties (such as asperities, hydrophobicity or hydrophilicity), and the load (L) applied on the surfaces (Eq. 3.37). Eq. 3.37 is also known as the Amonton's law (Chen and Stokes, 2012, Yakubov, 2014). F_f is the friction force.

$$\mu = \frac{F_f}{L} \tag{3.37}$$

With the target of reducing the friction coefficient, one effective method can be separating surfaces (Yakubov, 2014). Many methods of separating surfaces were suggested in different studies, such as magnetic forces; however, when it comes to oral processing tribology studies, the current achievable method is to put a thin fluid between two surfaces (Yakubov, 2014). When a thin layer fluid is between two surfaces, the viscosity of the fluid and the load of the surface can both determine the friction coefficient (Yakubov, 2014, Chen and Stokes, 2012, Bongaerts et al., 2007a). Therefore, the principle of tribological study is to investigate the condition of the fluid film (film thickness etc.) between surfaces (Stokes, 2012b), which leads to the lubrication study in Chapter 3.3.3.

3.3.3 Lubrication

Stribeck curve is one of the most effective methods to determine the friction behaviour of thin fluid film under different entrainment speeds between surfaces (Stachowiak and Batchelor, 2013). The surfaces for the lubrication test should be non-parallel, otherwise the lubrication film cannot lift the upper surface under high velocity (Stokes et al., 2013, Stokes, 2012b). The film geometry is dependent on the load applied on the upper surface, the viscosity of the fluid and the surface properties (Stokes, 2012b). Figure 3.11 shows an example of typical Stribeck curve, which contains three regimes: boundary regime, mixed regime and elasto hydrodynamic regime (Yakubov, 2014, Stokes, 2012b, Chen and Stokes, 2012). The Stribeck curve is plotted on a logarithmic scale. The y axis is the friction coefficient (μ), which can be calculated by Eq. 3.37. The x axis is the Stribeck parameter, which can be calculated by Eq. 3.38 below (Stachowiak and Batchelor, 2013). U is the entrainment speed, which is the fluid velocity and η is the viscosity of the fluid. L is known as the load applied on the upper surface.

$$S = \frac{\eta \times U}{L} \tag{3.38}$$

The entrainment speed of elasto hydrodynamic lubrication regime (EHD) is the highest among three regimes. When the entrainment speed is high enough, a lift force can be created by the fluid between surfaces on the upper surface, which leads to the decrease of the friction impact. The lift force is determined by the surface properties, the viscosity and the velocity of the fluid (Yakubov, 2014). As the lift force is the highest among three regimes, the asperity contacts between surfaces are avoided, which lead to little or no surface wear in this regime (Chen and Stokes, 2012). The friction force will be minimized when the film is at the same thickness to cover the asperities (Yakubov, 2014). The condition of the fluid film between surfaces mainly depends on the relative motion speed and the angle between surfaces. The thickness of the film is dependent on the fluid bulk viscosity of fluid and the entrainment speed between surfaces (de Vicente et al., 2006b). However, with the increase of the entrainment speed, the drag force caused by the fluid increases faster than the lift force. Therefore, the friction coefficient increases again with the velocity (Yakubov, 2014, Stokes, 2012b). At the first stage of food ingestion, the salivary film is thicker (suggested to be larger than 1 μm), indicating food bolus may experience EHD regime at first (Yakubov, 2014).

For the boundary regime, the entrainment speed is the lowest among three regimes. The amount of fluid between surfaces can be too little to provide lift force on the upper surface. The gap between surfaces is the smallest among three regimes and it is therefore suggested that the asperities between surfaces dominates this regime, indicating sever wear in boundary regime. Further, the frictional force is independent on the entrainment speed in this regime. However, the properties of fluid in the molecular level may also have impact on the friction coefficient in the boundary regime (Yakubov, 2014, de Vicente et al., 2006b, Stokes et al., 2013).

In the mixed regime, there is a thin layer of fluid between surfaces, but the lift force is not high enough to lift the upper surface due to high load or lack of speed (Yakubov, 2014). Unlike the elasto hydrodynamic regime, the asperities start to influence the lubrication behaviour in this regime. The value of frictional force between surfaces is between the frictional force in the elasto hydrodynamic regime and the frictional force in the boundary regime. The friction force in this regime is impacted by both fluid film properties and the surface asperities (de Vicente et al., 2006b). The wetting behaviour of the lubricant is fairly important in this regime as it can prevent fluid being squeezed out from surfaces (Yakubov, 2014).

During oral processing, the dominant lubrication regime is dependent on the properties of food (Chen and Stokes, 2012). For thicker fluids, the elasto hydrodynamic regime and the mixed regime tend to be the dominant regime during ingestion (Chen and Stokes, 2012, Malone et al., 2003). Some food can experience all regimes during oral processing. For example, when beverages are ingested, the thickness of the fluid is comparatively high, the bulk rheological properties (elasto hydrodynamic regime) govern the initial oral processing (Yakubov, 2014, Chen and Stokes, 2012). Over time after consumption, the thickness of the fluid is reduced. Therefore, the mixed lubrication regime governs this part of ingestion. When the fluid is consumed, the fluid left on the tongue and palate goes through boundary lubrication regime (de Vicente et al., 2006b, Chen and Stokes, 2012). Therefore, food may experience the Stribeck curve from right to left during digestion (Figure 3.11).

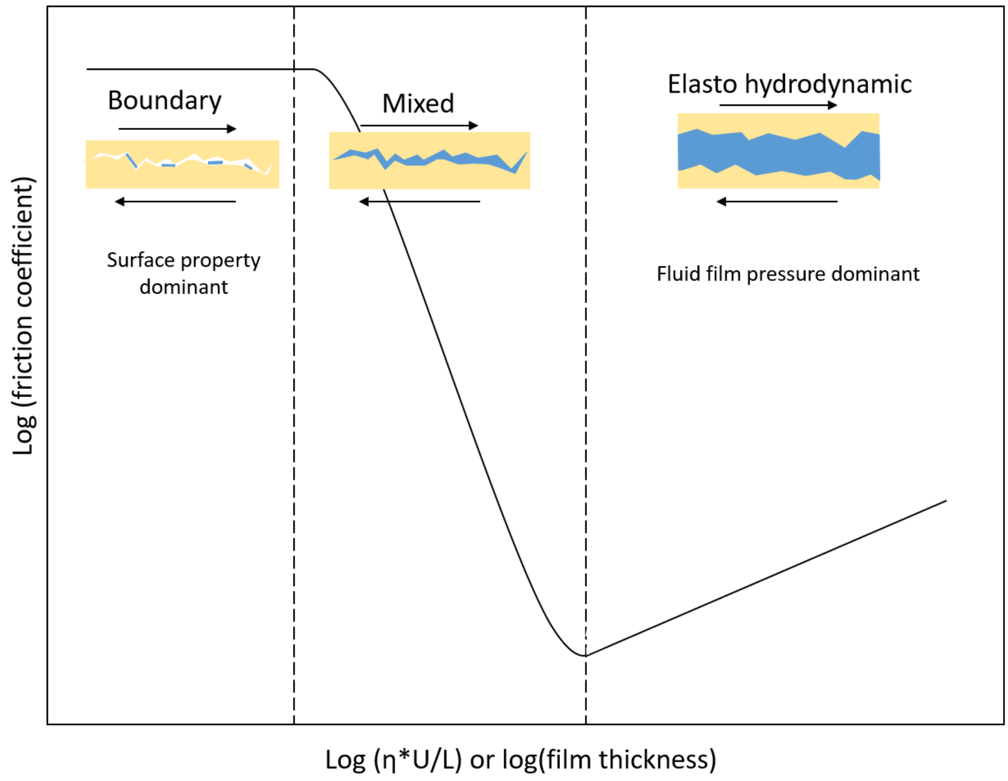

Figure 3.11. Stribeck curve with the y axis of friction coefficient and x axis of film thickness or η×U/L (*η* is the viscosity of the fluid, *U* is the entrainment speed and *L* is the load applied on the surface) (Yakubov, 2014, de Vicente et al., 2006a, Stachowiak and Batchelor, 2013)

3.3.4 Soft contract tribology

With the target of mimicking oral processing, many variables should be taken into consideration, for example, the roughness or the biochemical condition. As most surfaces in oral cavity are soft, the soft surfaces tribology should be focused when comes to oral tribological study. PDMS surfaces are widely used in mimicking oral cavity tribological study. There are different types of tribometers applied in oral tribological research, and among them all the mini traction machine has been well understood by researchers. MTM-2 mini traction machine was used to perform friction measurements (MTM-2, PCS Instruments Ltd., UK). Figure 3.12 shows the schematic figure of the equipment. The rubbing contact surfaces are PDMS (SYLGARD® 184 Silicon Elastomer Kit, Dow Corning, MI) ball with the radius of 0.95 cm and PDMS disk with the radius of 23 mm and the thickness of 4mm. Both PDMS surfaces are smooth and hydrophobic. The Young's modulus is 2.4 MPa (Bongaerts et al., 2007a). The normal force was applied on the ball during tribological tests. The friction force can be measured between the rotating disk and the rotating ball. The ball and the disk were under different speed and were driven by different motor systems. The slide-to-roll ratio (SRR) can be calculated by Eq. 3.39. v_{ball} is the velocity of the PDMS ball and v_{disk} is the velocoty of the surface in contact with the ball (Bongaerts et al., 2007b). The SRR ratio maintained constant during the test and the SRR is set at 50% in this research.

$$SRR = \frac{|v_{ball} - v_{disk}|}{U} \tag{3.39}$$

U (entrainment speed) can be calculated by Eq. 3.40.

$$U = \frac{(v_{ball} + v_{disk})}{2} \tag{3.40}$$

Two measurements were taken for every entrainment speed (v_{ball} > v_{disk}) and (v_{ball} < v_{disk}), and the average of these two measurement can eliminate the errors from the rolling friction (Bongaerts et al., 2007b, Yakubov et al., 2009).

The friction coefficient can be calculated by the Amonton's law (Eq. 3.37). The friction coefficient was measured five times in each entrainment speed. The test started from high entrainment speed (1000 mm/s) to low speed (1 mm/s) and the speed increased back to 1000 mm/s again.

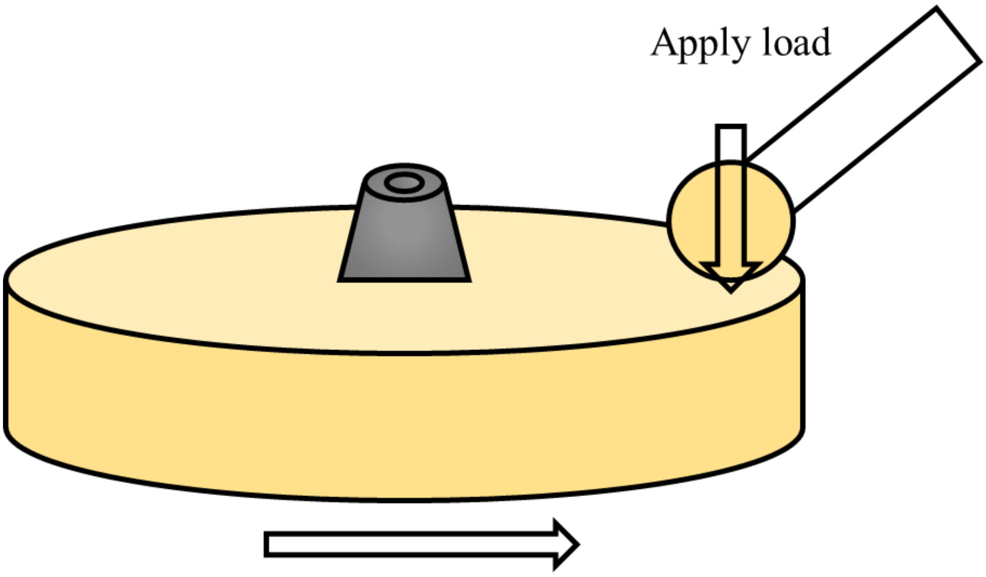

Figure 3.12. The schematic figure of the mini traction machine (MTM-2) set-up containing rotational ball and disc. All frictional measurement was carried out in this set-up.

Chapter 4 Characterisation of the molecular properties of scleroglucan as an alternative rigid rod molecule to xanthan gum for oropharyngeal dysphagia

Abstract

Scleroglucan (SG), a neutral (1-3) glucan with (1-6) glucan branches every third residue, is being considered as an alternative rod-like, shear thinning high molecular weight glucan based polysaccharide to xanthan gum for the management of patients with oropharyngeal dysphagia. It is therefore important to understand more fully its hydrodynamic properties in solution, in particular heterogeneity, molecular weight distribution and its behaviour in the presence of mucin glycoproteins. A commercially purified SG preparation produced by fermentation of the filamentous fungus *Sclerotium rolfsii* was analysed in deionised distilled water with 0.02% added sodium azide. Sedimentation velocity in the analytical ultracentrifuge showed the SG preparation to be unimodal at concentrations > 0.75 mg/ml which resolved into two components at lower concentration and with partial reversibility between the components. Sedimentation coefficient versus concentration plots showed significant hydrodynamic non-ideality. Self-association behaviour was confirmed by sedimentation equilibrium experiments with molecular weights between ~3 × 10^6 g/mol to ~5 × 10^6 g/mol after correcting for thermodynamic non-ideality. SEC-MALS-

viscosity experiments showed a transition between a rod-shape at lower molar masses to a more flexible structure at higher masses consistent with previous observations. Sedimentation velocity experiments also showed no evidence for potentially problematic interactions with submaxillary mucin.

4.1 Introduction

Oropharyngeal dysphagia is known as swallowing disorder in the upper aero digestive tract (Martino et al., 2000). The first polysaccharide to be considered for the management of dysphagia was starch but the pasty turbid products arising from poor solubility proved unpopular with patients. Xanthan gum (XG) – which gives clearer solutions – is now being considered and there has been no evidence of any residue left in the oral cavity after the use of xanthan gum based thickeners on dysphagia patients (Rofes et al., 2014).

XG is a large molecular weight (~ 3×10^6 g/mol) microbial/fungal polysaccharide which gives high viscosities and provides strong thickening to liquid based foods. The primary structure of xanthan gum consists of the cellulose-like backbone of (1,4)-linked β-D-*Glc*p residues substituted at O-3 of alternate glucose residues, with a trisaccharide side chain. The trisaccharide side chain consists of a β-D-*Man*p-(1,4)-β-D-*Glc*pA-(1,2)-α-D-*Man*p-(1→) unit. Non-carbohydrate substituents include an acetyl group at O-6 of the inner *Man*p residue and a pyruvate group at O-4,6 of the terminal *Man*p. The pyruvic acid content of XG can vary according to the producing bacterial strain. It is a dimeric helical polysaccharide (which adopts an extended conformation in solution (Berth et al., 1996) with a large persistence length (a measure of chain rigidity/flexibility of polysaccharides). The extended rod-like characteristics renders it susceptible to shear thinning in solution, a property which is desirable for managing dysphagia. SG, another microbial/fungal large molecular weight β-glucan based polysaccharide produced from the filamentous fungus *Sclerotium rolfsii*. It is being considered as an alternative rod-like, shear thinning high molecular weight β-glucan based polysaccharide. The possible uses of SG across a wide range of sectors has already been well described (see, for example, Morris and Harding (2009); Harding et al. (2017)). It has been considered for example for use in cosmetics (as part of skin and hair products), for application in pesticides (to assist binding to foliage), and, along with XG and other polysaccharides, as a water immobiliser and hydrogel (Survase, 2007) in drug delivery. A further aspect of water immobilization ability has been taken advantage of for binding water and providing high heat stability in oil well drilling fluids. In common with schizophyllan – another β(1→3)-linked glucan with β(1→6)-linked branches – an earlier study has suggested it may stimulate an immune response against tumour cells (Kurachi et al., 1990).

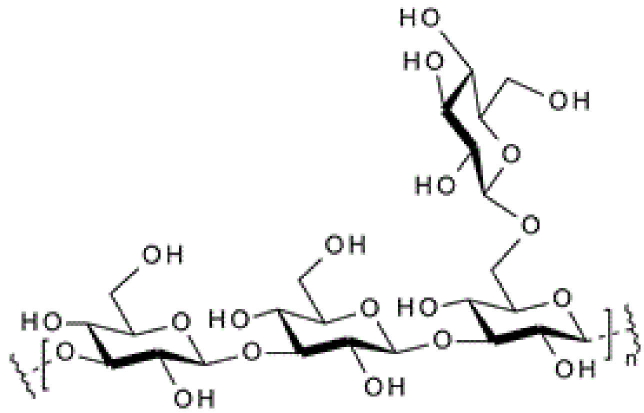

Figure 4.1 Primary structure of SG (Courtesy of Dr. C. Lawson, Carbosynth, Compton UK)

Key to these possibilities has been the size, conformation, and conformational rigidity of the SG molecule which has made it distinct from more flexible classes of polysaccharide. SG (Figure 4.1) is a beta-glucan whose primary structure is a backbone of repeating β(1→3)-linked glucose residues:

…→3) β-D-Glc*p*-(1→…

and approximately every third residue has a β(1→6)-linked D-glucose branch (Fariña et al., 1998, Rinaudo and Vincendon, 1982). Previous studies largely based on light scattering (Lecacheux et al., 1986, Yanaki et al., 1981, Yanaki and Norisuye, 1983) have suggested SG preparations have average molecular weights up to 6×10^6 g/mol, with considerable polydispersity. X-ray fibre diffraction studies have suggested that in an ordered form they exist as hydrogen-bond stabilized triple helices (Gawronski et al., 1999) with the β(1→6)-linked D-glucose branches protruding from the triple helical axis of the molecule. The existence of a trimeric structure has been supported by light scattering studies, by comparison of the molecular weights in non-dissociative and dissociative solvents for two different preparations – one sonicated, one not – of different molecular weight (Yanaki et al., 1981, Yanaki and Norisuye, 1983).

A consequence of the oligomeric helical structure is, in common with schizophyllan, an extended conformation in solution with a large persistence length (average projection from one end of the molecule to the original direction of the other end, in the limit the chain length $\rightarrow \infty$) namely ~ 200 nm (Biver et al., 1986). A consequence of the extended characteristics of the SG molecule is the shear thinning property of more concentrated solutions similar to XG which has also an extended conformation with high persistence lengths (Berth et al., 1996). However earlier papers have reported further associative effects beyond the "trimer" (Lecacheux et al., 1986, Yanaki and Norisuye, 1983).

It is therefore important to understand more fully its hydrodynamic properties in solution, in particular heterogeneity, molecular weight distribution and particularly its behaviour in the presence of mucin glycoproteins to check for the possibility of potentially problematic aggregation interactions, which can cause problems for dysphagia patients. We do this by taking advantage of recent advances in both sedimentation velocity and sedimentation equilibrium in the analytical ultracentrifuge

(AUC), together with advances in size-exclusion chromatography coupled to multi-angle light scattering and differential pressure viscometry (SEC-MALS).

4.2 Materials and methods

4.2.1 Materials

SG extracted from *Sclerotium rolfsii* was supplied from Carbosynth Ltd. (Compton, UK). It was suspended in triply distilled deionised water, and further purified by centrifugation and dialysis. The 0.2% (w/v) solution was centrifuged at 4850 g and 20.0 °C for 30 min to remove any supramolecular species. The supernatant was then dialyzed in water to remove any low molecular weight (<14 kDa maximum) impurities. Then the dialyzed supernatant was freeze dried in an Edwards Moduylo (York, UK) freeze drier. An appropriate amount of the freeze-dried SG sample was resuspended in a 0.02% sodium azide solution to prepare a 1% SG stock solution. Suspension in additional low molecular weight electrolyte to suppress any polyelectrolyte behaviour (as needed for example for the polyanionic XG) was unnecessary, as, unlike XG, SG is a neutral, uncharged polysaccharide. To prepare more diluted SG solutions (0.2% and 0.5%), the stock solution was diluted with the appropriate amount of aqueous solution of 0.02% (w/v) sodium azide and mixed on a magnetic stirrer at 20.0 °C for > 2 h.

For the interaction studies, human maxillary mucin was not available so bovine submaxillary mucin (Dinu et al., 2019) was used instead. For these experiments suspension in phosphate buffered saline, mimicking the inorganic conditions in the mouth, with a pH 6.8, ionic strength I=0.056 mol/L (and suppressing polyelectrolyte behaviour in the polyanionic mucin) was used (Sarkar et al., 2009).

4.2.2 Sedimentation velocity in the analytical ultracentrifuge

Sedimentation coefficient distributions were evaluated using the Beckman Optima XL-I analytical ultracentrifuge (Beckman Instruments, Palo Alto, USA). A volume of 400 µl of SG solution and matching amounts of solvent (water) were injected into appropriate channels of 12 mm double sector aluminium epoxy cells with sapphire windows. A range of concentrations from 0.075 to 2.0 mg/ml were studied. Solutions were centrifuged at 30000 to 45000 rpm at a temperature of (20.0 ± 0.1) °C. The data was analysed by using the least squares g(*s*) model in SEDFIT (Dam and Schuck, 2004). The weight average sedimentation coefficient '*s*' (in Svedbergs, S, with 1 S = 10^{-13} sec) for a particular component was then corrected to standard solvent conditions (the density and viscosity of water at a temperature of 20.0 ^{o}C), $s_{20,w}$ (Van Holde, 1971). A polyglucose partial specific volume $\bar{v}$ of 0.61 ml/g was used (Determann, 2012).

4.2.3 Sedimentation equilibrium in the analytical ultracentrifuge

Sedimentation equilibrium experiments were also performed on the Optima XL-I. 20 mm long optical path length double-sector cells (Nanolytics, Potsdam, Germany) with sapphire windows were loaded with 80 µl of dialysed sample and a matching amount of reference buffer dialysate in appropriate channels. The balanced cells were then loaded into an analytical 8-hole titanium rotor An50-Ti and placed in the AUC. After time was allowed for vacuum formation and for temperature equilibration (20.0 °C), the rotor was accelerated to 3000 rpm. Using the Rayleigh interference optical system, scans were taken every one hour and equilibrium was reached after approximately 72 h. Records of the relative concentration distribution of the solute at equilibrium was analysed to give the (whole distribution) apparent weight average molecular weight $M_{w,app}$ using the SEDFIT-MSTAR algorithm (Schuck et al., 2014). It uses the M^* function of Creeth and Harding (1982b) particularly suited for the analysis of difficult heterogeneous systems, and a 2nd method known as the hinge point used as an internal check on the result. Point (apparent) weight average molecular weights $M_{w,app}(r)$ were also estimated from local slopes of the ln$c(r)$ vs r^2 plots. SG solutions are known to be thermodynamically non-ideal, even in dilute solution (Lecacheux et al., 1986, Harding, 1992), and correction from apparent molecular weights to 'ideal' molecular weights M_w was made using the relation (Tanford, 1961) assumed valid in dilute solution (<0.5 mg/ml)

$$M_w = M_{w,\,app} \cdot (1 + 2BM_w c) \tag{4.1}$$

4.2.4 Capillary viscometry

Intrinsic viscosities were measured using a standard Schott-Geräte Ostwald 2 ml capillary viscometer, with automatic timing and water bath equilibrated to (20.00 ± 0.01) ^{o}C. A series of concentrations of SG solutions were injected to the reservoir of the capillary tube. Then the solutions were pumped to the upper line of the capillary. The time was measured when solution fell from the upper line to the bottom line of the capillary.

Relative specific viscosities η_r (the ratio of the solution viscosity to the solvent viscosity) were measured from the ratio of flow times of solution and solvent (because of high dilutions, c < 0.1mg/ml, no density correction was necessary (see, e.g., Harding (1997)) and reduced viscosities η_{red} obtained from

$$\eta_{red} = \frac{\eta_r - 1}{c} \tag{4.2}$$

The intrinsic viscosity [η] – the limiting value of the reduced viscosity at *c* = 0 was then estimated using three different extrapolation methods. Firstly the standard Huggins (1942) extrapolation:

$$\eta_{red} = [\eta] \cdot (1 + K_H[\eta]c) \tag{4.3}$$

K_H is the Huggins constant. Secondly the Kraemer (1938) extrapolation of the inherent viscosity

$\eta_{inh} = \ln \eta_r / c$:

$$\eta_{inh} = [\eta] \cdot (1 - K_K[\eta]c) \tag{4.4}$$

where K_K is the Kraemer constant, and finally the intrinsic viscosity was estimated at each concentration using the Solomon-Ciuta equation (Solomon and Ciută, 1962).

$$[\eta]_{SC} \sim (1/c) \cdot [2(\eta_{sp} - \ln(\eta_r))]^{1/2} \tag{4.5}$$

4.2.5 Size exclusion chromatography coupled to multi-angle light scattering (SEC-MALS) and differential pressure viscometer

A Schimadzu LC-20 HPLC system (Shimadzu Europe, Duisburg, Germany) comprising a DGU-20A degassing unit, LC-20AD solvent delivery system and SIL-20AHT autosampler, delivered 0.1 M sodium nitrate/0.02% azide at 0.5 mL/min to a Tosoh PWXL guard column. The guard column was serially connected to two Tosoh TSK-gel size-exclusion columns (G6000 PWXL followed by G5000 PWXL). Light scattering intensity was detected using a DAWN® HELEOS™ +8 eight angle light scattering photometer connected in series to an ViscoStar® II on-line differential pressure viscometer, Optilab® T-REX refractive index detector (Wyatt Technology Corporation, California, U.S.A.). The stock solution of 5.0 mg/ml was filtered through a 0.45 µm syringe filter (Whatman, Maidstone, England) - to remove any insoluble material or dust prior to injection - and then diluted to 1 and 2.5 mg/ml. A 100 µL aliquot of each solution was without further filtering injected onto the columns at ambient temperature. ASTRA™ (Version 6) software (Wyatt Technology Corporation, California, U.S.A.) was used to estimate the weight average $M_w(V_e)$ and relative viscosities η_r (V_e) as a function of elution volume V_e. A refractive increment (*dn/dc*) of SG is estimated to be similar as XG, which is ~ 0.14 mL/g (Lecacheux et al., 1986) and A_2 was set to zero.

The differential pressure drops from solution flow versus solvent flow yielded η_r and then the reduced viscosity η_{red} at each elution volume V_e was calculated from this form of Eq. 4.2.

$$\eta_{red}(V_e) = (\eta_r(V_e) - 1) / c(V_e) \qquad (4.2b)$$

Because no Huggins or Kraemer extrapolation to zero concentration is possible intrinsic viscosities at each elution volume $[\eta](V_e)$ were obtained using the Solomon-Ciuta equation as a function of elution volume V_e, in this form of Eq. 4.5b.

$$[\eta](V_e) \sim [1/c(V_e)] \cdot [2(\eta_{sp}(V_e)) - \ln(\eta_r(V_e))]^{1/2} \qquad (4.5b)$$

4.3 Results and discussion

4.3.1. Heterogeneity: Sedimentation coefficient and sedimentation coefficient distribution

Sedimentation velocity in the analytical ultracentrifuge showed the SG preparation was unimodal at concentrations > 0.75 mg/ml which resolved into two main components at lower concentration and with partial reversibility between the components (Figure 4.2), accounting for ~ 80% of the total distribution. What is interesting is the relative proportion of these two main components changes: increasing the loading concentration results in an increase in the 2nd higher molecular weight component compared with the other. Figure 4.3 shows this change: across a concentration range from 0.2 to 0.5 mg/ml results in a 5% drop of the lower molecular weight/slower sedimenting component and a corresponding increase in the higher molecular weight/faster sedimenting component was found. This behaviour is commensurate with a partially reversible association-dissociation. This trend is opposite to what might be expected from classical Johnston-Ogston effects (Johnston and Ogston, 1946) which can result in a diminution of the apparent concentration c_2 of the faster moving component with increase in total loading concentration c ($=c_1+c_2$). The fast component is impacted more by the hydrodynamic non-ideality. With the increase of the concentration, the fast component “2” is slowed down because it moves through the main slower component “1”. By contrast, the slow component is not slowed down as much as the fast component because it only needs to move through the solvent, which is less viscous. Therefore, there appears only one peak at higher concentrations where the slower component catches up the faster component. However, when the concentration is two low, there was not enough sensitivity for the AUC to catch the signal of two peaks. Therefore, there is again only one peak when the concentration is lower than 0.2 mg/ml.

(a) (b)

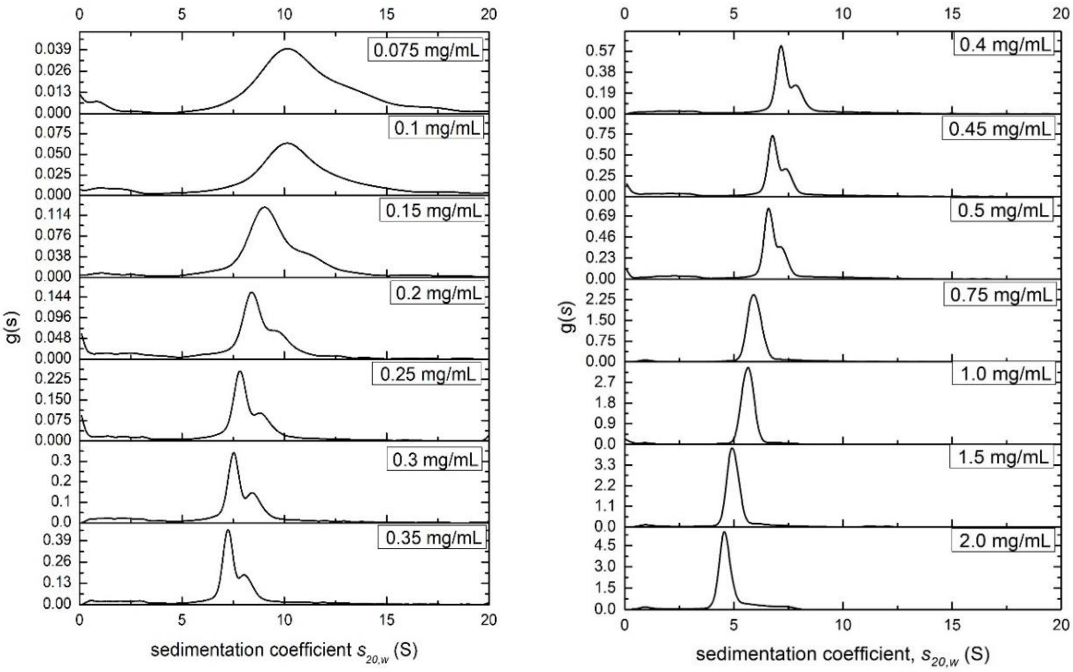

Figure 4.2 Sedimentation coefficient distributions g(*s*) vs $s_{20,w}$ for different loading concentrations of SG in deionized distilled water supplemented with 0.02% azide: (a) The loading concentration ranges from 0.075 mg/mL to 0.35 mg/mL; (b) The loading concentration ranges from 0.4 mg/mL to 2 mg/mL. Of the two main components on average (65.5 ± 2.5) % is the slower component and (34.5 ± 2.5) % is the faster component.

(a) (b)

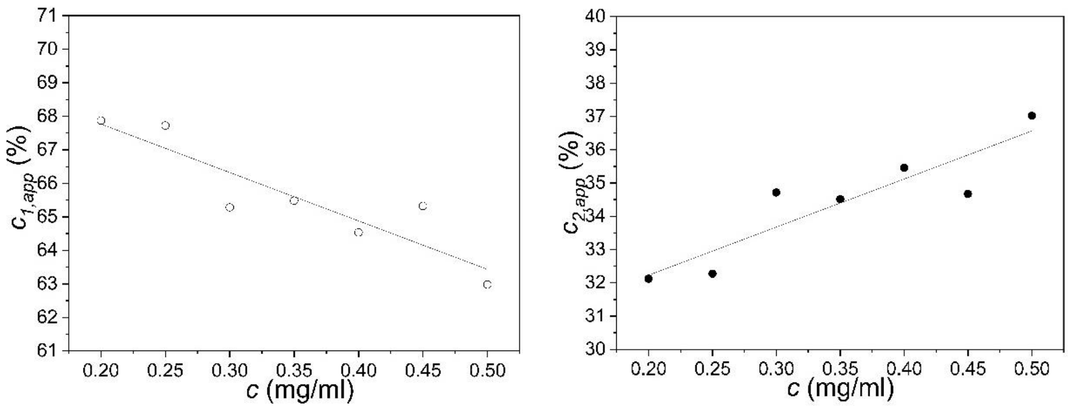

Figure 4.3 Plot of the relative concentration of (a) the 1st main component, c1, as a function of loading concentration c, and (b) the 2nd main component, c2, as a function of c.

The sedimentation coefficient versus concentration plots for both components showed significant hydrodynamic non-ideality (Figure 4.4), due to exclusion volume and viscosity effects. In Figure 4.4, *s* values had been corrected to standard conditions (density and viscosity of water at 20.0^{o}C). There appeared to be a discontinuity between 0.4 and 0.75 mg/ml after which the 2nd component has not resolved from the main peak. This could correspond to (i) the dilute solution limit or c* (Cuvelier and Launay, 1986): a similar value was seen for xanthan (Dhami et al., 1995); (ii) increased hydrodynamic non-ideality retarding more the faster component which is moving through a solution of the slower component. Linear extrapolation of datasets of $1/s_{20,w}$ vs total concentration, c, to c=0 for values of c<0.4mg/ml yielded estimates for the main (slower) component of $s^o_{20,w}$ = (13.0 ± 0.5)S and for the faster component of $s^o_{20,w}$ = (15.7 ± 1.3)S (Supplementary table 1).

(a) (b)

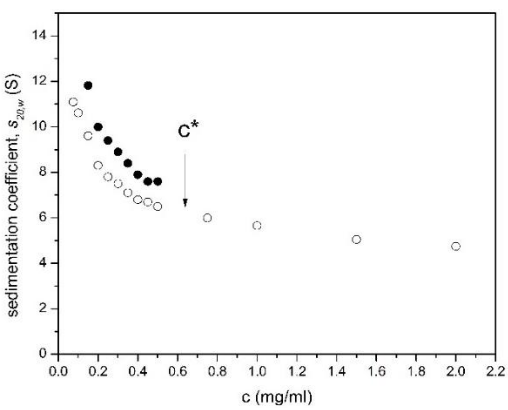

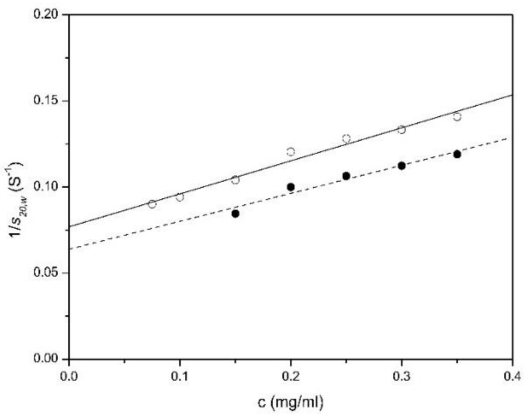

Figure 4.4 Plot of (apparent) sedimentation coefficient of SG in aqueous solution (water as solvent, supplemented with 0.02% azide) for the slower component (open circles) and faster component (solid circles) corrected to standard solvent conditions (viscosity, density of water at 20.0°C (b) extrapolation of the reciprocal of the sedimentation coefficient $s_{20,w}$ to zero concentration to yield $s^{o}_{20,w}$. Values of $s^{o}_{20,w}$ = (13.0 ± 0.5) S and $s^{o}_{20,w}$ = (15.7 ± 1.3) S for the slow and fast components were obtained.

4.3.2 Partially reversible self-association

The partially reversible self-association inferred from the sedimentation velocity results appear to be consistent with sedimentation equilibrium, with an increase in the (whole distribution) apparent weight average molecular weight $M_{w,app}$ as a function of loading concentration c (Figure 4.5a). This increase overcomes the effects of thermodynamic non-ideality which would normally lead to a decrease in $M_{w,app}$ with increase in concentration, c. This tendency to self-associate, also reported by

(Lecacheux et al., 1986) on the basis of low-angle light scattering measurements is not seen in xanthan which follows the classical decrease with c (Dhami et al., 1995): in such cases extrapolation to $c = 0$ effectively negates these effects to yield a true ideal weight average molecular weight. It is possible to compensate for these effects for a self-associating system if we have an estimate for the non-ideal contribution to $M_{w,app}$. In this regard, in the dilute solution region the relation given in Equation 4.1, namely $(1/M_{w,app}) = (1/M_w)(1 + 2BM_wc)$ applies where B is the 2nd thermodynamic virial coefficient. The factor $(1 + 2BM_wc)$ represents the factor by which $M_{w,app}$ underestimates the true or ideal weight average molecular weight M_w, at a concentration c. For SG $BM_w \sim 570$ ml/g (Harding, 1992, Lecacheux et al., 1986) and it is possible to convert the plot of $M_{w,app}$ vs c (Figure 4.5a) to M_w vs c (Figure 4.5b) further emphasizing the effect of self-association. From extrapolation we obtain an estimate for M_w^o, the value of M_w in the zero concentration limit, of ~ $(2.8 \pm 0.3) \times 10^6$ g/mol, comparable with that for xanthan (Dhami et al., 1995). Up to the apparent dilute solution limit, M_w rises to ~ 4.5×10^6 g/mol.

To examine the reversibility of the association we use the diagnostic technique of overlap of data-sets of point average apparent molecular weight $M_{w,app}(r)$ vs local (fringe) concentration $J(r)$ as a function of radial position r in an ultracentrifuge cell for different cell loading concentrations c (Creeth and Harding, 1982a, Nikolajski et al., 2014, Roark and Yphantis, 1969). For a completely reversible association-dissociation the different datasets obtained at different loading concentrations overlap and form part of the same curve. Compared to amino cellulose for example (Nikolajski et al., 2014) only partial overlap is seen (Figure 4.5c) indicating partial reversibility.

(a)

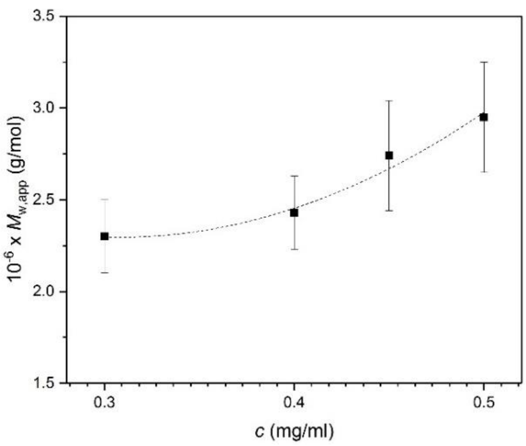

(b)

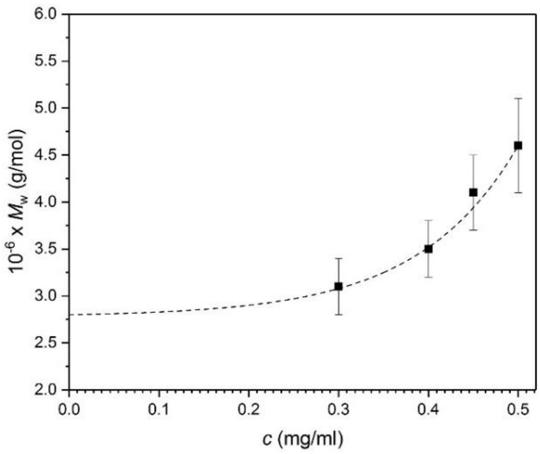

(c)

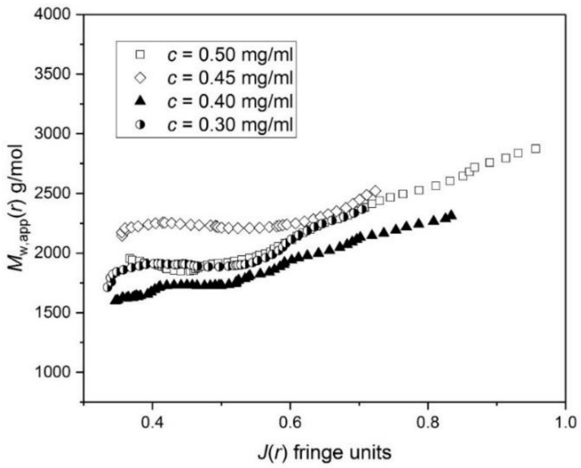

Figure 4.5 Sedimentation equilibrium of SG: (a) plot of (whole distribution) apparent weight average molecular weight $M_{w,app}$ versus cell loading concentration c SG in deionised distilled water supplemented with 0.02% azide.; (b) after correction for non-ideality, plot of (ideal) M_w versus c; (c) plot

of point or local average molecular weight $M_{w,app}(r)$ as a function of local (Rayleigh fringe) concentrations $J(r)$ at radial positions r for different cell loading concentrations.

4.3.3 Intrinsic viscosity

Figure 4.6 shows the different extrapolations to estimate the intrinsic viscosity [η] using the Ostwald viscometer. The assumption is made, as before with xanthan (Dhami et al., 1995) that due to the slow creeping flow conditions non-Newtonian flow effects are not significant. Flow time increments between solution and solvent were very large so very low concentrations could be employed, <0.05 mg/ml and well below the apparent c^*. Both the extrapolation methods – Huggins and Kraemer – gave very similar values for the intrinsic viscosity, (2191 ± 110) ml/g and (2192 ± 110) ml/g respectively. Within this concentration range the Solomon-Ciuta estimates for [η] at each concentration were reasonable and (unsurprisingly, since it is based on a combination of the two other extrapolation methods) gave an extrapolated value to c=0 in agreement with the other two. The intrinsic viscosity is lower than the intrinsic viscosities of XG measured in previous studies (Dhami et al., 1995).

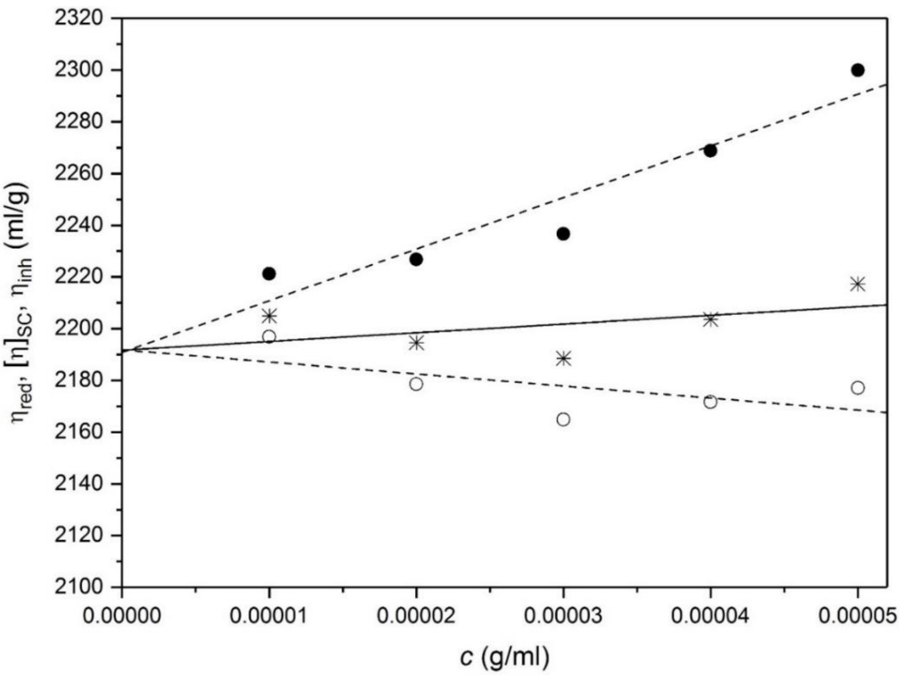

Figure 4.6 Intrinsic viscosity estimations from the Ostwald viscometer for SG in deionised distilled water supplemented with 0.02% azide. Filled circles – reduced viscosities η_{red}, yielding a value of [η] or (2191 ± 110) ml/g. Open circles – inherent viscosities η_{inh}, yielding a value of [η] or (2192 ± 110) ml/g. Stars – Solomon-Ciuta values $[\eta]_{SC}$ yielding a value of [η] or (2192 ± 110) ml/g.

4.3.4 Conformation

We use size exclusion chromatography coupled to multi-angle laser light scattering (SEC-MALS) to give an indication of the conformation/ chain rigidity of the SG. Although SEC-MALS is not the first method of choice for studying very large polymers due to the limit of resolution of the SEC columns , when coupled to an on-line differential pressure viscometer (and using the approximate Solomon-Ciuta equation to estimate [η]) equation, it is still possible to estimate the conformation from the dependence of the intrinsic viscosity $[\eta](V_e)$ relationship with $M_{w,app}(V_e)$ across a range of elution volumes V_e using for example the Mark-Houwink-Kuhn-Sakurada (MHKS) power law relation (see for example (Harding et al., 1991, Smidsrød and Andresen, 1979, Tsvetkov et al., 1971)).

$$[\eta] = M_w{}^a \tag{4.6}$$

Figure 4.7 shows the double logarithmic MHKS plot of $[\eta](V_e)$ versus $M_w(V_e)$: there appears a change in slope from a stiffish rod shape molecule (slope or "*a*" value of 1.14 ± 0.03) to a lower value as the molecular weight increases (a=0.76 ± 0.01), corresponding to a more flexible structure. We are limited to the molecular weight range we could look at due to the finite separation range of the SEC columns for high molecular weight material but nonetheless the trend is visible. This is reasonably similar to what was observed by Yanaki et al. (1981), although they found even stiffer rods at lower molecular weight. But those researchers did not have the benefit of on-line separation/viscosity/molecular weight instrumentation and their conclusions were limited to just two data points. We also observe considerable chain flexibility at higher molecular weights.

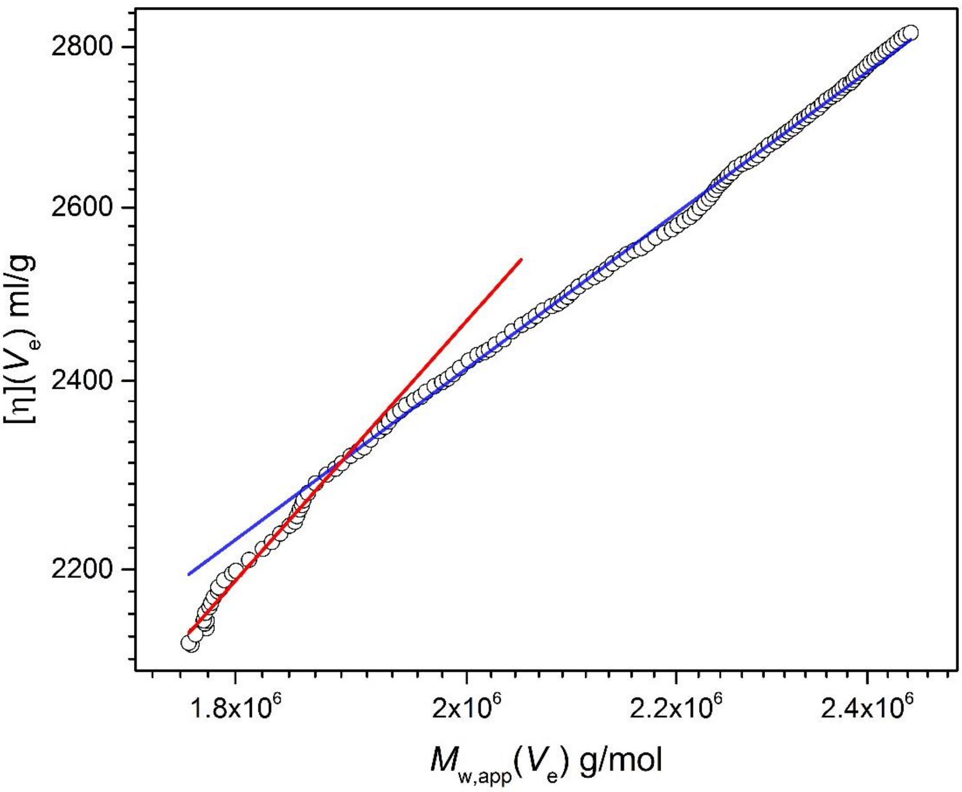

Figure 4.7 Mark-Houwink-Kuhn-Sakurada plot of SG of intrinsic viscosity [η](V_e) and weight average molecular weight M_w(V_e)as a function of elution volume V_e. The initial limiting slope (red) = (1.14 ± 0.03), corresponding to an extended rod-like structure. The final limiting slope at high molecular weight (blue) = (0.76 ± 0.01), corresponding to a more flexible structure.

These observations appear to further reinforce the earlier observations of Lecacheux et al. (1986) and Yanaki et al (1981, 1983) of a stiff conformation at lower molecular weights or chain lengths, becoming more flexible at higher molecular weights. We observe that the lower molecular weight structures (M ~ <2 × 10^6 g/mol) are stiff structures with xanthan-like properties (Berth et al., 1996) but above that they become considerably more flexible.

4.3.5 Molecular weight distribution and comparison with xanthan

As a final comparison with xanthan we can use the *Extended Fujita* method (Harding et al., 2011) to transform the sedimentation coefficient distribution g(*s*) at low concentration to a molecular weight distribution f(*M*) vs *M*. The approach uses the power-law or scaling relationship between the sedimentation coefficient and molecular weight, analogous to the MHKS equation for viscosity (Eq. 4.6) above (Harding et al., 1991, Smidsrød and Andresen, 1979, Tsvetkov et al., 1971):

$$s = \kappa_s M_w^b \qquad (4.7a)$$

where κ_s and b are characteristic coefficients related to conformation. For example, b = 0.4-0.5 for a coil type of conformation, ~0.15-0.2 for a rod conformation and ~0.67 for a spherical conformation. If κ_s and b are known then M_w can be found from:

$$M_w = \left(\frac{s}{\kappa_s}\right)^{1/b} \qquad (4.7b)$$

Fujita (1962) provided the basis for converting a (differential) distribution g(*s*) of the sedimentation coefficient *s* into a (differential) distribution f(*M*) of the molecular weight *M* for linear polymers, based on the assumption that the polymers behave as randomly coiled polymers in solution, with b = 0.5 in Eq. 4.7. the distribution function is

$$f(M) = g(s) \cdot (ds / dM) \tag{4.8}$$

where

$$ds / dM = b \cdot \kappa_s^{1/b} \cdot s^{(b-1)/b} \tag{4.9}$$

Therefore, to perform the transformation the conformation type or b needs to be known under the particular solvent conditions and at least one pair of s-M values is needed to define the κ_s from Eq. 4.10, and this is what we have now applied to the XG and SG.

Defining b and κ_s: we use the Tsvetkov et al. (1971) relation linking b with a:

$$b = \frac{2-a}{3} \tag{4.10}$$

Since a = 1.23 for xanthan (Morris and Harding, 2013), b = 0.26. For SG, from the (mean) MHKS a value of 0.95 (The average value of 1.14 and 0.76 from Figure 4.7), this leads to b = 0.35 across the distribution. To obtain κ_s we simply combine b with the "ideal" weight average molecular weight (Table 1) with the (weight average) sedimentation coefficient $s_{20,w}$, at the concentration used for the distribution, using Eq. 4.7. A loading concentration of 0.2 mg/ml is used to minimize non-ideality effects. This yields values of 0.197 for xanthan (Morris and Harding, 2013) and 0.0492 for SG, respectively. The corresponding transformations from g(s) vs s to f(M) vs M are given in Figure 4.8a for xanthan and Figure 4.8b for SG.

(a) (b)

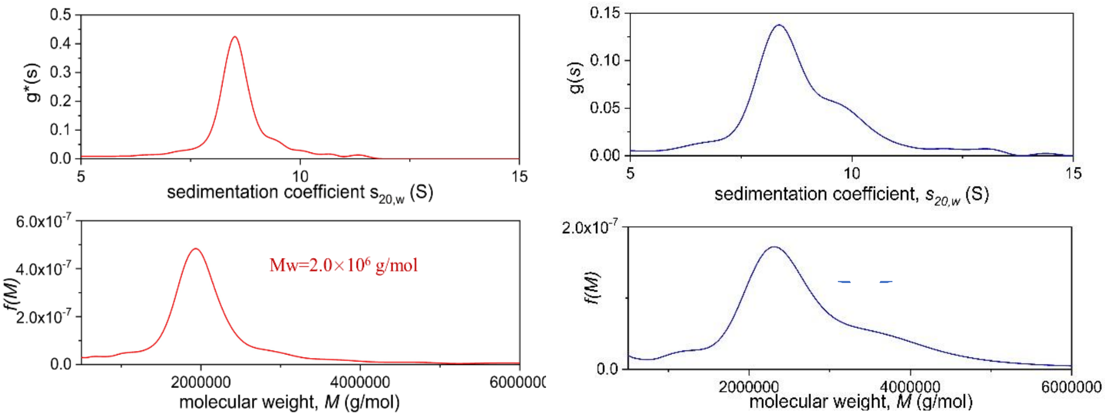

Figure 4.8 Transformation of sedimentation coefficient distributions g(*s*) vs *s* (for a loading concentration of 0.2 mg/ml) to molecular weight distributions f(*M*) vs *M*. (a) xanthan (b) SG. Distributions – and weight averages - are similar.

The g(*s*) profiles were obtained at a loading concentration of 0.2 mg/ml and the weight average sedimentation coefficient $s_{20,w}$ is combined with the weight average molecular weight. In terms of molecular weight distribution, it can be seen that both distributions are very similar. Although SG has a more marked 2nd component of higher molecular weight as we have previously observed.

4.3.6 Sedimentation of mixtures of SG with bovine submaxillary mucin

We explored using analytical ultracentrifugation to analyse the behaviour of mixtures of SG with submaxillary mucin (using bovine submaxillary mucin as the model mucin system - (Dinu et al., 2019)) to assay for the possible presence of deleterious large aggregation effects which might diminish the potential of SG as a dysphagia agent

(Rofes et al., 2014).

Experiments were conducted in phosphate buffered saline, mimicking the inorganic conditions in the mouth (and suppressing polyelectrolyte behaviour in the polyanionic mucin). The bovine submaxillary mucin (BSM) solution and each biopolymer solution were separately mixed with a weight ratio of 1:5. Figure 4.9 shows the sedimentation coefficient distribution plots for SG/BSM mixtures compared to controls, from the range 0-10 S (Figure 4.9a) and 10-1000 S (Figure 4.9b). From Figure 4.9a the reduction and slight retardation of the faster moving SG peaks on mixing may be due to Johnston-Ogston effects (faster components slowed down by the viscosity of the slower components – as considered above), but there is no evidence for faster moving large aggregates at least not in the size range up to 1000 S (Figure 4.9b).

(a) (b)

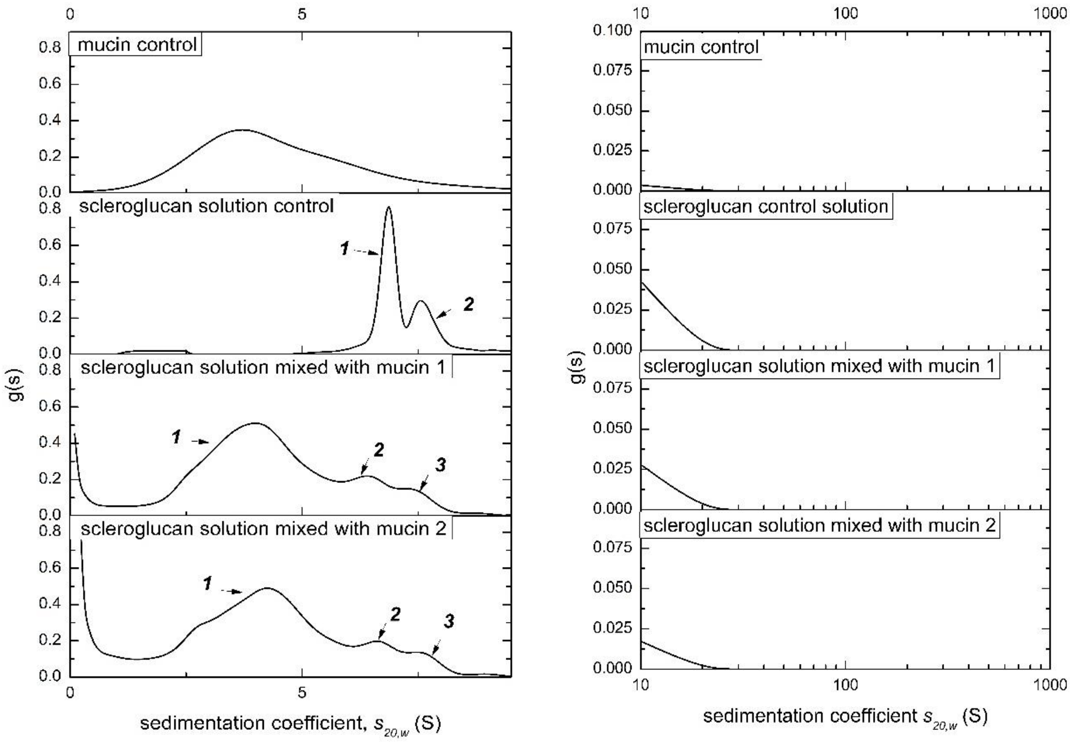

Figure 4.9 Sedimentation coefficient distributions g(*s*) vs $s_{20,w}$ for mixtures of SG with bovine submaxillary mucin (BSM). The number represents the number of peaks in the sedimentation coefficient distribution curve. (a) sedimentation coefficient range: 0.1 to 10 S; (b) 10 to 1000 S. Final loading concentrations: SG 0.42 mg/ml, BSM 0.50 mg/ml.

4.4 Concluding remarks

Our study confirms previous work that SG is a large and complex microbial polysaccharide in aqueous solution, consistent with previous observations of a tendency to self-associate beyond the trimeric, triple helical structure observed by others, and in a semi-reversible manner. In some ways it has properties similar to xanthan, another microbial/fungal polysaccharide with a β(1-4) backbone and of a similar molecular weight – and molecular weight distribution and which also exhibits complex properties. Encouragingly, in terms of its potential use for the treatment of dysphagia, SG showed no evidence from this study for significant interactions with submaxillary mucin, nor the formation of large mucoadhesive aggregates seen for other types of polysaccharide-mucin system & hence reduce the likelihood of choking. From the conformation work it seems that SG of molecular weight $<1.9 \times 10^6$ g/mol may be worthy of further consideration as an alternative to xanthan for the treatment/ management of patients with oropharyngeal dysphagia (Martino et al., 2000).

Chapter 5 Complex rheological properties of xanthan gum and scleroglucan, and their mixtures with mucin and human whole saliva

Abstract

Xanthan gum (XG) and scleroglucan (SG) exhibit a complex set rheological properties due to associative behaviour and the rod-like molecular conformation. The latter is important for the formation of the percolated-like network in semi-dilute solutions, leading to the high thickening effect. Both polymers find their use in medical nutritional applications, such as dysphagia, where they are used as low-concentration thickeners. The key difference between XG and SG is the non-charged nature of the latter, which enables its use in formulations with cationic molecules, such as proteins, where XG would cause precipitation and/or loss of stability. In this study, several rheological characterisation techniques, including steady shear rheology, small amplitude oscillatory shear spectroscopy, first normal stress difference measurements and capillary break-up rheometry have been used to investigate differences between SG and XG. In addition, the effect of saliva and submaxillary bovine mucin on complex rheological behaviour is examined in order to probe potential implications of XG/SG addition for oral lubrication and product texture. Amongst all techniques used in this study, the capillary break-up extensional rheometry was found to be most sensitive to the subtle rheological differences between two polysaccharides. Using solvents with different viscosities, i.e., water vs 40% sucrose solution, we show that two polymers are characterised by a marked difference in the characteristic relaxation time at shorter time scales, whilst at longer relaxation times their dynamics is similar.

We hypothesise that this behaviour is the manifestation of the transient self-association behaviour in solution. The data are consistent with the mechanism whereby XG supramolecular assemblies appear to be less stable compared to SG and hence, more easily disrupted by shear. Finally, we observe no major effect of saliva or mucin on complex rheological behaviour of SG, which is consistent with the data previously reported by Choi et al. (2014) for XG. Thus, the uncovered sets of rheological behaviour support the proposition that SG can be used as an effective, low-concentration thickener in medical nutrition applications, whilst due to its non-charged nature its use can open new formulation opportunities in a broad spectrum of pharmaceutical and food applications.

5.1 Introduction

Oropharyngeal dysphagia is often displayed by stroke patients and the elderly. Depending on the severity of their disorder, the patients can require an adjustment of product thickness to avoid aspiration. However, having to “modify” their foods and beverages prior to ingestion is psychologically challenging and often dysphagia sufferers will avoid eating or drinking in a social setting. This combined with the fact that a lone elderly can frequently simply forget to take on food or drink, and that thickening of foods and drinks can render these blander and unappetising, incidences of malnutrition among the elderly is on the increase. Many different biopolymers are available to thicken foods, imparting a range of rheological behaviours, texture properties and a display of different levels of sensitivity towards the environmental conditions in the food or beverage, e.g., pH, ionic strength, temperature, co-solutes. However, thickened food exhibit reduced flavour and taste. Therefore, new ingredients, in particular low concentration thickeners are required in order to develop new products with superior taste and flavour profiles that target improvement of nutrition, well-being and quality of life of elderly and vulnerable groups.

Xanthan gum (XG) is a common choice in dysphagia formulations due to its unique shear-thinning properties (Song et al., 2006a). These properties stem from the weak self-association behaviour and rod-like conformation of XG chains. To achieve the thickening effect, XG can be used at very low concentration, e.g., 0.05 wt%. This alleviates the problems of diminished flavour release and reduction of taste intensity that are common in thickened foods (Baines and Morris, 1988, Baines and Morris, 1989, Preininger, 2016). Scleroglucan (SG) was chosen as an analogous rod-like polysaccharide. In contrast to highly charged XG, SG is a neutral polysaccharide that was reported to adopt a triple helical supramolecular structure (Lecacheux et al., 1986, Yanaki and Norisuye, 1983), which can further self-associate in a partially reversible way (Li et al., 2020). This newly identified feature of SG's self-associative behaviour will become critical for proposing possible interpretations of rheological behaviour observed in this work. The shear thinning behaviour of XG and SG solutions are key factors in the way these hydrocolloids impact oral processing. During bolus formation, shear and normal forces play a key role, with material experiencing a mix of shear and elongational components of deformation (Stokes, 2012a). Therefore, different rheological techniques are applied in this work to study the difference between XG and SG.

During oral processing, saliva is brought in contact with food. Depending on the nature of the food or beverage, saliva has strong and complex effect on rheological properties of the bolus (Boehm et al., 2019, Boehm et al., 2020). When biopolymers are processed in the oral cavity, it interacts with teeth, tongue and palate and is incorporated into the food bolus before swallowing (Qazi et al., 2017, Newman et al., 2016). The analysis of oral processing of beverages and soft solids is complicated by the fact that saliva in itself is rheologically complex fluid (Stokes and Davies, 2007a), and hence the ratio of saliva/hydrocolloid solution will have a dramatic impact on the resulting rheological properties (Yakubov et al., 2015). Although mimicking saliva is very challenging (Yakubov, 2014), it is possible to utilise mucin solutions as a proxy for probing fundamental mechanisms of hydrocolloid – mucin interaction that can guide development of hypotheses to be subsequently tested *ex*/*in vivo*. Another reason for using model salivary proteins is to circumvent inherent variability of saliva and mitigate the impact of its degradation upon collection (Sarkar et al., 2019). The reconstituted saliva (RS) was prepared by dissolving bovine submaxillary mucin in the inorganic buffer solution. The inorganic buffer solution mimicking the inorganic environment of human whole saliva (Sarkar et al., 2009). Li et al. (2020) found that the mucin solution and biopolymer solutions have no interactions under AUC analysis, which may indicate that the HWS or RS have less impact on the rheological properties (Li et al., 2020). However, the concentrations of biopolymer solutions carried out under AUC analysis were ten times more diluted than in the work by Choi et al. (2014). Therefore, the rheological and extensional rheological behaviour of biopolymer solutions mixed with HWS or RS were also carried out in this chapter.

In this chapter, we report comparative investigation of shear and elongational rheological properties of two very similar rod-like polysaccharide thickeners: XG and SG. Several techniques were applied in this research, from approaches deeply rooted in flow profiling using rotational rheometry (steady shear and first normal stress tests), rheological oscillatory techniques (small amplitude oscillatory shear rheometry) (Stokes and Frith, 2008, Hyun et al., 2002) and extensional rheology approaches such as capillary breakup rheometry. Further, the interactions of the polysaccharide solutions with expectorated human whole saliva (HWS) as well as reconstituted saliva (RS) was investigated.

5.2 Material and Methods

5.2.1 Biopolymers and biopolymer solution preparation

5.2.1.1 Biopolymers

The two rod-like biopolymers used in this study were xanthan gum (Keltrol-T, CP Kelco, Surrey, UK) and scleroglucan (Carbosynth, Compton, UK). XG was used as received while SG was purified as described in Chapter 5.2.1.2. The molecular weight of xanthan gum is around 2,000 kDa. The molecular weight of scleroglucan is around 2,800 kDa (Li et al., 2020).

5.2.1.2 Biopolymer solution preparation

Xanthan gum solutions

The biopolymer solutions were prepared in double-distilled water (18.2 MΩ.cm). 0.02% (w/v) sodium azide (Sigma-Aldrich, Gillingham, UK) was added as an antimicrobial agent. Sodium chloride (Sigma-Aldrich, Gillingham, UK) was added to XG solutions to stabilize the helical structure of XG (Abbaszadeh et al., 2016). At first, a 1% (w/v) XG stock solution was prepared by slowing adding the appropriate amount of XG into an aqueous solution of 0.2% (w/v) sodium chloride while mixing on a magnetic stirrer. Then, the solution was heated up to 80 °C in order to make biopolymer solutions dissolve faster. The solution was stirred continuously at this temperature for one hour. Finally, the solution was cooled down to room temperature and left overnight before usage. To prepare working XG solutions (0.2% (w/v) and 0.5% (w/v)), the stock solution was diluted with the appropriate amount of aqueous solution of 0.2% (w/v) sodium chloride and mixed on a magnetic stirrer at 20 °C for at least 2 hours. 0.5% XG in 40% sucrose solution was also prepared by dispensing 0.5 g XG in 100 ml 40% sucrose solution and slowly heated up to 80 °C for two hours stirring. The 40% (w/v) sucrose solution was chosen as a solvent due to its higher viscosity compared to water and Newtonian behaviour. It can be used to identify the different relaxation behaviour of rod-like biopolymers i.e., XG and SG in different solvent.

Scleroglucan solutions

The SG as received was not fully soluble in water, therefore it was purified by centrifugation and dialysis. The 0.2% (w/v) turbid solution was centrifuged at 4850 g and 20 °C for 30 min. The supernatant was recovered by pouring out and then dialyzed in water to remove the low molecular weight impurities. Then the dialyzed supernatant was freeze dried in freeze dryer (Freeze Dryer Modulyo, Edwards, York, UK). An appropriate amount of the freeze-dried SG sample was then dispensed in 0.02% sodium azide solution to prepare a 1% SG stock solution. During the solution preparation, the solution was heated up to 80 °C for one hour. To prepare more diluted SG solutions (0.2% (w/v) and 0.5% (w/v)), the stock solution was diluted with the appropriate amount of aqueous solution of 0.02% (w/v) sodium azide and mixed on a magnetic stirrer at 20 °C for at least 2 hours. 0.5g SG was also dispensed in 100 ml 40% sucrose solution and was heated up to 80 °C with three hours stirring.

5.2.2 Saliva sample preparation

Mechanically stimulated human whole saliva (HWS) was collected from one donor (female, 28 years old, non-smoking). As saliva properties vary, the saliva samples were always collected between 8.30 to 10.30 am, and the donor was requested to not eat or drink (with the exception of water) for at least 2 hours before saliva collection. The donor also brushed the teeth after breakfast to remove as much food debris as possible. Prior to saliva collection, the donor rinsed the mouth with bottled water (Buxton natural mineral water) for at least 30 seconds to remove remaining food debris. Then, a 10 min rest period was imposed to allow the oral cavity to return to a neutral condition and to avoid dilution of donated saliva with the water. For saliva collection, the donor was asked to chew on a small piece of laboratory film (Parafilm, Bermis Flexible Packaging, Neenah, USA) and expectorate the in-mouth collected volume of saliva every 30 seconds into centrifuge tube. This total collection time was 6 minutes. The expectorated saliva from the first 30 seconds was discarded as it may contain food debris. During collection, saliva samples were kept on ice to minimise the saliva degradation. Then, the saliva samples were centrifuged at 10,000 g and 4 °C for 30 mins, and the resulting supernatant collected. The supernatant was used to mix with the biopolymer solutions for further experiment.

5.2.3 Reconstituted saliva composition and preparation

Saliva mimetic solution of bovine submaxillary mucin (BSM) (Sigma-Aldrich, Gillingham, UK) was prepared using an aqueous solution of the composition detailed in Table 5.1 followed by the protocol described in Sarkar et al. (2009). These inorganic components and their concentrations are representative of HWS. The BSM was dissolved into this solution at the concentration of 30 mg/mL. This has comparable steady shear viscosity to that of HWS (Sarkar et al., 2009, Gal et al., 2001). There are little publications focusing on comparing the extensional rheological behaviour of mucin solution and human whole saliva. The 1.2 mg/mL BSM solution was also prepared because this is the average concentration of mucin in human whole saliva (Kejriwal et al., 2014). However, addition of 1.2 mg/ml BSM solution to XG or SG solutions resulted in no effect on the capillary break-up behaviour (Supplementary Table 2 and Supplementary Table 3). The prepared reconstituted saliva should be kept in 4 °C fridge. The reconstituted saliva cannot be stored in freezer as mucins could not disperse again after freezing.

Table 5.1 The inorganic components in reconstituted saliva

Component	**Chemical formula**	**Concentration (g/L)**
Sodium chloride	$NaCl$	1.594
Ammonium nitrate	NH_4NO_3	0.328
Potassium phosphate	KH_2PO_4	0.636
Potassium chloride	KCl	0.202
Potassium citrate	$K_3C_6H_5O_7.H_2O$	0.308
Uric acid sodium salt	$C_5H_3N_4O_3Na$	0.021
Urea	H_2NCONH_2	0.198
Lactic acid sodium salt	$C_3H_5O_3Na$	0.146

5.2.4 Biopolymer-saliva and reference mixture preparation

The centrifuged human whole saliva supernatant (HWS) and each biopolymer solution were separately mixed with a weight ratio of 1:5. The concentrations of XG and SG solution used were both 0.5% (w/v). 0.5% of biopolymer solutions were chosen to be used in the extensional rheological analysis as 0.5% is the concentration of XG usually be used in thickened food products (Choi et al., 2014). The mixing process took place in an ice water bath. For each saliva and biopolymer solution combination, six different stirring times were utilised in capillary break-up test (2 min, 5 min, 30 min, 60 min, 90 min and 120 min). The control and BSM samples were prepared under the same condition, with the exception that the aliquot of saliva was replaced with double-distilled water or BSM solutions, respectively.

5.2.5 Steady shear and oscillatory shear rheological analysis

All of the shear rheological measurements were analysed under 20 °C by using the stress-controlled rheometer (MCR 301, Anton Paar, Graz, Austria). The geometry used in the research is cone plate 50-2, indicating that the diameter of the geometry has 50 mm diameter with 2° cone angle. Each biopolymer solution was measured at least three times. For the steady shear rheological measurement, the shear rate ranges from 0.01 s^{-1} to 1000 s^{-1}. 10 points were collected per decade. For the amplitude strain sweep test, the angular frequency was set at 1.59 Hz (10 rad/s) (Mezger, 2014). The strain ranged from 0.01% to 1000%. For the frequency sweep test, the angular frequency ranges from 10 rad/s to 0.1 rad/s. The shear strain was set at 10%, which was taken from the linear viscoelastic range from amplitude sweep test.

5.2.6 Normal stress analysis

The measurement were carried at a temperature of 20 °C by using the stress-controlled rheometer (MCR 302, Anton Paar, Graz, Austria). The geometry used in this research is parallel plate with the plate diameter of 50 mm and the gap of 50 μm. The gap error correction was applied in accordance with the protocol described in Davies and Stokes (2005). Triplicate analyses were carried out for each of the biopolymer solution. The first normal stress difference was measured between the shear rate range of 1000 s^{-1}s to 10000 s^{-1}. The parallel plate correction was applied to the raw data in accordance with the method described in (Davies and Stokes, 2008).

5.2.7 Filament break-up and data analysis

The extensional rheological tests were carried out at 20 °C using capillary break-up extensional rheometer (CaBER-1, Thermofisher Haake, Kalsruhe, Germany). Air temperature and humidity probe allow the humidity in the chamber to be maintained above 70% (mimicking the in vivo oral biology environment). The operating principle of this method is based on formation of a capillary bridge upon rapid separation of two cylindrical plates and monitoring the dynamics of the fluid column thinning. The thinning is followed by a laser micrometre at the midpoint of the filament length. For all measurements, 790 μL of the sample was placed between the fixed plate and moving plate (diameter 6 mm). The initial gap was set at 3 mm. The strike time for the measurement was set at 20 ms and the final gap was set to 10 mm. Thus, the aspect ratio (AR = gap height between top and bottom plates / plate diameter) at the beginning of the test was 0.5 and at the end of the strike 1.67 (Hencky strain = 1.2). Each sample was measured for at least 10 repeats, with a fresh aliquot being loaded for each replicate. Data analysis was performed using Haake CaBER software.

The decay of the mid-point diameter of biopolymer solutions have two regions, an exponential region and a linear region (Stelter et al., 2002, McKinley, 2005). In the linear region, the Bond number << 1 indicating the radius of the filament is extremely small. The biopolymer relaxation time (λ) and the steady state apparent extensional viscosity (η_e) were determined by fitting initial exponential and final linear region of the relationship of the midpoint diameter versus time using Eq. 5.1 and Eq. 5.2, respectively (Anna and McKinley, 2001, Kheirandish et al., 2008, Stelter et al., 2002).

$$D(t) = D_0 \exp(-\frac{t}{3\lambda}) \tag{5.1}$$

$$\eta_e = -\frac{\sigma}{dD(t)/dt} \tag{5.2}$$

D is the diameter of the mid-point of the filament. D_0 is the mid-point diameter at time = 0 (equals to the diameter of the plate, D_0 = 6 mm). σ is the surface tension of the fluid.

Previous studies on xanthan gum showed that the surface tension of the 0.5% (w/v) solutions is in the range 67 – 69 mN/m, which is similar to the surface tension of water (Muthamizhi et al., 2014, Lee et al., 2012). The surface tension of human whole saliva is around 47 to 57 mN/m (Kirkness et al., 2000, Vijay et al., 2015, Christersson et al., 2000). However, when HWS mixed with polysaccharide in ratio (by weight) less than 1:5, HWS is found to have less influence on surface tension than polysaccharide. Therefore, the surface tension in this research is assumed to be not too dissimilar to pure water.

5.3. Results and Discussion

5.3.1 Shear rheological analysis

The rheological properties of biopolymer solutions themselves under different concentrations were investigated in this research. These concentrations are all above the c* (Li et al., 2020, Cuvelier and Launay, 1986). Figure 5.1 displays the steady shear rheological behaviour of XG and SG solution in the concentration range of 0.2 % to 1 %. Both XG and SG solutions have comparable shear-thinning behaviour. The viscosity of SG solution is slightly higher than XG solution under low shear rate range of 0.01 to 1 s^{-1}. Further, the shear viscosity difference between XG and SG becomes larger when lowering the concentration of biopolymer solution, which can be caused by different entangled structure of XG and SG under still state. The viscosities of XG and SG solution are moderately comparable in the shear range of 1 to 1000 s^{-1}, which also in good agreement with the data reported by Lafforgue (Lafforgue et al., 2018).

Some disagreement can be pointed with the viscosity data reported for SG by Moresi et al. (2001), which found 1% SG solutions to be ~ 40 times more viscous than our own findings. With regards to XG, our findings are found to be consistent and in good agreement with many previous studies (see for example, Phillips and Williams (2009)).

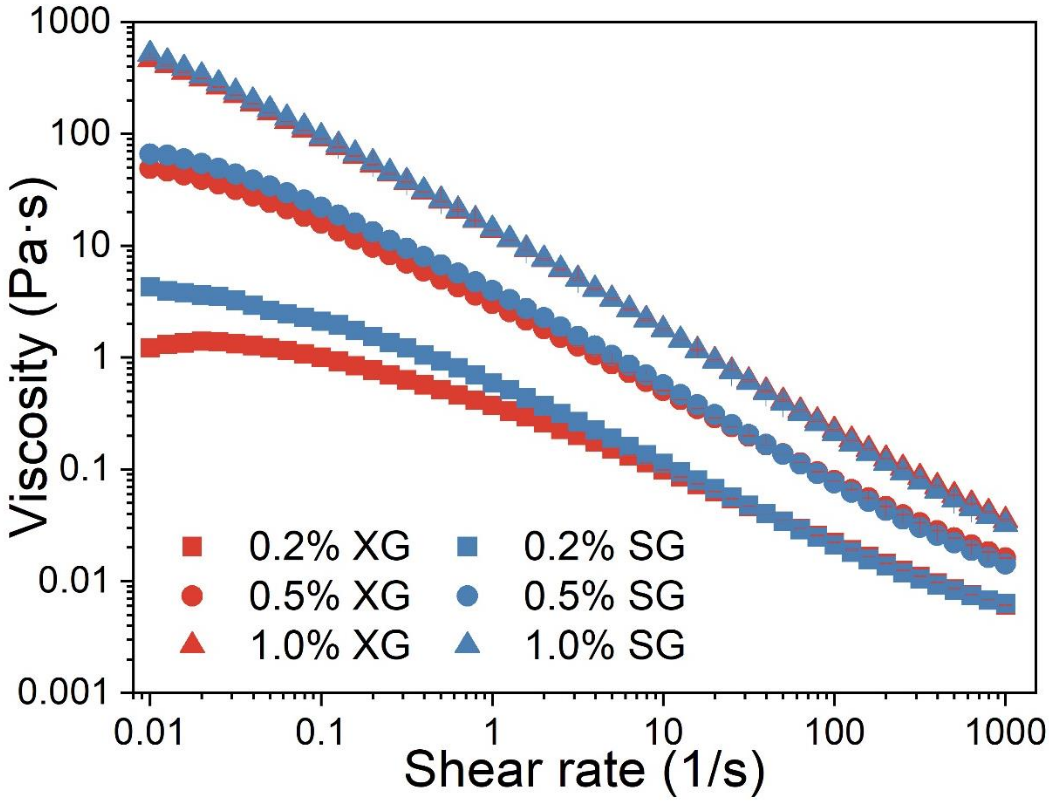

Figure 5.1 The shear rheological rheological properties of XG (red symbols) and SG (blue symbols) solution (water as the solvent) with the concentration of 0.2% (square), 0.5% (circle) and 1% (triangle) at 20°C

Figure 5.2a shows the results of the small amplitude oscillatory shear tests. The viscoelastic moduli (amplitude sweep test) of 0.2%, 0.5% and 1% XG and SG solution are found to be comparable, with both moduli increasing with concentration. The storage moduli are higher than the loss moduli for all concentrations tested for both XG and SG solutions within the LVE range. For both XG and SG solutions with the concentration of 1%, G” has an overshooting phenomenon at the cross point (flow point) with the G’ in this experiment, which can occur in concentrated dispersions. This phenomenon is also consistent with several previous research (Song et al., 2006b, Hyun et al., 2002, Lafforgue et al., 2018). Ren et al. (2020) suggested that this phenomenon is caused by the release of large amount of deformation energy.

The frequency sweep test shows a typical viscoelastic behaviour with both moduli increasing with concentration (Figure 5.2b). The general trend, SG solutions show higher storage and loss moduli compared to XG solutions of the same concentration. The 0.5% and 1% solutions exhibit elasticity dominated (G’>G”) viscoelastic behaviour within the frequency range tested (0.1 – 10 rad/s). For the 0.2% XG and SG solutions, the cross-over point is observed at ω 2 rad/s and 6 rad/s for XG and SG, respectively. When the concentration is 0.2%, the tanδ of SG is lower than XG (Figure 5.2c). With the increase of concentrations, the differences of tanδ between XG and SG become smaller. For the frequency sweep test, the tanδ of XG is slightly higher than SG when under same concentrations, and the differences become bigger with the increase of angular frequency (Figure 5.2d). Further, for both XG and SG solutions, the complex viscosity is slightly higher than steady shear viscosity (Supplementary figure 1) (Cox and Merz, 1958). Since complex viscosity is analysed by the oscillatory test, the curve of complex viscosity can have a turning point when the frequency goes higher than a certain point. Previous research done by Lopes da Silva et al. (1993) suggested that this phenomena can be caused by high associations among molecules or the presence of entangled network (Augusto et al., 2013). Due to the artefacts of the rheometer, some noise data points were removed for 0.2% SG solution in Figure 5.2d.

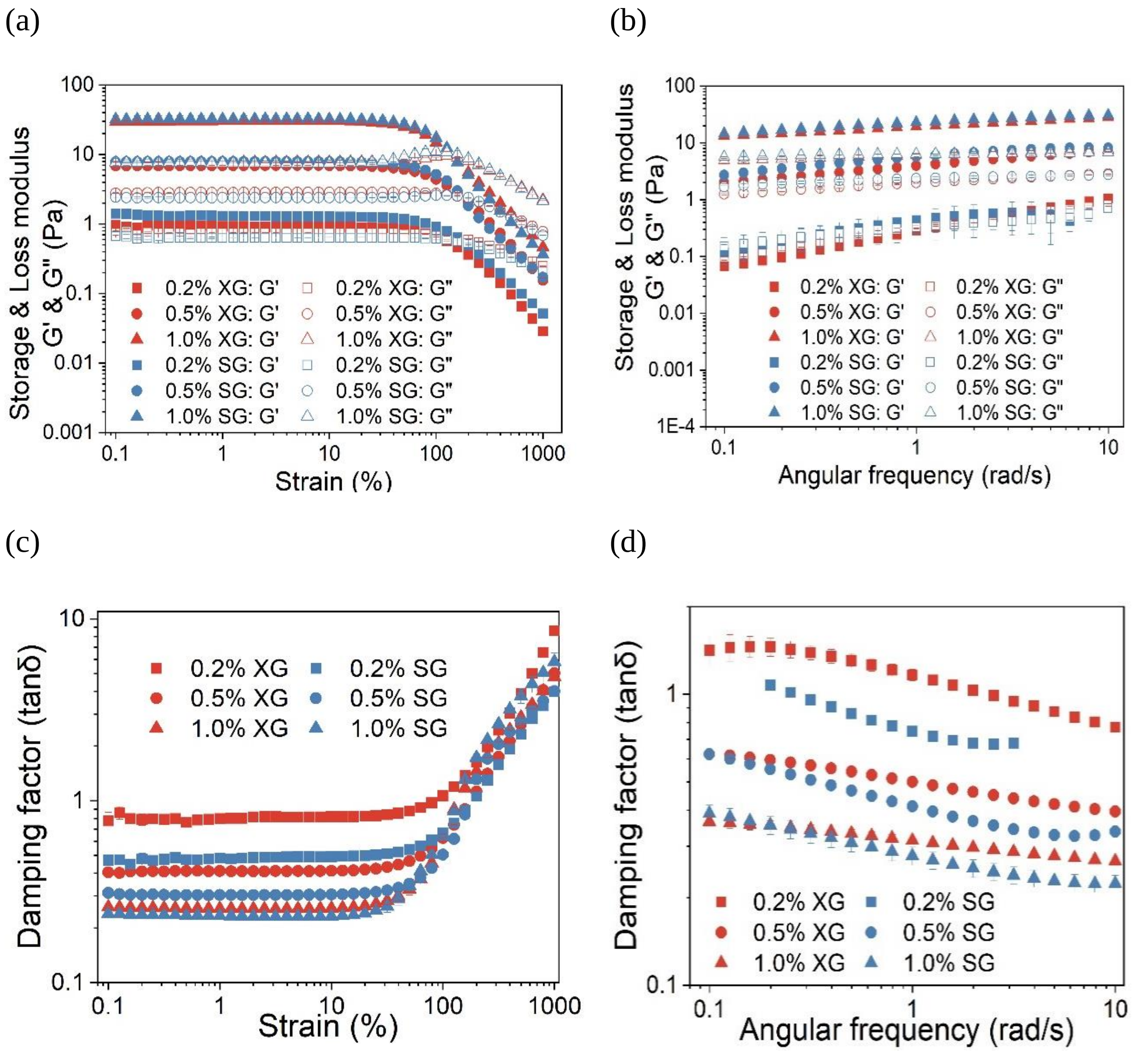

Figure 5.2 The small deformation rheological analysis of XG (red symbols) and SG (blue symbols) solution with the concentration of 0.2% (square), 0.5% (circle) and 1% (triangle) at 20°C. (a): amplitude sweep test: storage modulus (full symbols)

and loss modulus (void symbols), (b): frequency sweep test: storage modulus (full symbols) and loss modulus (void symbols), (c): amplitude sweep test: damping factor (tanδ), (d) frequency sweep test: damping factor (tanδ)

5.3.2 Normal Stress analysis

To probe viscoelastic behaviour further, the normal stress difference profiles were measured using narrow gap parallel plate rheometry (Davies and Stokes, 2008). The normal stress (i.e., the component of the stress tensor orthogonal to the shear plane) can be viewed as a measure of polymer resistance to stretching in response to the shear force (Song et al., 2006a), which in turn alters the streamlines of the flow generating stress components in the direction perpendicular to the shear plane. Figure 5.3 shows the 1st normal stress difference data of the 0.5% XG aqueous solution and the 0.5% SG aqueous solution. For relatively dilute biopolymer solutions, the normal forces are relatively weak. However, N_1 increases with the shear rate, enabling detection at higher values of $\dot{\gamma}$. For experiments in water shown in Figure 5.3a, the practical range of shear rates with detectable normal force is found between 1000 to 10000 s^{-1}. SG shows higher N_1 values compared to XG, suggesting that SG is characterised by the higher values of the 1st normal force coefficient Ψ_1, which is proportional to the characteristic relaxation modulus (G_i) and characteristic relaxation time τ_i. In order to disentangle contributions of G_i and τ_i, we use 40% sucrose solution as a Newtonian solvent. As expected (Zirnsak et al., 1999), the values of N_1 are higher than in aqueous solutions of XG and SG, however, the difference between two biopolymers reduces to below experimental error. These results suggest that the key difference between XG and SG is primarily associated with relaxation spectrum rather than the characteristic modulus of the polymer chain. If the latter would be the factor, the difference in N_1 between XG and SG would remain regardless of solvent viscosity or, equivalently, regardless of characteristic elongation time. Further analysis of the dependency of N_1 on $\dot{\gamma}$, shows that the for XG in water the scaling parameter is ~3/2 suggesting dilute like behaviour (i.e. away from the stretching limit of the polymer chain), whilst in 40% sucrose it reduces to ~0.8, which approaches the value of 2/3 predicted for the rigid rod structure in accordance with a dumbbell FENE-P model (Bird et al., 1987, Doi and Edwards, 1986). For SG, the scaling exponent is very close to the theoretical prediction of 2/3 (for water and 40% sucrose), suggesting that short and long relaxation processes correspond to fundamentally the same structure. This is in contrast to XG, where it is possible to suggest that XG undergoes some level of structural change between water and 40% sucrose leading to the observed differences in viscoelastic response. It is also possible to suggest that potential mechanism may be associated with weak self-association of XG, whereby at short relaxation times, the response is dominated by XG single chains, whilst longer term relaxation is dominated by more rod-like double strand assemblies. These findings are consistent with the values of power exponent for XG, varied from 0.09 to 1.47, reported across different concentrations and solvents (Zirnsak et al., 1999, Escudier et al., 1999, Wei et al., 2014, Stokes et al., 2001).

(a) (b)

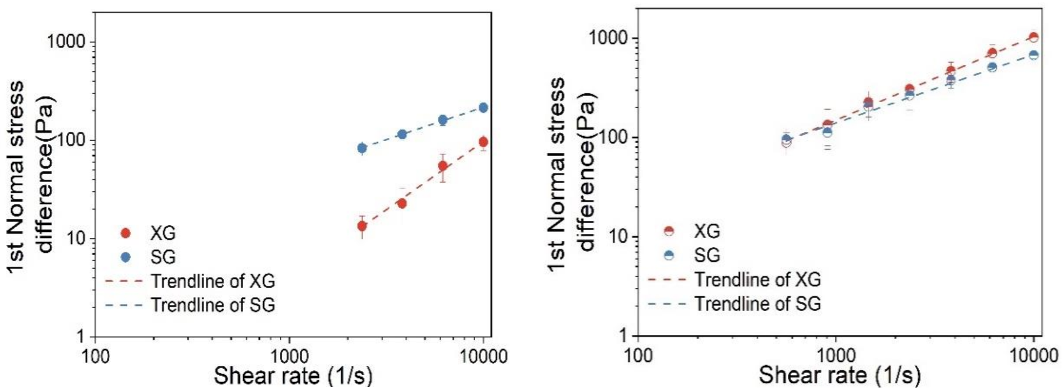

Figure 5.3. The first normal stress of XG solution and SG solution at 20 °C in a logarithm scale. (a): water as the continuous phase: The trendline of XG is $y=0.00028x^{1.39}$; The trendline of SG is $y=0.50x^{0.66}$ (b): 40% sucrose solution as the solvent: The trendline of XG is $y=0.45x^{0.84}$; The trendline of SG is $y=1.2x^{0.69}$

5.3.3 Shear rheological analysis of mixing biopolymers with HWS and RS

XG and SG have comparable shear rheological behaviour and linear viscoelasticity under the same concentration. It is hypothesized that they may also have similar rheological behaviour when mixed with HWS or RS respectively. Figure 5.4 shows the shear rheological properties of biopolymer solutions mixed with water (control samples), HWS or RS for 5 min. The mucin concentration of RS is 30 mg/ml, as it was previously suggested that this concentration of mucin can mimic the rheological behaviour of the HWS (Sarkar et al., 2009, Gal et al., 2001). The viscosities of both XG and SG solutions are higher when the continuous phase is 40% sucrose solution.

HWS and RS has little impact on the biopolymer solutions under steady shear rheological analysis. This finding also corresponds to the finding of the previous research made by Choi et al. (2014).

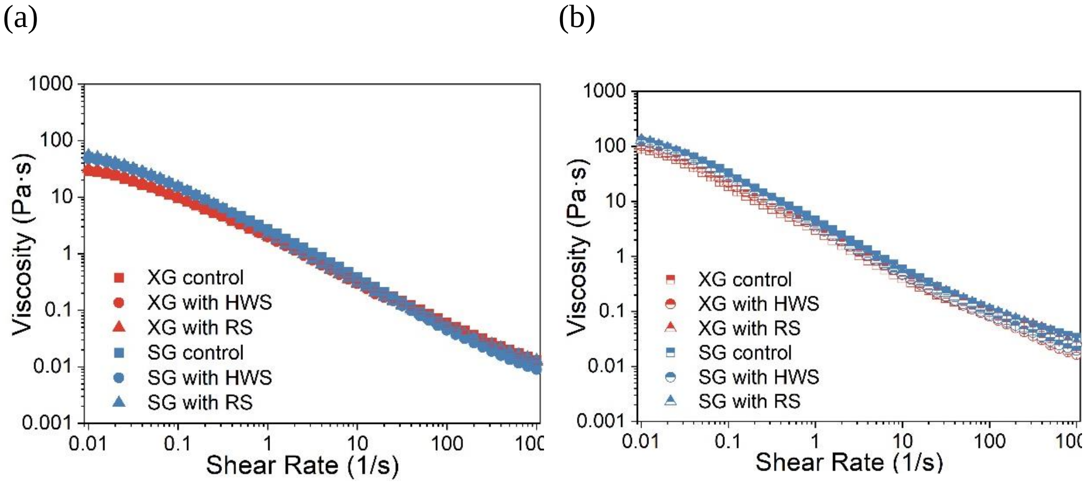

Figure 5.4. The shear rheological properties of 0.5% XG control samples (red square symbols), 0.5% XG with HWS samples (red circle symbols) and 0.5% XG with RS samples (red triangle symbols); 0.5% SG control samples (blue square symbols), 0.5% SG with HWS samples (blue circle symbols) and 0.5% SG with RS samples (blue triangle symbols) (a): water as the continuous phase (full symbol), (b): 40% sucrose solution as the continuous phase (half-filled symbol) at 20 °C

The storage and loss moduli of biopolymer solutions (40% sucrose solution as the solvent) are higher than the aqueous solutions (Figure 5.5a and Figure 5.5b), indicating that XG/SG in 40% sucrose solutions have more gel-like structures (Figure 5.5c, 5.5d, 5.5g and 5.5h). Moreover, SG has more elastic dominant structure than XG as tanδ of

SG is slightly lower (Figure 5.5e, 5.5f, 5.5g and 5.5h). It is also possible to suggest that 40% sucrose introduces changes in solvent quality, resulting in different degree of interaction between hydrocolloid polysaccharides and mucin/salivary proteins. Like steady shear rheological measurement, it is also found the addition of HWS and RS have little or no impact on the biopolymer solutions, which prompts the same finding that addition of saliva (at concentrations explored) has minimum impact on rheological properties of hydrocolloids (Choi et al., 2014). These results suggest that small changes in relaxation profile within mixed biopolymer systems is amplified by dissolving polymers in more viscous matrix.

(a)

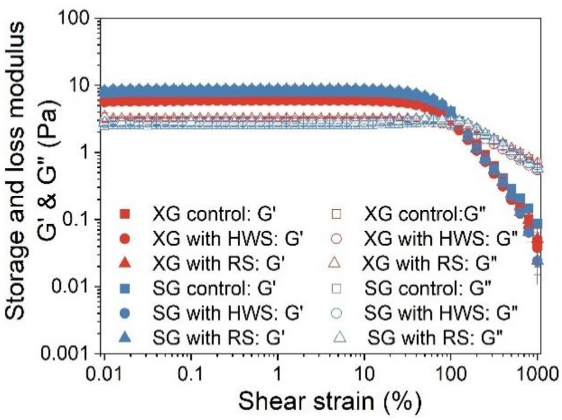

(b)

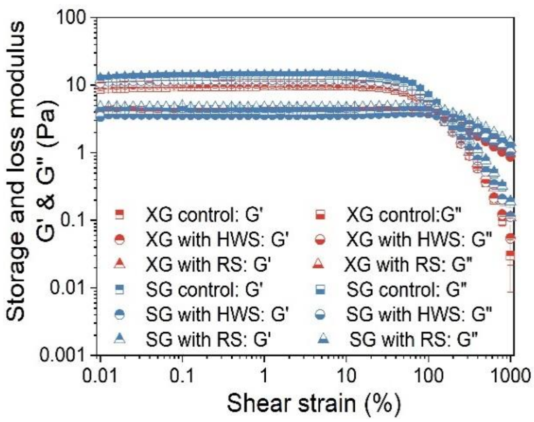

(c)

(d)

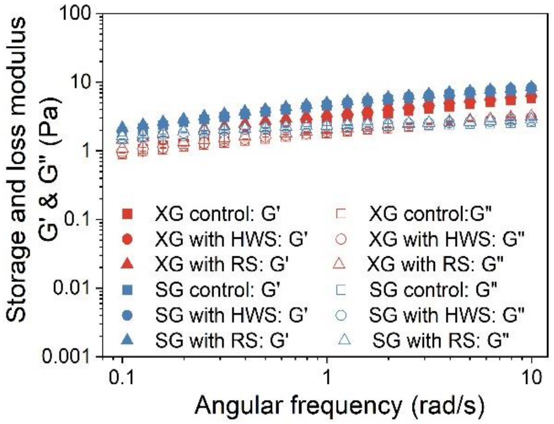

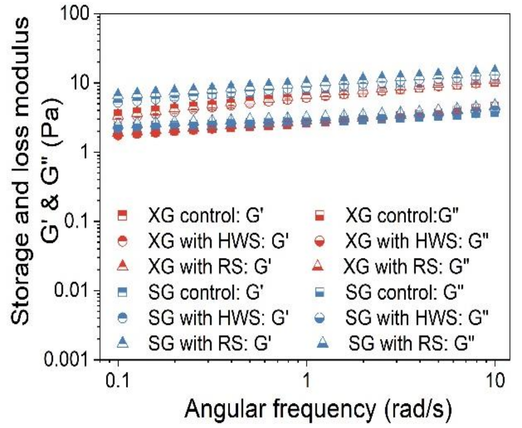

(e) (f)

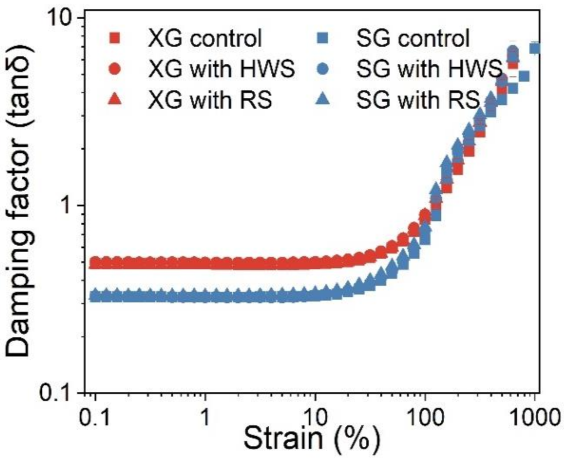

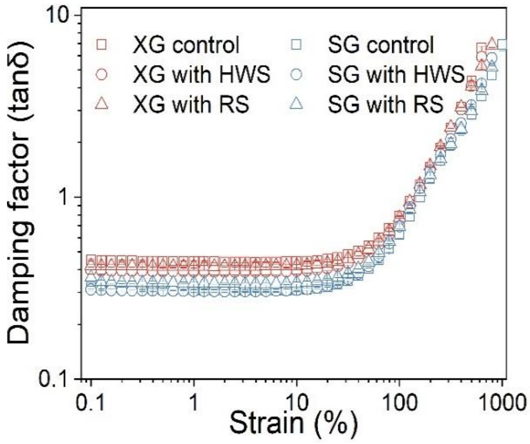

(g) (h)

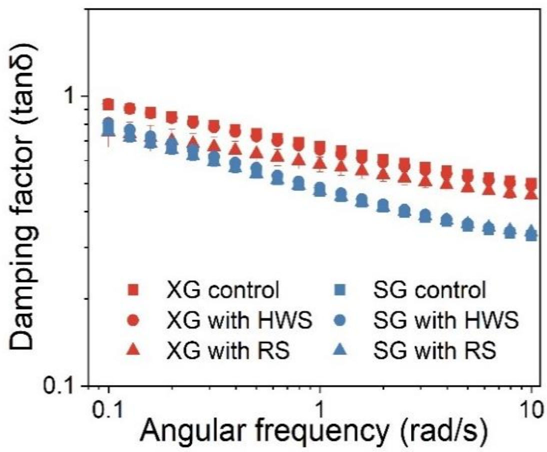

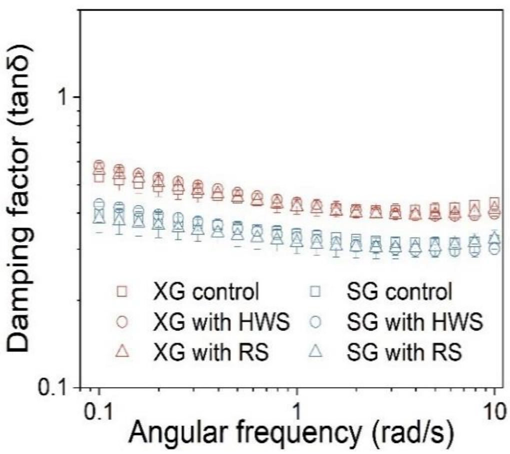

Figure 5.5. The small deformation rheological analysis of 0.5% XG control samples (red square symbol), 0.5% XG with HWS samples (red circle symbol) and

0.5% XG with RS samples (red triangle symbol); 0.5% SG control samples (blue square symbol), 0.5% SG with HWS samples (blue circle symbol) and 0.5% SG with RS samples (blue triangle symbol) (a): Amplitude sweep test of XG and SG dissolved in water: full symbol represents the storage modulus and void symbol represents the loss modulus, (b): Amplitude sweep test of XG and SG dissolved in 40% sucrose solution: top filled symbol represents the storage modulus and bottom filled symbol represents the loss modulus, (c): frequency sweep test of XG and SG dissolved in water: full symbol represents the storage modulus and void symbol represents the loss modulus, (d): frequency sweep test of XG and SG dissolved in 40% sucrose solution: top filled symbol represents the storage modulus and bottom filled symbol represents the loss modulus, (e) amplitude sweep test of XG and SG dissolved in water: damping factor (tanδ), (f) amplitude sweep test of XG and SG dissolved 40% sucrose solution: damping factor (tanδ), (g) frequency sweep test of XG and SG dissolved in water: damping factor (tanδ), (h) frequency sweep test of XG and SG dissolved in 40% sucrose solution: damping factor (tanδ) at 20 °C

5.3.4 Extensional Rheological analysis of control and saliva samples

5.3.4.1 Aqueous biopolymer solutions mix with HWS or RS

The extensional rheological behaviour of mixing hydrocolloids with HWS or RS will be explained in this section. Figure 5.6 shows the decay in the normalized diameter of

XG and SG solution samples with time. It was shown that both XG solution and SG solution have two regimes, i.e., exponential regime and linear regime. This was also validated by previous researchers (Stelter et al., 2002, McKinley, 2005). The relaxation time can be calculated by Eq. 5.1 from the exponential region in the filament break-up curve. The steady state extensional viscosity can be calculated by Eq. 5.2 from the linear region of the filament break-up curve, which are mainly impacted by the surface tension and the slope of the linear region of the filament break-up curve.

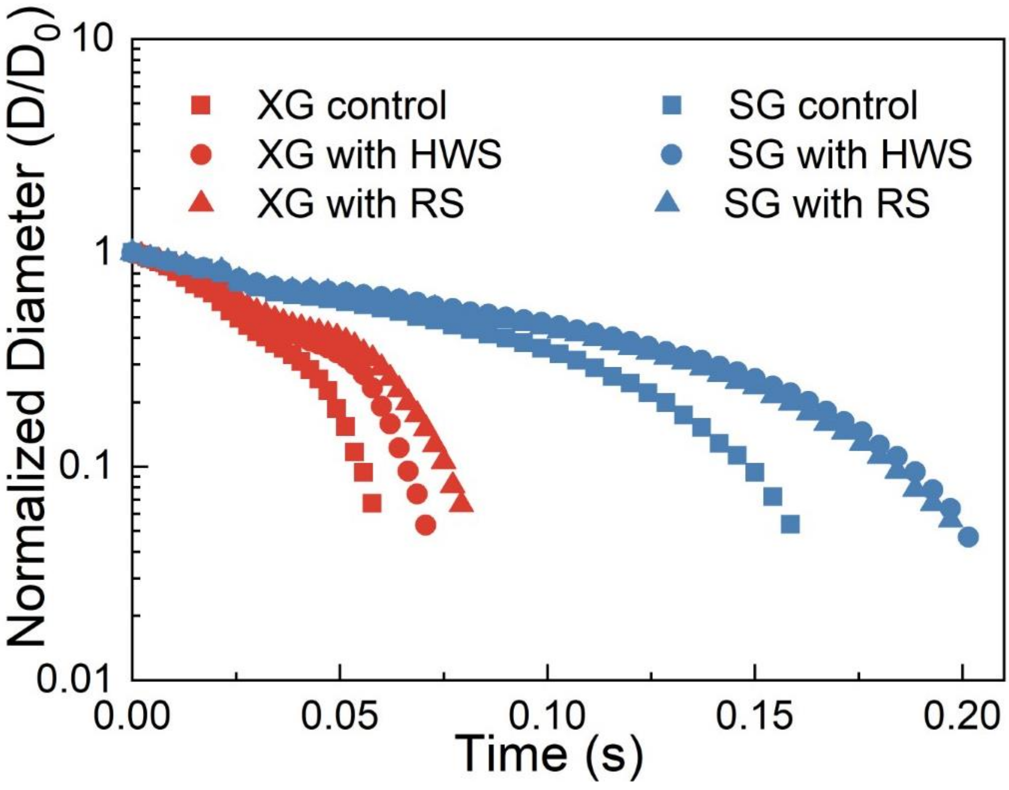

Figure 5.6. The normalized diameter of 0.5% XG (red symbol) and 0.5% SG solution (blue symbol) mixed with water (square symbol), HWS (circle symbol) or RS (triangle symbol) as a function of time with the mixing stirring time under 2 min at 20 °C (water as the solvent)

Figure 5.7 shows the filament break-up time, the relaxation time and the steady state extensional viscosity of the biopolymer solutions mixed with water (control samples), HWS or RS under different stirring time. The concentrations of the biopolymer solutions are 0.5% for carrying out the extensional rheological analysis. The filament break-up time of XG solutions and SG solutions were measured by several previous studies (see for example (Turcanu et al., 2015, Sousa et al., 2011, Japper-Jaafar et al., 2009)), and the values of filament break-up time can vary with different final gap setting and different strike time. The filament break-up time, the relaxation time and the steady state extensional viscosity of SG solutions were two times higher than the XG solution. This result was not expected from the analysis of the steady shear rheological behaviour of 0.5% XG and SG solutions (see Figure 5.1 for reference). In line with the hypothesis formulated based on the examination of the normal force data, it is possible to suggest that faster relaxation modes in XG may contribute to the faster filament breakup. In addition, the stability of supra-molecular association can play a significant role. These data are consistent with previous AUC data (Chapter 4) suggesting that SG assemblies may be more stable compared to that formed in XG solutions.

More surprisingly, it is found that mixtures or biopolymer solutions with HWS or RS show a markedly longer break-up time compared to pure polysaccharide. Although there is no clear explanation of these observations, we can propose that interaction between salivary proteins and polysaccharide hydrocolloid may occur during the extensional deformation of polysaccharides. It is possible to hypothesise that in the extended state, where conformation flexibility is reduced, the reduction in entropy may be compensated by the condensation of salivary proteins and mucins onto the extended polysaccharide chains. Addressing this hypothesis would require future research and probing the detailed structure and molecular alignment during liquid bridge formation.

Unlike the trend in filament break-up time and relaxation time, the steady state extensional viscosity of XG control samples is higher than the HWS samples (Figure 5.7c). It may be caused by the negative charged of XG. When mixed with HWS, the charges on inorganic compounds and the charged salivary proteins (such as mucin or glycoproteins) may have the repulsion force to the side chain of XG, which may influence the steady state extensional viscosity. However, for the RS, the charges are less complex than the HWS, which lead to different extensional viscosity. For the SG solutions, the steady state extensional viscosity of HWS samples is slightly higher than the RS samples and control samples (Figure 5.7c).

From the processing perspective, the effect of the stirring time on the filament break-up time, relaxation time and steady state extensional viscosity was also explored. The effect of time and saliva "aging" is well documented, and it was hypothesised that stirring time will expose the effect of saliva proteolytic degradation and its impact on extensional rheology of XG and SG. It is suggested that RS can be more stable than HWS under ANOVA test (Supplementary table 4). However, the observed changes of hydrocolloids-HWS mixture samples are within the experimental error. Two possible explanations have been proposed; first, the saliva degradation is offset by the dilution effect, and second, most of the degradation occurs within first 2 minutes of mixing, with further mixing time having little effect.

(a)

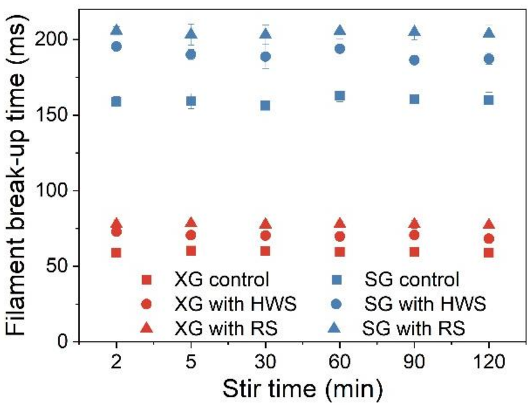

(b)

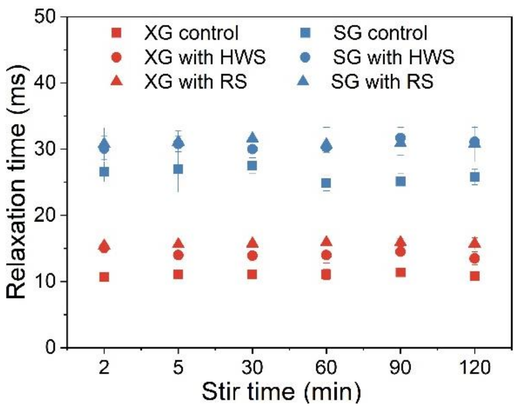

(c)

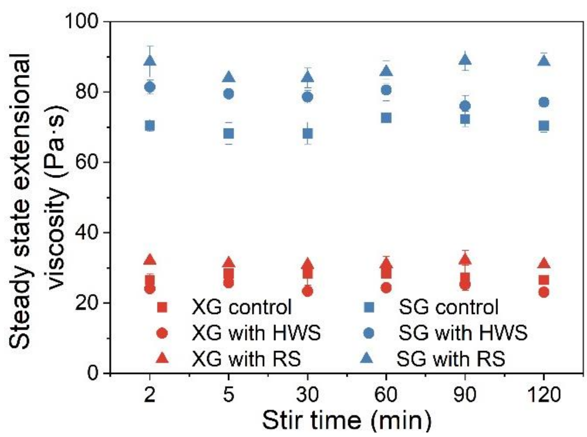

Figure 5.7. (a) The filament break-up time, (b) relaxation time, (c) steady state extensional viscosity of control (square symbol), HWS samples (circle symbol) and RS samples (triangle symbol) of XG (red symbol) and SG solution (blue symbols) under different stir time

5.3.4.2 Biopolymer solutions (40% sucrose solution as the solvent) mix with HWS or RS

With the target of investigating the HWS or RS on the biopolymer solutions under higher viscosity, 40% sucrose solution as the continuous phase. Both XG and SG solutions have more gel like structure under shear rheological analysis (Figure 5.5). It is also found that when mixed biopolymer solutions with HWS, the results were impacted by the deterioration of human whole saliva (Figure 5.7 and Supplementary table 2 and 3). Therefore, 5 min stirring time was chosen in this experiment. Figure 5.8 shows the filament break-up time, the relaxation time and the steady state extensional viscosity of the biopolymer solutions (40% sucrose solution as the solvent) mixed with water (control samples), HWS or RS under 5 min stir time. SG solutions have higher filament break-up time, relaxation time and steady state extensional viscosity than XG. When mixed biopolymer solutions with HWS or RS, the filament-break up time, relaxation time and steady state extensional viscosity was prolonged except the steady state extensional viscosity of xanthan gum. Moreover, when compared data of both 0.5% XG and 0.5% SG dissolved in water under 5 min stirring time (Supplementary figure 2), it is found that the differences of filament break-up time, relaxation time and between the XG and SG are smaller, which also corresponds to the 1st normal stress difference results.

(a) (b)

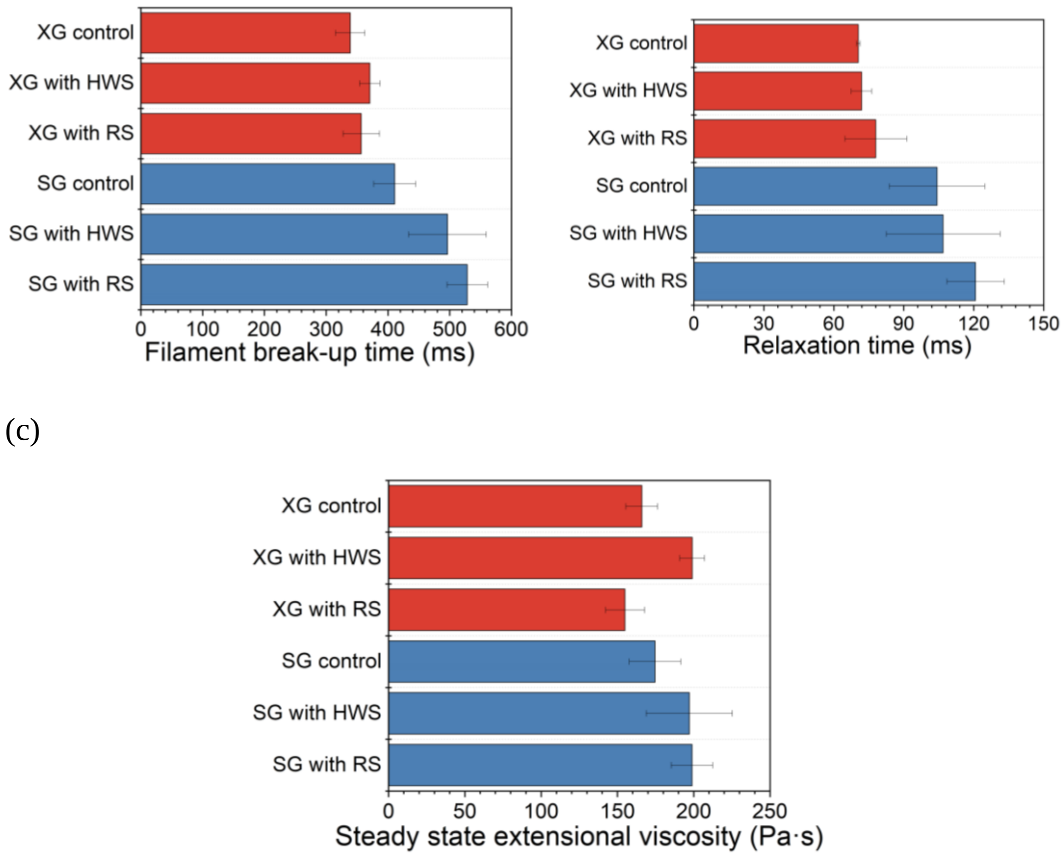

Figure 5.8. The (a) filament break-up time, (b) relaxation time, (c) steady state extensional viscosity of control, HWS samples and RS samples of XG and SG solution (40% sucrose solution as the solvent)

5.4 Conclusions

In this research, it is found that XG and SG have similar steady shear and viscoelastic behaviour. However, subtle changes in dynamics and stability of supra-molecular assemblies were revealed by analysing differences in the 1st normal stress difference and extensional rheological behaviour. Further, when biopolymer solutions were mixed with HWS or RS, steady shear and oscillatory shear rheological measurement are not sensitive enough to detect the small difference. For the extensional rheological measurement, the filament break-up time and relaxation time were prolonged for both XG and SG solutions. RS have comparable results as HWS, and RS is more stable than HWS. The hydrocolloids-HWS mixtures and hydrocolloids-RS mixtures have comparable filament break-up time, relaxation time and apparent steady state extensional viscosity. However, the ANOVA test of hydrocolloid-HWS show that the filament break-up time, relaxation time and apparent steady state extensional viscosity decrease with the increasing stirring time (Supplementary table 4).

Turcanu et al. (2015) found that when XG solution is mixed with acidic saliva, the filament break-up time and relaxation were significantly prolonged. For future research, the mechanism of different types of stimulated saliva with biopolymer solutions can be studied. Further, the biopolymer solutions may also be mixed with other different food proteins than mucin (such as casein). Moreover, the biopolymer solutions can also be mixed with other salivary proteins with lubrication property, such as PRPs. These studies may help to understand and to build different food system and saliva proxy.

It was previously reported that XG has better flavour release ability than many random coil food industry polysaccharides such as guar gum (Cook et al., 2003). The insights gained in this research may also help to further explain observations on taste perception from rigid rod versus random coil food thickeners. Previous research done by Choi et al. (2014) compared CMC with XG, and found that HWS have less noticeable impact on CMC compared to XG. However, CMC does not have comparable molecular weight as XG. Dextran is a random coil polysaccharide and different types of dextran products have different molecular weight. The molecular weight of dextran T2000 is ~ 2 million Dalton, which is comparable to XG and SG. Some trial experiment of using dextran (T2000) were done. When the concentration of dextran solution is 20%, it has comparable filament break-up time as 0.5% XG solution (Supplementary table 5). Unlike the extensional rheological behaviour of CMC biopolymer (Choi et al., 2014), the difference between the control sample and saliva samples of dextran solutions are more significant. However, dextran T2000 does not have comparable thickening effect as XG or SG. In future research, random coil polysaccharide with higher viscosity and comparable molecular weight can be compared with XG or SG, for example pullulan (P800).

Chapter 6 Probing interactions of xanthan gum and scleroglucan with bovine submaxillary mucin and human whole salivary surface films using soft-contact tribology

Abstract

Xanthan gum (XG) and scleroglucan (SG) are both rod-like polysaccharides that form entangled solution. The small differences of molecular conformation between XG and SG can be detected under high-shear (1,000 s^{-1} to 10,000 s^{-1}) rheological behaviour (Chapter 5). Here we evaluate how these changes in high shear behaviour would impact their lubrication properties and whether these differences may have impact on their interaction with salivary films. The results show that XG and SG solutions with matched viscosity show similar tribological behaviour between hydrophobic PDMS substrates. SG solutions have higher friction coefficient than XG under the same concentration. Concentrations have little impact on friction coefficient for SG. When substrates are modified with a film formed by bovine submaxillary mucin (BSM) the SG shows high friction compared to XG, which we associate with changes in the micro hydrodynamic behaviour during BSM desorption. In comparison, the highly lubricated films formed using whole human saliva remained unperturbed by the presence of both thickeners.

6.1 Introduction

Many food research and development tasks require making a choice of an instrumental technique for characterising flow and lubrication behaviour of food biopolymers and for exploring their interactions with other ingredients or biological interfaces. Combining different instrumental techniques presents a powerful approach that enables capturing different aspects of biopolymers behaviour at different length and time scales (Stokes et al., 2013, Witt and Stokes, 2015, Stribiţcaia et al., 2020, Krop et al., 2020). In the context of food product development, however, the combined approaches may present a number of practical challenges. Complexity of experimental design, difficulty of execution and results interpretation, as well as availability of instrumentation and considerable time investment, may restrict wide adoption and impede practical utilisation. To address this problem and provide a simple comparison of instrumental techniques, we seek to examine the flow, viscoelastic and lubrication behaviour of two very similar hydrocolloid thickeners: xanthan gum (XG) and scleroglucan (SG). It is expected that different techniques would show selective sensitivity. Further, we seek to utilise techniques to examine the interaction of hydrocolloids with salivary protein, including human whole saliva (HWS) and reconstituted saliva (RS). The results of using rheological techniques were explained in Chapter 5, which found that XG and RS have comparable steady shear rheological behaviour and linear viscoelasticity. However, XG and SG have different non-linear viscoelastic behaviour and elongational rheological behaviour. In this chapter, we seek to utilise tribological tools to extend the study.

There are limitations of rheological model when comes to oral processing. Upon ingestion of food products, the rheological behaviour analysis of food systems is more applicable in the first stage of oral processing. With the time of mastication, tribological analysis starts to play a more important role as food has been processed into smaller particles in micrometre scale (Stokes et al., 2013, Stokes, 2012b, Chen and Stokes, 2012, Yakubov, 2014). Shewan and Stokes (2020) also claimed that rheology focuses more on the properties of the material while tribology focuses more on the properties of the system. The limitation of rheological test also becomes more obvious when it comes to semi-fluid or fluid food products (Chen and Stokes, 2012). Further, the surface properties also cannot be analysed by solely rheological tests. Tribological study may help to determine the sensory aspect of food products as rheological study cannot analyse the sensory aspects of food products, such as astringency (mayonnaise as an example) (Stokes, 2012b). It is therefore important to identify the tribological properties of SG and XG solutions, and the mixture of SG/XG solutions with HWS or RS. When processed food in oral cavity, most surfaces in the oral cavity are soft except the teeth (Yakubov et al., 2009, Yakubov, 2014). Thus, soft contact tribology can mimic the oral lubrication environment better, which gives a more accurate prediction than hard surface tribological study in oral processing area.

Saliva plays a significant role during food and beverage ingestion. Previous studies stated that proteins in saliva, such as mucin, proline-rich protein and statherin have the function of lubrication in oral cavity, and mucin is believed as the best lubricant among them all (Cárdenas et al., 2007, Douglas et al., 1991, Bongaerts et al., 2007b, Boze et al., 2010, Humphrey and Williamson, 2001). Mucin is also highly viscoelastic among salivary proteins. It has both hydrophilic and hydrophobic zones, which may lead to hydrophobicity of HWS (Cárdenas et al., 2007). Cárdenas et al. (2007) compared the absorbed films formed by MUC5B and saliva, who suggested that the MUC5B can play an important role of the anchoring layer of salivary films. Mucin also tend to be the dominant protein to provide saliva the barrier properties (Cone, 2009, Stokes et al., 2013). It was found that 30 mg/ml mucin solution can mimic the rheological behaviour of HWS (Sarkar et al., 2009, Gal et al., 2001), which was also confirmed in Chapter 5. Therefore, it is worth to extending the tribological study to test whether RS can be a proxy for HWS to circumvent the deterioration of HWS. Further, RS can be easily prepared and using RS may circumvent the biological risk of collecting and using HWS (such as the risk of getting infection with hepatitis B). There were few studies regarding on the differences of the tribological behaviour of RS and HWS, and their mixture with rod like hydrocolloid solutions.

In this chapter, it is aimed to underly the tribological properties of rod-like shape polysaccharide solutions (XG and SG) by plotting Stribeck curves under different concentrations. Further, we investigate the interaction of the polysaccharide solutions (XG and SG) with expectorated human whole saliva as well as model mucin formulation, based on bovine submaxillary mucin and a cocktail of salts mimicking the ionic environment of human saliva. Last but not least, the kinetic tests were also carried out with the target of investigating the film formation of HWS or RS under boundary lubrication.

6.2 Materials and methods

6.2.1 Materials and solution preparation

The two rod-like biopolymers used in this study were xanthan gum (Keltrol-T, CP Kelco, Surrey, UK) and scleroglucan (Carbosynth, Compton, UK). XG was used as received while SG was dialyzed, freeze-dried and re-dissolved as solutions. Details of purifying SG can be found in Chapter 5.2.1.2. All water used in experiments was reverse osmosis treated water (DI water) with resistivity of 18.2 MΩcm (Satorius Stedim).

1% (w/v) XG and SG stock solutions were prepared respectively in the first place. 0.2% (w/v) sodium chloride solution was used as the solvent for dissolving XG solution. During dissolving process, the solution was heated up slowly to 80 °C for one hour under gentle stirring. After preparation, the 1% (w/v) stock solution was cooled down in room temperature and left overnight before further dilution and usage. SG stock solution was prepared by using the same protocol while using double-distilled water as the solvent.

0.5% (w/v) XG and SG in 40% sucrose solution were also prepared with the target of increasing the viscosity of the solvent while maintaining its Newtonian rheological behaviour. The detailed solution preparation protocol can be found in Chapter 5.2.1.2.

For the kinetic tests, 0.1% (w/v) biopolymer solutions (XG/SG) were prepared in PBS buffer (pH = 6.8, I = 0.056) (Sarkar et al., 2009). The buffer is used to minimise changes of ionic environment upon contact with saliva (Macakova et al., 2011, Macakova et al., 2010).

6.2.2 Saliva/reconstituted saliva collection and mixture preparation

The mechanically stimulated saliva was collected from a single donor (female, 29 years old, non-smoking). Saliva was obtained in the morning and the donor was asked not to eat or drink for at least 2 h before saliva donation. The volunteer was asked to chew on a 5cm × 5cm of parafilm (Parafilm, Bermis Flexible Packaging, Neenah, USA) to donate saliva. The detailed collection protocol can be found in Chapter 5.2.2. The collected saliva was centrifuged at 10,000 g for 30 min at 4 °C and used immediately after the donation.

The reconstituted saliva was prepared by dissolving 3% (w/v) bovine submaxillary mucin (BSM) in PBS buffer. The protocol of preparing PBS can be found in Chapter 5.2.3. The BSM solution was stirred for 30 min at 4 °C. The prepared reconstituted saliva should be kept at 4 °C for storage and should be used within two weeks.

For the Stribeck tests, the biopolymer solutions were mixed with HWS/RS with the weight ratio of 1:5 for 5 min. The mixing ratio was followed the protocol published by Choi et al. (2014). The control samples were produced by mixing biopolymer solutions with double distilled water.

6.2.3 Stribeck tests

MTM-2 mini traction machine was used to perform friction measurement (MTM-2, PCS Instruments Ltd., UK). The rubbing contact surfaces are polydimethylsiloxane (PDMS) (SYLGARD® 184 Silicon Elastomer Kit, Dow Corning, MI) ball with the radius of 0.95 cm and PDMS disk with the radius of 23 mm and the thickness of 4mm. The Young's modulus is 2.4 MPa (Bongaerts et al., 2007a). Both PDMS surfaces are smooth and hydrophobic. The schematic figure of the equipment can be found in Figure 3.12. The normal force was applied on the ball during tribological tests. The friction force can be measured between the rotating disk and the rotating ball. In a typical MTM experiment, the ball and disc are driven independently at velocities v_{ball} and v_{disk} respectively, yielding the entrainment speed $U = (v_{\text{ball}} + v_{\text{disk}})/2$. The relative motion of the moving ball and disc determine the slide-to-roll ratio, SRR = $|v_{\text{ball}} - v_{\text{disk}}|/U$. In all experiments, the SRR was set at 0.5 (50%). To prevent offset errors, lateral force measurements are taken at each entrainment speed when $v_{\text{ball}} > v_{\text{disk}}$ and

$v_{ball} < v_{disk}$, both rotating in the same direction, and the average was taken. Further details of the soft contact friction experiments are also presented elsewhere (Yakubov et al., 2009, Bongaerts et al., 2007a).

During the test, a load, L, is applied onto the ball and the normal force is measured using a strain gauge installed on the leaf spring of the MTM. In all experiments, L was set to 1 N. The lateral friction force, F_f, and the normal load yield the friction coefficient, $\mu = F_f / L$. One way of representing friction in different lubrication regimes is using a Stribeck curve, in which the friction coefficient is plotted against the product of U and the viscosity. For each entrainment speed, at a constant SRR, five friction measurements are taken and averaged. To test for hysteresis, each entrainment speed is tested twice in the same experiment; measurements are first taken from the highest speed 1000 mm/s and the speed is stepwise decreased to the lowest speed of 1 mm/s, after which the speed is increased again to 1000 mm/s. The tests were done with an inset to reduce the sample volume to 17 ml per run.

6.2.4 Friction measurement with the dynamic tribology protocol (DTP)

Here we utilise the Dynamic Tribology Protocol (DTP) to probe the interaction of the salivary film with hydrocolloids. DTP has been utilised before (Rossetti et al., 2009, Yakubov et al., 2015) and has recently received a thorough development by (Fan et al., 2021). During a typical DTP test performed using MTM, the pre-adsorbed salivary pellicle is formed on hydrophobic PDMS surfaces, and friction coefficient at constant speed is recorded as a function of time. At specific time point the hydrocolloid solution is added to the MTM chamber, and the temporal response of friction is recorded. Upon the exposure of salivary film to hydrocolloid the interaction changes the properties of the surface film resulting in changes in the friction coefficient. Typically, saliva is characterised by very low friction coefficient (μ = 0.005-0.05), and the binding of HWS/RS to the hydrocolloid results in the loss of lubrication during the measurement. In all experiments, the pre-adsorbed salivary film was formed on hydrophobic PDMS as an oral mimic (contact angle ca. 100°) (Rossetti et al., 2009).

The DTP curves of polysaccharide interaction with pre-adsorbed salivary/mucin film were recorded using MTM-2 at constant speed of 6 mm/s. Under this speed, HWS or RS can form a film on the hydrophobic PDMS surface with high lubrication (Rossetti et al., 2009, Bongaerts et al., 2007b). The pot was open during the experiment. 0.1% (w/v) biopolymer solutions were used in these tests. 400 μl HWS (or saliva mimetic BSM solution) was transferred by pipette slowly on the disk in the first place to let the saliva form a thin film. The friction coefficient was recorded to monitor the formation process of salivary film. Then 40 mL of 0.1% (w/v) XG or SG solutions (PBS buffer as the solvent) were poured into the pot and the DTP temporal friction response was recorded with the rate of 1 reading/s. The DTP measurements were carried out at 35 °C, mimicking the temperature of the surfaces in oral cavity.

6.3 Results and discussions

6.3.1 Concentration dependence of the Stribeck behaviour of XG and SG

Here the tribological behaviour of XG and SG under different concentrations by plotting Stribeck curves was explored (Figure 6.1). Stribeck curve is one of the most effective way to investigate the friction behaviour of thin fluid film under different entrainment speed between surfaces (Stachowiak and Batchelor, 2013). The film geometry is dependent on the load applied on the upper surface, the viscosity of the fluid and the surface properties (Stokes, 2012b). Stribeck curves have three regimes, which are boundary regime, mixed regime and elasto hydrodynamic regime (Chen and Stokes, 2012, Stokes, 2012b, Yakubov, 2014). When the entrainment speed is low, the asperities on surfaces can lock the surfaces and lead to wear during the movement, indicating high friction coefficient. When the entrainment speed is high, the fluid film between surfaces can give upper surface a lift force, and the friction coefficient is the smallest. However, with the increase of the entrainment speed, the drag force caused by the surface movement increases faster than the lift force. The friction coefficient will increase again. Between these two regimes, there is a mixed regime, where only a thin layer of fluid is trapped between surfaces. The minimal friction coefficient is at the turning point of the mixed regime and the elasto hydrodynamic regime (de Vicente et al., 2006a).

The y axis of the Stribeck curve is the fiction coefficient and the x axis is $\eta \times U$ (reduced velocity). η is the bulk viscosity of biopolymer solutions and U is the entrainment speed. The unit of $\eta \times U$ is N/m. The low shear viscosity $\eta_{0.01}$ (shear rate at 0.01 s^{-1}) applied in Figure 6.1a and the high shear viscosity (shear rate at 1000 s^{-1}) was applied in Figure 6.1b (Supplementary table 6). The viscosity data were measured by MCR-301 rheometer. The detailed data and method can be in found in Chapter 5. The tribological data under each $\eta \times U$ in the Stribeck curve was measured twice with the target of investing hysteresis. For most Strbeck curves, the results of friction coefficient overlap for both measurements. Since XG solution and SG solution under same concentration have comparative viscosity, the Stribeck curves of XG solution and SG solution under the same concentration are in the similar position. The friction coefficient of XG is in good agreement with several previous publications (see for example (Chojnicka-Paszun and de Jongh, 2014, Stokes et al., 2011, de Vicente et al., 2005)). Further, the friction coefficient of SG also corresponds to research done by Garrec and Norton (2012), who reported friction coefficient of different concentrations of SG at several entrainment speed from boundary regime and mixed regime. SG solutions has higher friction coefficient than XG solutions in the boundary regime under the same concentration. SG solutions also have slightly stronger drop than XG under same concentrations in the mixed regime. As can be seen from Figure 6.1b, most of the data overlap in the mixed regime, which indicates that the viscosity is the dominant factor in this regime in the tribological contacts (Stokes, 2012b). Further, concentrations have little influence on friction coefficient in the boundary regime and the mixed regime for SG solutions. Both XG and SG solutions have nonparallel boundary region, which is caused by the unstable measurement on smooth PDMS surface at low entrainment speed (Xu and Stokes, 2020, Selway et al., 2017). For 1% SG and XG solutions, a clear increase trend can be found in the elasto hydrodynamic regime as the drag force on the upper surface from the fluid can be stronger than low concentration solutions.

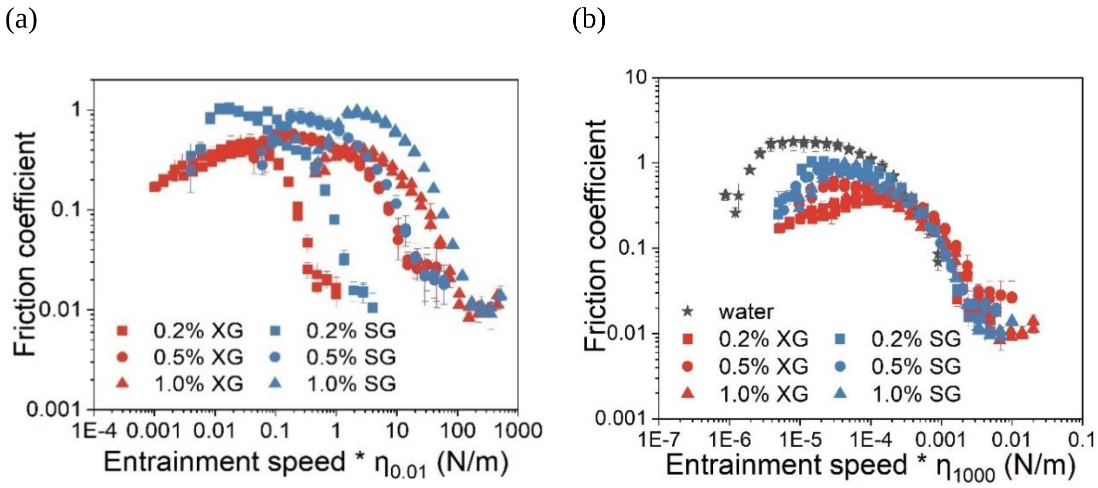

Figure 6.1. Stribeck curves of XG solutions (red symbols) and SG (blue symbols) solution (water as the solvent) with the concentrations of 0.2% (square), 0.5% (circle) and 1% (triangle) at 25 °C: (a) friction coefficient vs $U\times\eta_{0.01}$, (b) friction coefficient vs $U\times\eta_{1000}$ (Each entrainment speed in the Stribeck curve was measured twice to test for hysteresis)

Figure 6.2 show Stribeck curves of comparing XG and SG dissolved in water and in 40% sucrose solution. The x axis is U × the low shear viscosity (viscosity with the shear rate of 0.01 s^{-1}) in Figure 6.2a and the x axis is U × the high shear viscosity (viscosity with the shear rate of 1000 s^{-1}) in Figure 6.2b (Supplementary table 6). The friction coefficient of XG in 40% sucrose solution is higher than XG aqueous solutions. On the other hand, the friction coefficient of SG in 40% sucrose solution and SG aqueous solution in the mixed regime are comparable. The friction coefficient of XG and SG solutions (40% sucrose as the solvent) are more comparable than aqueous solutions, which corresponds to previous results of N_1 and extensional rheological measurement in Chapter 5. The curves of XG in 40% sucrose solution and SG in 40% sucrose solution collapse in the mixed regime in Figure 6.2b, suggesting that viscosity is the dominant parameter in this regime. When dissolved biopolymers (XG and SG) in 40% sucrose solution, the elasto hydrodynamic regimes are extended and the boundary regime is shortened because 40% sucrose solution can provide bigger drag force than water.

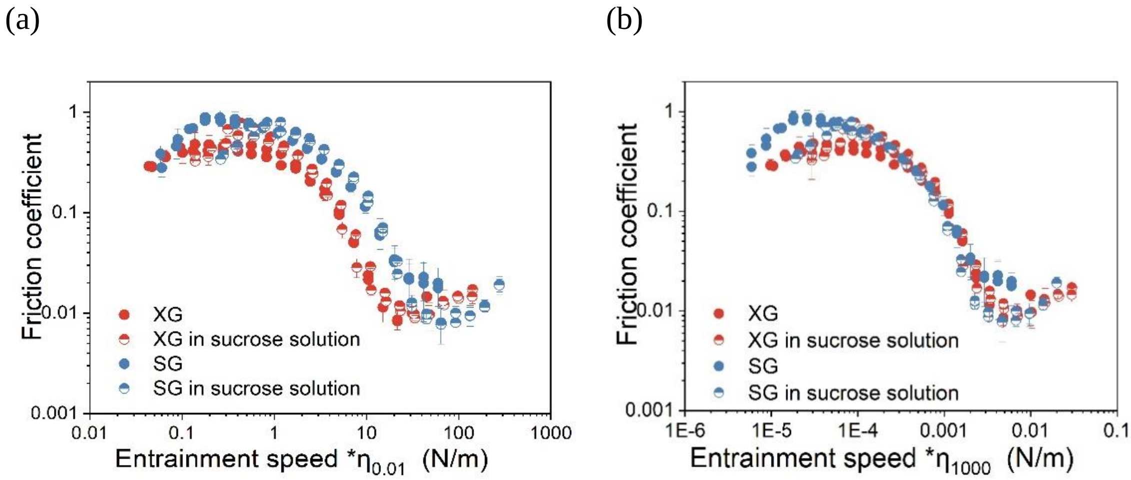

Figure 6.2. Stribeck curves of comparing 0.5% XG solutions (red symbols) and 0.5% SG solutions (blue symbols) in water or in 40% sucrose solution at 25 °C: (a) friction coefficient vs $U\times\eta_{0.01}$: water as solvent (full symbol) and 40% sucrose

solution as the solvent (top full symbol), (b) friction coefficient vs $U \times \eta_{1000}$: water as solvent (full symbol) and 40% sucrose solution as the solvent (top full symbol) (Each entrainment speed in the Stribeck curve was measured twice to test for hysteresis)

6.3.2 Effect of addition of RS and HWS on Stribeck behaviour

Figure 6.3 shows the Stribeck curves of mixing 0.5% polysaccharide solutions with HWS or RS respectively. It is found that the friction coefficient of XG-HWS and XG-RS mixtures are lower than the control samples in the boundary lubrication regime, and the difference between XG-HWS mixture and control samples is more obvious. The Stribeck curves of XG-HWS mixture samples and XG-RS mixture samples overlap in the mixed lubrication regime due to comparable viscosity of these samples. On the contrary, HWS or RS have little influence on the friction coefficient changes of SG solutions. The SG control samples and SG-HWS or SG-RS mixtures have similar Stribeck curves, which collapse through the whole three lubrication regimes. During the tribological tests, some HWS or RS in the samples may attached to the PDMS surface (Macakova et al., 2010, Yakubov et al., 2009). As XG is negatively charged, there may be some extra external interactions between the salivary or mucin films and the XG solution, which leads to lower friction coefficient in the boundary lubrication regime. SG may have higher propensity to prevent adsorption of salivary proteins or BSM, which may inhibit protein films formation. Further, this result may also suggest that SG and XG have different interfacial adsorption behaviour.

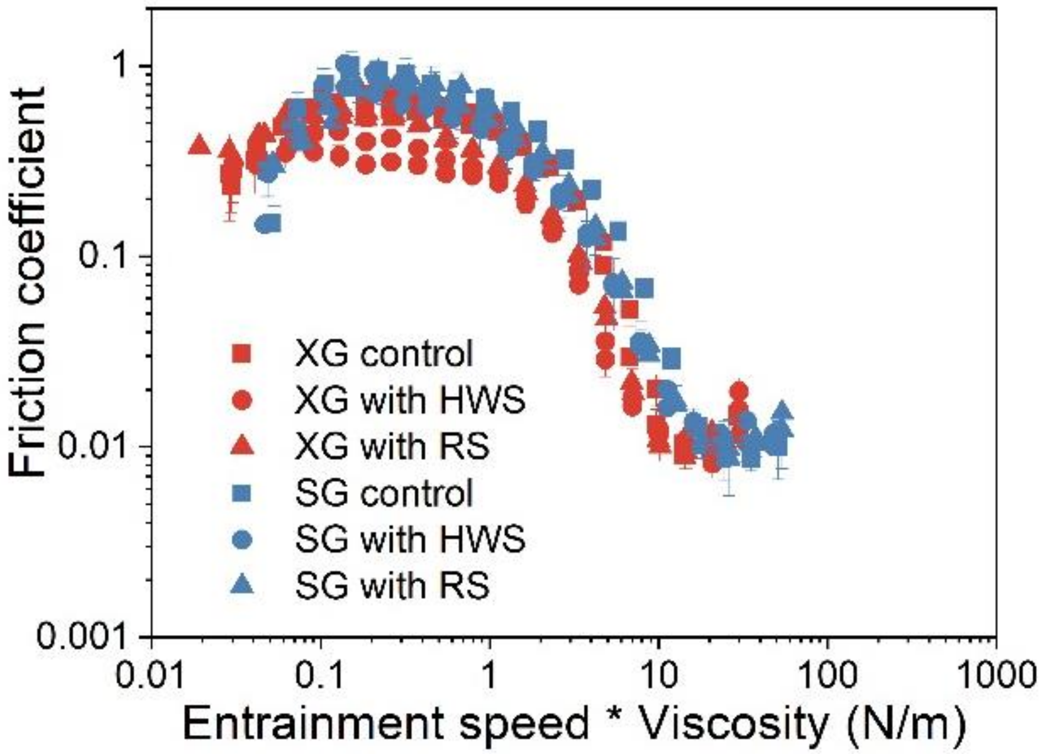

Figure 6.3. Stribeck curves of XG and SG solutions mixed with RS or HWS at 25 °C (Each entrainment speed in the Stribeck curve was measured twice to test for hysteresis)

To probe the effect further of different solvent on biopolymer solutions mixed with HWS or RS, 0.5% XG and SG solutions (40% sucrose solution as the solvent) were mixed with HWS or RS respectively. When compared Figure 6.4 with Figure 6.3, it is found the increase in elasto hydrodynamic regime is more obvious than aqueous solvent due to higher drag force supplied by 40% sucrose solution. Unlike the aqueous solutions, the Stribeck curves of all samples collapse in the elasto hydrodynamic regime, which indicates that the fluid pressure is similar for all these samples. Further, the Stribeck curves of XG-HWS mixture and XG-RS mixture are more comparable with the XG control samples. It can be suggested that the higher viscosity of the solvent can reduce the adsorption of salivary proteins/BSM to the PDMS surfaces. The difference of friction coefficient between SG control and SG-HWS mixture or SG-RS mixture samples can also be negligible.

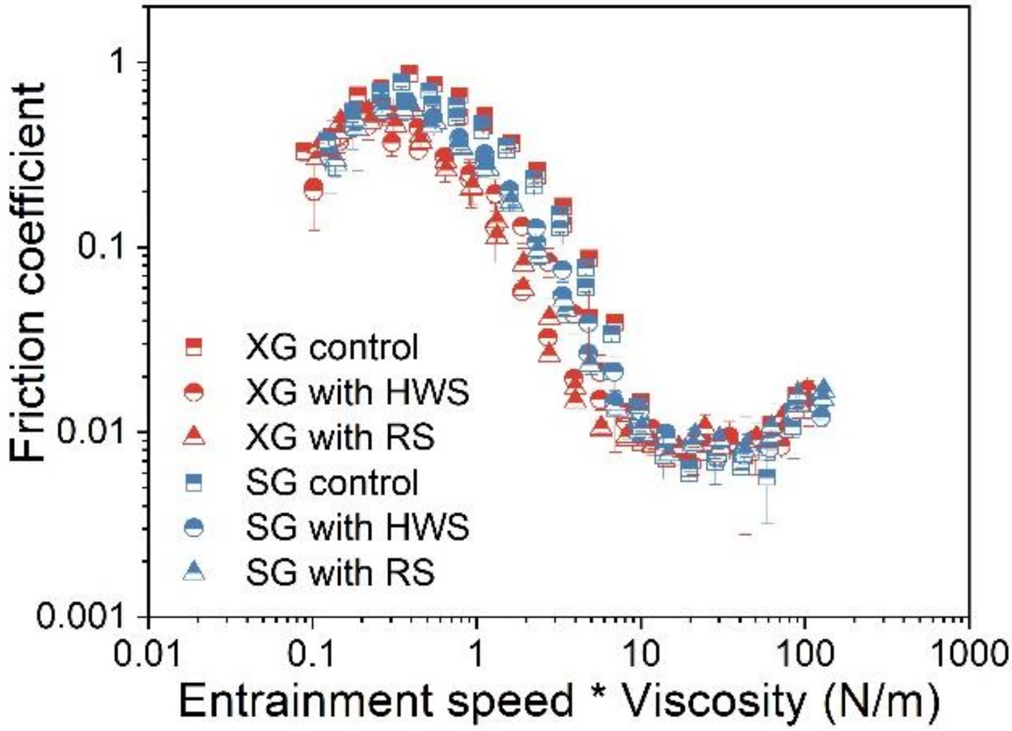

Figure 6.4. Stribeck curves of XG and SG solutions (40% sucrose solution as the solvent) mixed with RS or HWS at 25 °C (Each entrainment speed in the Stribeck curve was measured twice to test for hysteresis)

6.3.3 Kinetics of hydrocolloid/mucin interaction and comparison with whole human saliva

There is not an obvious difference of mixing biopolymer solution with HWS or RS in Stribeck curves, especially the SG solutions. Therefore, it is worth to investigate salivary film or saliva proxy film behaviour by taking DTP tests. HWS and RS are both charged, and they can form films during the low-speed lubrication regime (Macakova et al., 2010, Yakubov et al., 2009). In this test, 400 μl HWS or RS were transferred to the disk slowly under low rotating speed in order to form a thin layer of HWS or RS. The data were recorded in full symbols in Figure 6.5. It is found at this stage, the friction coefficient of HWS and RS are quite comparable, both ranges from 0.03 to 0.12, which corresponds to the friction coefficient measured by previous researchers (Macakova et al., 2010, Bongaerts et al., 2007b, Madsen et al., 2014, Macakova et al., 2011). The similar results of RS and HWS may also suggest that mucin is the main component that provide saliva the lubrication property. Further, it is also suggests that mucin can absorb in hydrophobic surfaces quickly as HWS, which corresponds to the study of Feldötö et al. (2008).

In the second stage, 40 ml XG or SG solutions were poured into the pot of MTM machine, the friction coefficient are presented in void symbols. With the target of mimicking the beverage ingestion in the oral cavity, biopolymers were dissolved in PBS buffer in this test. It is found that the friction coefficient of hydrocolloids-HWS mixtures remained stable. However, for the hydrocolloids-RS mixtures, the friction coefficient increases immediately after pouring the biopolymer solutions in the pot. SG-RS mixture has higher fiction coefficient than XG-RS mixture, which corresponds to the Stribeck curve in Figure 6.1.

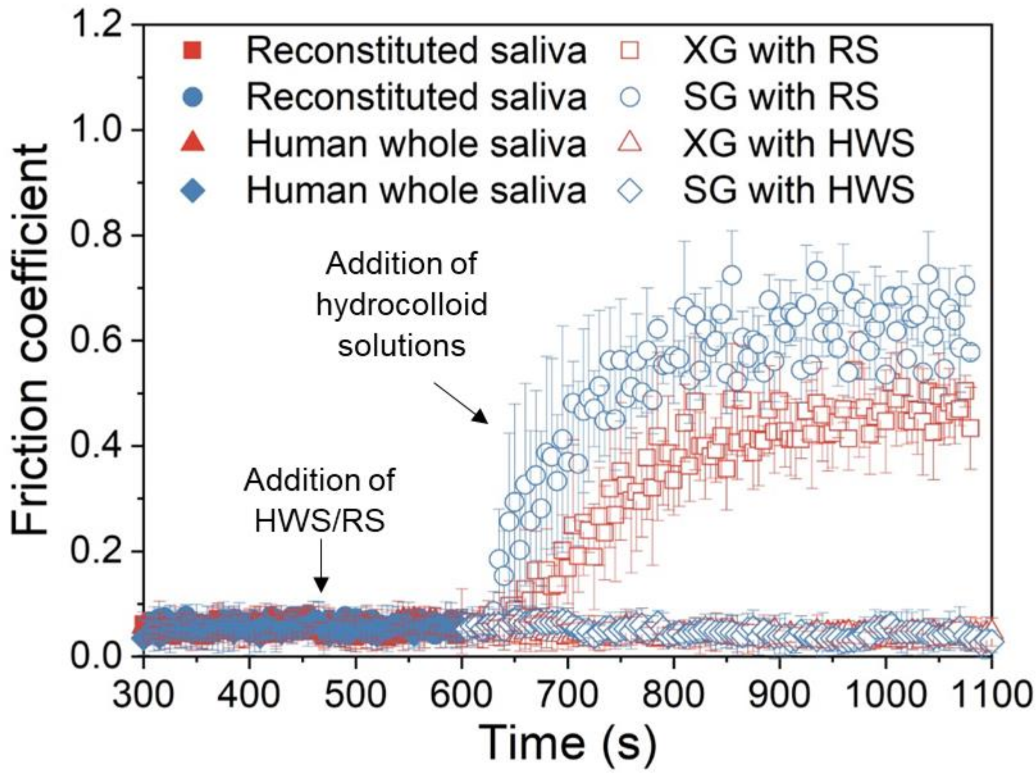

Figure 6.5. Comparison of steady state values of coefficient of friction for XG and SC solutions deposited on pre adsorbed BSM and HWS surface films at 35 °C: Full symbols indicate the HWS or RS film (solely), the corresponding void symbols indicate the friction coefficient after pouring biopolymer solutions (Triplet analysis was done for each sample)

When compared results of hydrocolloids-RS mixture samples with hydrocolloids-HWS mixture samples, it is suggested that the film formed by RS is different as the adsorbed film formed by HWS, which is in good agreement with many previous research (see for example (Kesimer and Sheehan, 2008, Raynal et al., 2002, Yakubov et al., 2014). Most of these studies suggested that mucin cannot mimic the gelling properties of saliva, which implies that the physical properties of HWS cannot fully reproduced by the MUC5B solution. Further, Cárdenas et al. (2007) reported that the film properties of HWS and MUC5B are still different under buffer rinsing and SDS solution rinsing due to different structures. MUC5B in saliva can also bind small molecule protein to form a larger cross-linking structure with the presence of calcium (Yakubov, 2014, Raynal et al., 2003, Wickström et al., 2009). Therefore, with lack of small salivary or non-glycosylated proteins in the anchoring layer for MUC5B film, mucin film cannot mimic the salivary film fully in tribological study (Macakova et al., 2011).

6.4 Conclusion

It is found that SG have higher friction coefficient than XG. The concentration has little influence on friction coefficient of SG solutions. Like the results from N_1 and elongational rheological tests (Chapter 5), when dissolved XG or SG in the 40% sucrose solutions, the difference between XG and SG is minimised.

It is found that SG-HWS/RS and control samples have comparable Stribeck curves, indicating that SG have higher propensity to inhibit salivary films formation. XG-salivary mixtures have lower friction coefficient than control samples, however, the difference is negligible. Therefore, it is possible to suggest that SG can be an alternative hydrocolloid to XG for food and oral care formulations. RS and HWS have different film behaviour in the DTP test, indicating that RS cannot replace HWS in the tribology study due to different film structure on soft surfaces.

Chojnicka-Paszun and de Jongh (2014) reported that XG have better lubrication properties than many commercial random coil polysaccharides including negatively charged pectin when under the same viscosity. Therefore, for the future research, it is worth to compare the lubrication properties of SG with other commercial random coil polysaccharides to investigate whether the rod structure can be a factor influencing tribological properties.

7. Conclusions and Future work

To summarise, there are two main targets of this PhD research: (a) To study the hydrodynamic properties of scleroglucan (SG), which is a possible alternative to xanthan gum (XG); (b) To investigate the interactions between XG/SG solutions and human whole saliva (HWS) /reconstituted saliva (RS). Therefore, at the first stage of the research, the molecular properties of SG were studied by using AUC and SEC-MALS. Further, the rheological and tribological studies were carried out in vitro that mimicked oral processing conditions. The main conclusions are listed in the following subsections: a) The molecular characterisation in Chapter 7.1; b) The rheological characterisation in Chapter 7.2; c) The tribological characterisation in Chapter 7.3.

7.1 Molecular characterisation

The results of SG's molecular characterisation can be summarised into the following key findings:

1. SG has two components with partial reversibility

Sedimentation velocity analysis showed the SG preparation was unimodal at concentrations > 0.75 mg/ml. The unimodal was resolved into two main components at concentrations lower than 0.75 mg/ml and with partial reversibility between the components. These two components account for around 80% of the total distribution and the fast component is impacted more by the hydrodynamic non-ideality than the slow component.

2. SG has partially self-association behaviour

The apparent weight average molecular weight ($M_{w,app}$) increases with the increase of the loading concentration. Usually, for polysaccharides without self-association behaviour, $M_{w,app}$ decreases with the increasing concentration under the thermodynamic non-ideality impact.

3. The molecular weight is around 2.8 million Dalton

For sedimentation equilibrium analysis, when extrapolated $M_{w,app}$ to zero concentration, the value of M_w^o is estimated to be ~ (2.8 ± 0.3) x 10^6 g/mol. Further, similar molecular weight is confirmed by using *Extended Fujita* method. For XG, the molecular weight is ~ 2.0 x 10^6 g/mol.

4. The intrinsic viscosity is around 2191 ml/g

The Huggins and Kraemer extrapolation methods demonstrated very similar values for the intrinsic viscosity, which are (2191 ± 110) ml/g and (2192 ± 110) ml/g respectively.

5. No evidence of interaction between SG and BSM was found by using AUC

The BSM solution (3 mg/ml) and SG solution (0.5 mg/ml) were separately mixed with a weight ratio of 1:5. There was no obvious interactions and aggregations between BSM and SG by conducting sedimentation velocity experiment.

In general, SG has a tendency to self-associate beyond the triple helical structure. It has a comparable molecular weight as XG. Further, when mixed SG with BSM, no evidence of significant interactions between SG and BSM were found.

7.2 Rheological study

Five key results from the rheological study were summarised below:

1. XG and SG have comparable steady shear rheological behaviour and linear viscoelasticity

XG or SG solution with 0.2%, 0.5% and 1% concentration solutions were studied by shear rheological tests and small amplitude oscillatory shear tests. XG and SG showed comparable shear rheological behaviour, particularly in the shear rate range of 1 to 1000 s^{-1}. For 0.5% and 1.0% XG or SG solutions, they have elastic dominant behaviour under the frequency range of 0.1 to 10 rad/s as G' > G".

2. XG and SG have different non-linear viscoelasticity and elongational rheological properties

SG has higher 1st normal stress difference than XG solution, indicating SG and XG have different relaxation spectrum. Further, SG solutions have two times higher filament break-up time, relaxation time and steady state extensional viscosity than XG solutions under the same concentration.

3. When XG and SG dissolved in 40% sucrose solution, the differences between XG and SG are smaller

When dissolving XG and SG in water, SG solution has higher 1st normal stress difference and filament break-up time. However, when dissolved in 40% sucrose solution, the differences between XG and SG were minimised. Further, when using CaBER to study XG/SG in 40% sucrose solution, the differences between XG and SG is also smaller than aqueous solution.

4. CaBER is a sensitive technique to investigate the impact when added HWS/RS

When XG or SG solutions were mixed with human whole saliva (HWS) or reconstituted saliva (RS), the filament break-up time and relaxation time were prolonged for both XG and SG solutions. For the steady state apparent extensional viscosity, XG-HWS mixture is lower than the control samples, which can be explained by the negatively charged side chain of XG. However, for SG solutions, the apparent extensional viscosity of SG-HWS/RS mixtures is higher than the SG control samples. Thus, it is suggested that SG may interact with HWS, especially the salivary proteins (such as mucins or glycoproteins) in a slightly different way than XG.

5. RS can be a proxy for HWS in rheological study

RS can be a replacement for HWS in rheological study as biopolymer solutions-HWS mixtures and biopolymer solutions-RS mixtures have comparable results under shear and elongational rheological tests. Further, the CaBER results of biopolymer solutions-RS mixtures varied little with the increasing stir time at room temperature. On the other hand, the CaBER results of rod-like biopolymer solutions-HWS mixtures decrease with the increase of stir time. It is further suggested that RS is more stable than HWS at room temperature.

In summary, XG and SG have comparable shear rheological behaviour and linear viscoelasticity. But SG has higher first normal stress difference and higher filament break-up time than XG. When mixed XG or SG with salivary samples, CaBER is the most sensitive technique to detect the differences between biopolymer solutions-HWS mixtures and control samples.

7.3 Tribological study

The results from tribological study were outlined in the following areas:

1. SG has higher friction coefficient than XG

SG solution has slightly higher friction coefficient than that of XG solution under the same concentration (Figure 6.1). Further, the friction coefficient of SG decreases more remarkably than XG in the mixed regime.

2. Concentrations have limited impact on friction coefficient of SG solution

The concentrations had no significant impact on the friction coefficient changes of SG solution, especially in the boundary and the mixed regime. For 1% SG solution, the elasto hydrodynamic regime has an obvious increase compared to lower concentrations (0.2% and 0.5%).

3. When XG/SG were dissolved in 40% sucrose solution, the differences of Stribeck curves between XG and SG were minimised

When XG/SG were dissolved in 40% sucrose solution, it was found that XG and SG solution had more comparable Stribeck curves than that in aqueous solution, which correspond to the results of 1st normal stress difference test and elongational tests. Therefore, it is suggested there is no significant difference between XG and SG when they were mixed with 40% sucrose solution.

4. When mixed XG with HWS/RS, the friction coefficient becomes lower

When mixing XG with HWS/RS, the friction coefficient becomes lower compared with control samples, especially in aqueous solution. When dissolved in 40% sucrose solution, the impact of adding HWS/RS can be negligible. However, the Stribeck curves of control, HWS/RS mixed samples of SG solutions are comparable. It is further suggested that SG may have higher propensity to inhibit salivary films formation than XG.

5. RS cannot be a replacement of HWS in tribological study

RS and HWS illustrated different film behaviours in the DTP test because HWS have two functional layers which cannot be precisely mimicked by BSM. The film formed by RS is not stable as the friction coefficient increase immediately after pouring biopolymer solutions in the pot. Therefore, RS cannot replace HWS in the tribology study due to the different film structure on soft surfaces.

To summarise the results from tribological studies, SG has slightly higher coefficient than XG. Concentrations have limited influence on the Stribeck curves of SG. Unlike XG, when mixed SG with HWS/RS, the Stribeck curves are comparable with the Stribeck curves of control samples. Last but not least, RS cannot be a proxy of HWS in the tribological study.

In conclusion, CaBER can be the most sensitive technique to detect the differences of viscoelastic behaviour. Further, SG can be an effective alternative to XG due to apparent similarities of flow behaviour under steady shear conditions and a closely matching set of linear viscoelastic properties.

7.4 Future directions

In this section, four aspects of future research directions will be suggested based on the conclusions and speculations.

1. XG/SG solutions can be mixed with acid stimulated saliva

The mechanically stimulated saliva is applied in this research. Stokes and Davies (2007b) reported that 0.025% citric acid stimulated saliva was more elastic than mechanically stimulated saliva. Therefore, with the target of understand the oral processing under different conditions, the future research can also focus on investigating rheological and tribological behaviour of biopolymer solutions-acid stimulated saliva mixtures.

2. Mixing other food proteins with polysaccharide solution

In this work the BSM solution was used as the proxy of human whole saliva to study the interactions. For the future research, with the target of developing new food systems, different types of food proteins can be mixed with biopolymer solutions, such as casein or prolamins, which may help to understand and to build different food systems and saliva proxy.

3. Preparing different concentrations of XG/SG solutions in Newtonian solvents with different concentrations

It is observed that when dissolved XG/SG in more viscosified Newtonian solvent (40%

sucrose solution in this research), the rheological and tribological behaviour differences between XG and SG are minimised. For future research, different concentrations from dilute, semi-dilute and concentrated regimes of XG and SG solutions can be made to conduct the rheological and tribological tests. Furthermore, XG/SG can be dissolved in different concentrations of sucrose solution to compare the differences (e.g., 10%, 20% or 30%).

4. The random coil polysaccharides with comparable molecular weight can be compared with XG/SG.

In this research, the rod-like polysaccharides XG and SG solutions and their mixtures with salivary proteins were studied. Previous research done by Choi et al. (2014) reported that when mixed CMC with HWS, the increase of filament break-up time of CMC-HWS mixture is less obvious compared to XG-HWS mixture. However, CMC has much lower molecular weight than XG or SG. Therefore, it is worth to compare random coil polysaccharides with comparable molecular weight with XG/SG, and dextran (T2000) could fit into these criteria. Some trial experiments of mixing dextran (T2000) solutions with HWS/RS were done using CaBER in this research (Supplementary table 5), and it was found that HWS/RS can prolong the filament break-up of dextran solution. However, the concentration of dextran solution used in this project is ~ 20%, indicating dextran T2000 may not have comparable high thickening effectiveness as rod-like biopolymer. Therefore, some other random coil polysaccharides (for example pullulan P800) with higher thickening effect can be compared with XG/SG in the future research.

References

ABBASZADEH, A., LAD, M., JANIN, M., MORRIS, G. A., MACNAUGHTAN, W., SWORN, G. & FOSTER, T. J. 2015. A novel approach to the determination of the pyruvate and acetate distribution in xanthan. *Food Hydrocolloids,* 44**,** 162-171.

ABBASZADEH, A., MACNAUGHTAN, W., SWORN, G. & FOSTER, T. J. 2016. New insights into xanthan synergistic interactions with konjac glucomannan: A novel interaction mechanism proposal. *Carbohydrate Polymers,* 144**,** 168-177.

ANDREW, T. R. 1977. Extracellular Microbial Polysaccharides. *In:* SANDFORD, P. A. & LASKIN, A. I. (eds.) *ACS symposium series.*

ANNA, S. L. & MCKINLEY, G. H. 2001. Elasto-capillary thinning and breakup of model elastic liquids. *Journal of Rheology,* 45**,** 115-138.

ANSARI, S. A., MATRICARDI, P., MEO, C. D., ALHAIQUE, F. & COVIELLO, T. 2012. Evaluation of rheological properties and swelling behaviour of sonicated scleroglucan samples. *Molecules (Basel, Switzerland)* [Online], 17.

APS, J. K. M. & MARTENS, L. C. 2005. Review: The physiology of saliva and transfer of drugs into saliva. *Forensic Science International,* 150**,** 119-131.

AUGUSTO, P. E. D., FALGUERA, V., CRISTIANINI, M. & IBARZ, A. 2013. Viscoelastic Properties of Tomato Juice: Applicability of the Cox–Merz Rule. *Food and Bioprocess Technology,* 6**,** 839-843.

BABA HAMED, S. & BELHADRI, M. 2009. Rheological properties of biopolymers drilling fluids. *Journal of Petroleum Science and Engineering,* 67**,** 84-90.

BAINES, Z. & MORRIS, E. 1988. Effect of polysaccharide thickeners on organoleptic attributes. *Gums and stabilisers for the food industry***,** 193-201.

BAINES, Z. & MORRIS, E. 1989. Suppression of perceived flavour and taste by food hydrocolloids. *Food colloids,* 75**,** 184-192.

BAIS, D., TREVISAN, A., LAPASIN, R., PARTAL, P. & GALLEGOS, C. 2005. Rheological characterization of polysaccharide–surfactant matrices for cosmetic O/W emulsions. *Journal of Colloid and Interface Science,* 290**,** 546-556.

BANSIL, R., STANLEY, E. & LAMONT, J. T. 1995. Mucin biophysics. *Annual review of physiology,* 57**,** 635-657.

BANSIL, R. & TURNER, B. S. 2006. Mucin structure, aggregation, physiological functions and biomedical applications. *Current Opinion in Colloid & Interface Science,* 11**,** 164-170.

BARNES, H. A. 2000. *A Handbook of Elementary Rheology,* The University of Wales Institute of Non-Newtonian Fluid Mechanics.

BENNA-ZAYANI, M., KBIR-ARIGUIB, N., TRABELSI-AYADI, M. & GROSSIORD, J. L. 2008. Stabilisation of W/O/W double emulsion by polysaccharides as weak gels. *Colloids and Surfaces A: Physicochemical and*

Engineering Aspects, 316**,** 46-54.
BERTH, G., DAUTZENBERG, H., CHRISTENSEN, B. E., HARDING, S. E., ROTHER, G. & SMIDSRøD, O. 1996. Static Light Scattering Studies on Xanthan in Aqueous Solutions. *Macromolecules,* 29**,** 3491-3498.
BETTELHEIM, F. A. & DEY, S. K. 1965. Molecular parameters of submaxillary mucins. *Archives of Biochemistry and Biophysics,* 109**,** 259-265.
BEWERSDORFF, H. W. & SINGH, R. P. 1988. Rheological and drag reduction characteristics of xanthan gum solutions. *Rheologica Acta,* 27**,** 617-627.
BIRD, R. B., CURTISS, C. F., ARMSTRONG, R. C. & HASSAGER, O. 1987. *Dynamics of Polymeric Liquids, Volume 2: Kinetic Theory,* New York, John Wiley & Sons, Inc.
BIVER, C., LESEC, J., ALLAIN, C. & SALOME, L. 1986. Rheological behavior and low temperature sol-gel transition of scleroglucan solutions. *Polymer,* 27**,** 351.
BLUHM, T. L., DESLANDES, Y., MARCHESSAULT, R. H., PéREZ, S. & RINAUDO, M. 1982. Solid-state and solution conformation of scleroglucan. *Carbohydrate Research,* 100**,** 117-130.
BOBEK, L. A., TSAI, H., BIESBROCK, A. R. & LEVINE, M. J. 1993. Molecular cloning, sequence, and specificity of expression of the gene encoding the low molecular weight human salivary mucin (MUC7). *The Journal of biological chemistry,* 268**,** 20563-20569.
BOEHM, M. W., YAKUBOV, G. E., DELWICHE, J. F., STOKES, J. R. & BAIER, S. K. 2019. Enabling the Rational Design of Low-Fat Snack Foods: Insights from In Vitro Oral Processing. *Journal of Agricultural and Food Chemistry,* 67**,** 8725-8734.
BOEHM, M. W., YAKUBOV, G. E., STOKES, J. R. & BAIER, S. K. 2020. The role of saliva in oral processing: Reconsidering the breakdown path paradigm. *Journal of Texture Studies,* 51**,** 67-77.
BONGAERTS, J. H. H., FOURTOUNI, K. & STOKES, J. R. 2007a. Soft-tribology: Lubrication in a compliant PDMS–PDMS contact. *Tribology International,* 40**,** 1531-1542.
BONGAERTS, J. H. H., ROSSETTI, D. & STOKES, J. R. 2007b. The Lubricating Properties of Human Whole Saliva. 27**,** 277-287.
BOOTH, A. N., HENDRICKSON, A. P. & DEEDS, F. 1963. Physiologic effects of three microbial polysaccharides on rats. *Toxicol Appl Pharmacol,* 5**,** 478-84.
BOZE, H., MARLIN, T., DURAND, D., PéREZ, J., VERNHET, A., CANON, F., SARNI-MANCHADO, P., CHEYNIER, V. & CABANE, B. 2010. Proline-Rich Salivary Proteins Have Extended Conformations. *Biophysical Journal,* 99**,** 656-665.
BRIGAND, G. 1993. CHAPTER 17 - SCLEROGLUCAN. *In:* WHISTLER, R. L. & BEMILLER, J. N. (eds.) *Industrial Gums (Third Edition).* London: Academic Press.
CADMUS, M. C., ROGOVIN, S. P., BURTON, K. A., PITTSLEY, J. E., KNUTSON,

C. A. & JEANES, A. 1976. Colonial variation in Xanthomonas campestris NRRL B-1459 and characterization of the polysaccharide from a variant strain. *Can J Microbiol,* 22**,** 942-8.

CAMMACK, R., ATTWOOD, T., CAMPBELL, P., PARISH, H., SMITH, A., VELLA, F. & STIRLING, J. 2006. *Oxford Dictionary of Biochemistry and Molecular Biology,* OUP Oxford.

CAMPESE, M., SUN, X., BOSCH, J. A., OPPENHEIM, F. G. & HELMERHORST, E. J. 2009. Concentration and fate of histatins and acidic proline-rich proteins in the oral environment. *Archives of oral biology,* 54**,** 345-353.

CáRDENAS, M., ELOFSSON, U. & LINDH, L. 2007. Salivary Mucin MUC5B Could Be an Important Component of in Vitro Pellicles of Human Saliva: An in Situ Ellipsometry and Atomic Force Microscopy Study. *Biomacromolecules,* 8**,** 1149-1156.

CARNALI, J. O. 1991. A dispersed anisotropic phase as the origin of the weak-gel properties of aqueous xanthan gum. *Journal of Applied Polymer Science,* 43**,** 929-941.

CARPENTER, G. H. 2012. Role of Saliva in the Oral Processing of Food. *In:* JIANSHE CHEN, L. E. (ed.) *Food Oral Processing: fundamentals of eating and sensory perception.* WILEY-BLACKWELL.

CHAUDHARI, N. & ROPER, S. D. 2010. The cell biology of taste. *Journal of Cell Biology,* 190**,** 285-296.

CHEETHAM, N. W. H. & NIK NORMA, N. M. 1989. The effect of pyruvate on viscosity properties of xanthan. *Carbohydrate Polymers,* 10**,** 55-60.

CHEN, J. & STOKES, J. R. 2012. Rheology and tribology: Two distinctive regimes of food texture sensation. *Trends in Food Science & Technology,* 25**,** 4-12.

CHOI, H., MITCHELL, J. R., GADDIPATI, S. R., HILL, S. E. & WOLF, B. 2014. Shear rheology and filament stretching behaviour of xanthan gum and carboxymethyl cellulose solution in presence of saliva. *Food Hydrocolloids,* 40**,** 71-75.

CHOJNICKA-PASZUN, A. & DE JONGH, H. H. J. 2014. Friction properties of oral surface analogs and their interaction with polysaccharide/MCC particle dispersions. *Food Research International,* 62**,** 1020-1028.

CHRISTERSSON, C. E., LINDH, L. & ARNEBRANT, T. 2000. Film-forming properties and viscosities of saliva substitutes and human whole saliva. *European Journal of Oral Sciences,* 108**,** 418-425.

COLE, J. L., LARY, J. W., P MOODY, T. & LAUE, T. M. 2008. Analytical ultracentrifugation: sedimentation velocity and sedimentation equilibrium. *Methods in cell biology,* 84**,** 143-179.

COLLINS, L. M. & DAWES, C. 1987. The surface area of the adult human mouth and thickness of the salivary film covering the teeth and oral mucosa. *J Dent Res,* 66**,** 1300-2.

CONE, R. A. 2009. Barrier properties of mucus. *Advanced Drug Delivery Reviews,*

61, 75-85.
COOK, D. J., HOLLOWOOD, T. A., LINFORTH, R. S. T. & TAYLOR, A. J. 2003. Oral Shear Stress Predicts Flavour Perception in Viscous Solutions. *Chemical Senses,* 28, 11-23.
COVIELLO, T., MATRICARDI, P., BALENA, A., CHIAPPERINO, B. & ALHAIQUE, F. 2010. Hydrogels from scleroglucan and ionic crosslinkers: Characterization and drug delivery. *Journal of Applied Polymer Science,* 115, 3610-3622.
COVIELLO, T., PALLESCHI, A., GRASSI, M., MATRICARDI, P., BOCCHINFUSO, G. & ALHAIQUE, F. 2005. Scleroglucan: a versatile polysaccharide for modified drug delivery. *Molecules (Basel, Switzerland),* 10, 6-33.
COX, W. P. & MERZ, E. H. 1958. Correlation of dynamic and steady flow viscosities. *Journal of Polymer Science*, 28, 619-622.
CREETH, J. M. & HARDING, S. E. 1982a. A simple test for macromolecular heterogeneity in the analytical ultracentrifuge. *The Biochemical journal,* 205, 639-641.
CREETH, J. M. & HARDING, S. E. 1982b. Some observations on a new type of point average molecular weight. *Journal of Biochemical and Biophysical Methods,* 7, 25-34.
CUVELIER, G. & LAUNAY, B. 1986. Concentration regimes in xanthan gum solutions deduced from flow and viscoelastic properties. *Carbohydrate Polymers,* 6, 321-333.
DAM, J. & SCHUCK, P. 2004. Calculating Sedimentation Coefficient Distributions by Direct Modeling of Sedimentation Velocity Concentration Profiles. *Methods in Enzymology.* Academic Press.
DAVIES, G. A. & STOKES, J. R. 2005. On the gap error in parallel plate rheometry that arises from the presence of air when zeroing the gap. *Journal of Rheology,* 49, 919-922.
DAVIES, G. A. & STOKES, J. R. 2008. Thin film and high shear rheology of multiphase complex fluids. *Journal of Non-Newtonian Fluid Mechanics,* 148, 73-87.
DAVISON, P. & MENTZER, E. 1982. Polymer Flooding in North Sea Reservoirs. *Society of Petroleum Engineers Journal,* 22, 353-362.
DE MOURA, M. R. V. & MORENO, R. B. Z. L. 2019. Concentration, Brine Salinity and Temperature effects on Xanthan Gum Solutions Rheology. *Applied Rheology,* 29, 69-79.
DE VICENTE, J., SPIKES, H. A. & STOKES, J. R. 2006a. Viscosity Ratio Effect in the Emulsion Lubrication of Soft EHL Contact. *Journal of Tribology,* 128, 795-800.
DE VICENTE, J., STOKES, J. R. & SPIKES, H. A. 2005. Lubrication properties of non-adsorbing polymer solutions in soft elastohydrodynamic (EHD) contacts.

Tribology International, 38**,** 515-526.
DE VICENTE, J., STOKES, J. R. & SPIKES, H. A. 2006b. Soft lubrication of model hydrocolloids. *Food Hydrocolloids,* 20**,** 483-491.
DEALY, J. M. & WANG, J. 2013. Viscosity and Normal Stress Differences. *Melt Rheology and its Applications in the Plastics Industry.* Dordrecht: Springer Netherlands.
DEMELER, B. 2010. Methods for the Design and Analysis of Sedimentation Velocity and Sedimentation Equilibrium Experiments with Proteins. *Current Protocols in Protein Science,* 60**,** 7.13.1-7.13.24.
DEMELER, B., NGUYEN, T.-L., GORBET, G. E., SCHIRF, V., BROOKES, E. H., MULVANEY, P., EL-BALLOULI, A. A. O., PAN, J., BAKR, O. M., DEMELER, A. K., HERNANDEZ URIBE, B. I., BHATTARAI, N. & WHETTEN, R. L. 2014. Characterization of Size, Anisotropy, and Density Heterogeneity of Nanoparticles by Sedimentation Velocity. *Analytical Chemistry,* 86**,** 7688-7695.
DENNY, P. C., DENNY, P. A., KLAUSER, D. K., HONG, S. H., NAVAZESH, M. & TABAK, L. A. 1991. Age-related Changes in Mucins from Human Whole Saliva. *Journal of Dental Research,* 70**,** 1320-1327.
DETERMANN, H. 2012. *Gel Chromatography Gel Filtration · Gel Permeation · Molecular Sieves: A Laboratory Handbook,* Springer Science & Business Medi.
DHAMI, R., HARDING, S. E., JONES, T., HUGHES, T., MITCHELL, J. R. & TO, K.-M. 1995. Physico-chemical studies on a commercial food-grade xanthan--I. Characterisation by sedimentation velocity, sedimentation equilibrium and viscometry. *Carbohydrate Polymers,* 27**,** 93-100.
DINU, V., GILLIS, R. B., MACCALMAN, T., LIM, M., ADAMS, G. G., HARDING, S. E. & FISK, I. D. 2019. Submaxillary Mucin: its Effect on Aroma Release from Acidic Drinks and New Insight into the Effect of Aroma Compounds on its Macromolecular Integrity. *Food Biophysics,* 14**,** 278-286.
DODDS, M. W. J., JOHNSON, D. A. & YEH, C.-K. 2005. Health benefits of saliva: a review. *Journal of Dentistry,* 33**,** 223-233.
DOI, M. & EDWARDS, S. F. 1986. *The theory of polymer dynamics,* Oxford, Oxford University Press.
DOOLITTLE, A. K. 1952. Studies in Newtonian Flow. III. The Dependence of the Viscosity of Liquids on Molecular Weight and Free Space (in Homologous Series). *Journal of Applied Physics,* 23**,** 236-239.
DOUGLAS, W. H., REEH, E. S., RAMASUBBU, N., RAJ, P. A., BHANDARY, K. K. & LEVINE, M. J. 1991. Statherin: A major boundary lubricant of human saliva. *Biochemical and Biophysical Research Communications,* 180**,** 91-97.
ESCUDIER, M. P., PRESTI, F. & SMITH, S. 1999. Drag reduction in the turbulent pipe flow of polymers. *Journal of Non-Newtonian Fluid Mechanics,* 81**,** 197-213.

EWOLDT, R. H., WINTER, P., MAXEY, J. & MCKINLEY, G. H. 2010. Large amplitude oscillatory shear of pseudoplastic and elastoviscoplastic materials. *Rheologica Acta,* 49**,** 191-212.

FAN, N., SHEWAN, H. M., SMYTH, H. E., YAKUBOV, G. E. & STOKES, J. R. 2021. Dynamic Tribology Protocol (DTP): Response of salivary pellicle to dairy protein interactions validated against sensory perception. *Food Hydrocolloids,* 113**,** 106478.

FANG, Y., TAKAHASHI, R. & NISHINARI, K. 2004. Rheological characterization of schizophyllan aqueous solutions after denaturation–renaturation treatment. *Biopolymers,* 74**,** 302-315.

FARIñA, J. I., SIñERIZ, F., MOLINA, O. E. & PEROTTI, N. I. 1998. High scleroglucan production by Sclerotium rolfsii: Influence of medium composition. *Biotechnology Letters,* 20**,** 825-831.

FARIñA, J. I., SIñERIZ, F., MOLINA, O. E. & PEROTTI, N. I. 2001. Isolation and physicochemical characterization of soluble scleroglucan from Sclerotium rolfsii. Rheological properties, molecular weight and conformational characteristics. *Carbohydrate Polymers,* 44**,** 41-50.

FELDöTö, Z., PETTERSSON, T. & DĖDINAITĖ, A. 2008. Mucin−Electrolyte Interactions at the Solid−Liquid Interface Probed by QCM-D. *Langmuir,* 24**,** 3348-3357.

FINNERTY, W. R. 2000. Production and Uses of Biopolymers. *In:* JOSHUA LEDERBERG, M. A., BARRY BLOOM, DAVID HOPWOOD, ROGER HULL, BARBARA IGLEWSKI, ALLEN LASKIN, STEPHEN OLIVER, MOSELIO SCHAECHTER, WILLIAM SUMMERS (ed.) *Encyclopedia of Microbiology.* second ed. New York.

FOSTER, T. J. & MITCHELL, J. R. 2012. Physical Modification of Xanthan Gum. *Gums and Stabilisers for the Food Industry 16.* The Royal Society of Chemistry.

FRANçOIS, N. J., ROJAS, A. M. A., DARAIO, M. E. & BERNIK, D. L. 2003. Dynamic rheological measurements and drug release kinetics in swollen scleroglucan matrices. *Journal of Controlled Release*, 90**,** 355-362.

FUJITA, H. 1962. *Mathematical theory of sedimentation analysis,* New York, Academic Press.

FUJIWARA, K. & OHASHI, S. 1982a. *Material for food and baked confectionery dough*. Japan patent application JP56050170A.

FUJIWARA, K. & OHASHI, S. 1982b. *Material for pastry of japanese unbaked cake*. Japan patent application JP56050175A.

FUJIWARA, K. & OHASHI, S. 1982c. *Material for pastry of rice cracker food*. Japan patent application JP56050172A.

FUJIWARA, K. & OHASHI, S. 1982d. *Material for pastry of steamed food*. Japan patent application JP56050173A.

FUJIWARA, K. & OHASHI, S. 1982e. *Preparation of solid instant drink*. Japan

patent application JP56050171A.
GAL, J.-Y., FOVET, Y. & ADIB-YADZI, M. 2001. About a synthetic saliva for in vitro studies. *Talanta,* 53**,** 1103-1115.
GARCíA-OCHOA, F. & CASAS, J. A. 1994. Apparent yield stress in xanthan gum solutions at low concentrations. *The Chemical Engineering Journal and the Biochemical Engineering Journal,* 53**,** B41-B46.
GARCíA-OCHOA, F., SANTOS, V. E., CASAS, J. A. & GóMEZ, E. 2000. Xanthan gum: production, recovery, and properties. *Biotechnology Advances,* 18**,** 549-579.
GARREC, D. A. & NORTON, I. T. 2012. The influence of hydrocolloid hydrodynamics on lubrication. *Food Hydrocolloids,* 26**,** 389-397.
GARRETT, J. R., EKSTRöM, J. & ANDERSON, L. C. 1999. *Neural mechanisms of salivary gland secretion,* Karger Medical and Scientific Publishers.
GAWRONSKI, M., PARK, J. T., MAGEE, A. S. & CONRAD, H. 1999. Microfibrillar structure of PGG-Glucan in aqueous solution as triple-helix aggregates by small angle x-ray scattering. *Biopolymers,* 50**,** 569-578.
GIBBINS, H. L., PROCTOR, G. B., YAKUBOV, G. E., WILSON, S. & CARPENTER, G. H. 2014a. Concentration of salivary protective proteins within the bound oral mucosal pellicle. *Oral Diseases,* 20**,** 707-713.
GIBBINS, H. L., YAKUBOV, G. E., PROCTOR, G. B., WILSON, S. & CARPENTER, G. H. 2014b. What interactions drive the salivary mucosal pellicle formation? *Colloids and Surfaces B: Biointerfaces,* 120**,** 184-192.
GIDLEY, M. J. & NISHINARI, K. 2009. Chapter 2.2 - Physico-chemistry of (1,3)-β-Glucans. *In:* BACIC, A., FINCHER, G. B. & STONE, B. A. (eds.) *Chemistry, Biochemistry, and Biology of 1-3 Beta Glucans and Related Polysaccharides.* San Diego: Academic Press.
GRIMINGER, P. & FISHER, H. 1966. Anti-hypercholesterolemic action of scleroglucan and pectin in chickens. *Proc Soc Exp Biol Med,* 122**,** 551-3.
GULREZ, S. K. H., AL-ASSAF, S., FANG, Y., PHILLIPS, G. O. & GUNNING, A. P. 2012. Revisiting the conformation of xanthan and the effect of industrially relevant treatments. *Carbohydrate Polymers,* 90**,** 1235-1243.
HAHN BERG, I. C., LINDH, L. & ARNEBRANT, T. 2004. Intraoral Lubrication of PRP-1, Statherin and Mucin as Studied by AFM. *Biofouling,* 20**,** 65-70.
HALLECK, F. E. 1970. *Animal food products for reducing plasma cholesterol levels*. United States patent application 54107966A.
HANNIG, C., HANNIG, M., KENSCHE, A. & CARPENTER, G. 2017. The mucosal pellicle – An underestimated factor in oral physiology. *Archives of Oral Biology,* 80**,** 144-152.
HANNOTE, M., FLORES, F., TORRES, L. & GALINDO, E. 1991. Apparent yield stress estimation in xanthan gum solutions and fermentation broths using a low-cost viscometer. *Chemical engineering journal,* 45**,** B49-B56.
HARDING, S. E. 1989. The Macrostructure of Mucus Glycoproteins in Solution. *In:*

TIPSON, R. S. & HORTON, D. (eds.) *Advances in Carbohydrate Chemistry and Biochemistry.* Academic Press.
HARDING, S. E. 1992. Sedimentation analysis of polysaccharides. *In:* HARDING, S. E. & HORTON, J. C. (eds.) *Analytical Ultracentrifugation in Biochemistry and Polymer Science.* Cambridge UK: Royal Society of Chemistry.
HARDING, S. E. 1997. The intrinsic viscosity of biological macromolecules. Progress in measurement, interpretation and application to structure in dilute solution. *Progress in Biophysics and Molecular Biology,* 68**,** 207-262.
HARDING, S. E. 2005a. Analysis of polysaccharide size, shape and interactions.
HARDING, S. E. 2005b. Challenges for the modern analytical ultracentrifuge analysis of polysaccharides. *Carbohydrate Research,* 340**,** 811-826.
HARDING, S. E. 2013. Intrinsic Viscosity. *In:* ROBERTS, G. C. K. (ed.) *Encyclopedia of Biophysics.* Berlin, Heidelberg: Springer Berlin Heidelberg.
HARDING, S. E. & JOHNSON, P. 1985a. The concentration-dependence of macromolecular parameters. *The Biochemical journal,* 231**,** 543-547.
HARDING, S. E. & JOHNSON, P. 1985b. Physicochemical studies on turnip-yellow-mosaic virus. Homogeneity, relative molecular masses, hydrodynamic radii and concentration-dependence of parameters in non-dissociating solvents. *The Biochemical journal,* 231**,** 549-555.
HARDING, S. E., SCHUCK, P., ABDELHAMEED, A. S., ADAMS, G., KöK, M. S. & MORRIS, G. A. 2011. Extended Fujita approach to the molecular weight distribution of polysaccharides and other polymeric systems. *Methods,* 54**,** 136-144.
HARDING, S. E., TOMBS, M. P., ADAMS, G. G., PAULSEN, B., INNGJERDINGEN, K. T. & BARSETT, H. 2017. *An introduction to polysaccharide biotechnology, second edition,* Boca Raton, USA, CRC Press.
HARDING, S. E., TOMBS, M. P., ADAMS, G. G., PAULSEN, B. S., INNGJERDINGEN, K. T. & BARSETT, H. 2018. *An introduction to polysaccharide biotechnology,* CRC Press.
HARDING, S. E., VARUM, K., STOKKE, B. & SMIDSRøD, O. 1991. Molecular weight determination of polysaccharides. *Advances in Carbohydrate Analysis,* 1**,** 63-144.
HARVEY, N. M., CARPENTER, G. H., PROCTOR, G. B. & KLEIN, J. 2011a. Normal and frictional interactions of purified human statherin adsorbed on molecularly-smooth solid substrata. *Biofouling,* 27**,** 823-835.
HARVEY, N. M., YAKUBOV, G. E., STOKES, J. R. & KLEIN, J. 2011b. Normal and Shear Forces between Surfaces Bearing Porcine Gastric Mucin, a High-Molecular-Weight Glycoprotein. *Biomacromolecules,* 12**,** 1041-1050.
HAWARD, S. J., ODELL, J. A., BERRY, M. & HALL, T. 2011. Extensional rheology of human saliva. *Rheologica Acta,* 50**,** 869-879.
HAY, D. I. & SCHLESINGER, D. H. 1977. Human salivary statherin : A peptide inhibitor of calcium phosphate precipitation. *Calcium-Binding Proteins and*

*Calcium Function***,** 401-408.
HAYES, D., LAUE, T. & PHILO, J. 1995. SEDNTERP. *University of New Hampshire*.
HENSKENS, Y. M. C., VAN DER VELDEN, U., VEERMAN, E. C. I. & AMERONGEN, A. V. N. 1993. Protein, albumin and cystatin concentrations in saliva of healthy subjects and of patients with gingivitis periodonitis. *Journal of Periodontal Research,* 28**,** 43-48.
HENSKENS, Y. M. C., VEERMAN, E. C. I., MANTEL, M. S., VAN DER VELDEN, U. & NIEUW AMERONGEN, A. V. 1994. Cystatins S and C in Human Whole Saliva and in Glandular Salivas in Periodontal Health and Disease. *Journal of Dental Research,* 73**,** 1606-1614.
HENSON, B. S. & WONG, D. T. 2010. Collection, Storage, and Processing of Saliva Samples for Downstream Molecular Applications. Humana Press.
HOLZWARTH, G. 1978. Molecular weight of xanthan polysaccharide. *Carbohydrate Research,* 66**,** 173-186.
HOLZWARTH, G. & PRESTRIDGE, E. B. 1977. Multistranded helix in xanthan polysaccharide. *Science,* 197**,** 757.
HU, S., LOO, J. A. & WONG, D. T. 2007. Human Saliva Proteome Analysis. *Annals of the New York Academy of Sciences,* 1098**,** 323-329.
HUGGINS, M. L. 1942. The Viscosity of Dilute Solutions of Long-Chain Molecules. IV. Dependence on Concentration. *Journal of the American Chemical Society,* 64**,** 2716-2718.
HUMPHREY, S. P. & WILLIAMSON, R. T. 2001. A review of saliva: Normal composition, flow, and function. *Journal of Prosthetic Dentistry,* 85**,** 162-169.
HYUN, K., KIM, S. H., AHN, K. H. & LEE, S. J. 2002. Large amplitude oscillatory shear as a way to classify the complex fluids. *Journal of Non-Newtonian Fluid Mechanics,* 107**,** 51-65.
JAPPER-JAAFAR, A., ESCUDIER, M. P. & POOLE, R. J. 2009. Turbulent pipe flow of a drag-reducing rigid “rod-like” polymer solution. *Journal of Non-Newtonian Fluid Mechanics,* 161**,** 86-93.
JENSEN, J. L., LAMKIN, M. S. & OPPENHEIM, F. G. 1992. Adsorption of Human Salivary Proteins to Hydroxyapatite: A Comparison Between Whole Saliva and Glandular Salivary Secretions. *Journal of Dental Research,* 71**,** 1569-1576.
JINDAL, N. & SINGH KHATTAR, J. 2018. Chapter 4 - Microbial Polysaccharides in Food Industry. *In:* GRUMEZESCU, A. M. & HOLBAN, A. M. (eds.) *Biopolymers for Food Design.* Academic Press.
JOHNSTON, J. P. & OGSTON, A. G. 1946. A boundary anomaly found in the ultracentrifugal sedimentation of mixtures. *Transactions of the Faraday Society,* 42**,** 789.
KANG, K. S. & PETTITT, D. J. 1993. CHAPTER 13 - XANTHAN, GELLAN, WELAN, AND RHAMSAN. *In:* WHISTLER, R. L. & BEMILLER, J. N. (eds.) *Industrial Gums (Third Edition).* London: Academic Press.

KASHIWAGI, Y., NORISUYE, T. & FUJITA, H. 1981. Triple helix of Schizophyllum commune polysaccharide in dilute solution. 4. Light scattering and viscosity in dilute aqueous sodium hydroxide. *Macromolecules,* 14**,** 1220-1225.

KEJRIWAL, S., BHANDARY, R., THOMAS, B. & KUMARI, S. 2014. Estimation of Levels of Salivary Mucin, Amylase and Total Protein in Gingivitis and Chronic Periodontitis Patients. *Journal of Clinical and Diagnostic Research : JCDR,* 8**,** ZC56-ZC60.

KESIMER, M. & SHEEHAN, J. K. 2008. Analyzing the functions of large glycoconjugates through the dissipative properties of their absorbed layers using the gel-forming mucin MUC5B as an example. *Glycobiology,* 18**,** 463-472.

KHEIRANDISH, S., GUYBAIDULLIN, I., WOHLLEBEN, W. & WILLENBACHER, N. 2008. Shear and elongational flow behavior of acrylic thickener solutions. *Rheologica Acta,* 47**,** 999.

KIRKNESS, J. P., AMIS, T. C., WHEATLEY, J. R. & CHRISTENSON, H. K. 2000. Determining the Surface Tension of Microliter Amounts of Liquid. *Journal of Colloid and Interface Science,* 232**,** 408-409.

KITAMURA, S., HORI, T., KURITA, K., TAKEO, K., HARA, C., ITOH, W., TABATA, K., ELGSAETER, A. & STOKKE, B. T. 1994. An antitumor, branched (1 → 3)-β-d-glucan from a water extract of fruiting bodies of Cryptoporus volvatus. *Carbohydrate Research,* 263**,** 111-121.

KOOL, M. M., GRUPPEN, H., SWORN, G. & SCHOLS, H. A. 2013. Comparison of xanthans by the relative abundance of its six constituent repeating units. *Carbohydrate Polymers,* 98**,** 914-921.

KRAEMER, E. O. 1938. Molecular Weights of Celluloses and Cellulose Derivates. *Industrial & Engineering Chemistry,* 30**,** 1200-1203.

KRAVCHUK, O. & STOKES, J. R. 2013. Review of algorithms for estimating the gap error correction in narrow gap parallel plate rheology. *Journal of Rheology,* 57**,** 365-375.

KROP, E. M., HETHERINGTON, M. M., MIQUEL, S. & SARKAR, A. 2020. Oral processing of hydrogels: Influence of food material properties versus individuals' eating capability. *Journal of Texture Studies,* 51**,** 144-153.

KURACHI, K., OHNO, N. & YADOMAE, T. 1990. Preparation and antitumor activity of hydroxyethylated derivatives of 6-branched (1.RAR.3)-.BETA.-D-glucan, SSG, obtained from the culture filtrate of Sclerotinia sclerotiorum IFO 9395. *CHEMICAL & PHARMACEUTICAL BULLETIN,* 38**,** 2527-2531.

KUSY, R. P. & SCHAFER, D. L. 1995. Rheology of stimulated whole saliva in a typical pre-orthodontic sample population. *Journal of Materials Science: Materials in Medicine,* 6**,** 385-389.

LAFFORGUE, O., SEYSSIECQ, I., PONCET, S. & FAVIER, J. 2018. Rheological properties of synthetic mucus for airway clearance. *Journal of Biomedical*

Materials Research Part A, 106**,** 386-396.

LAMM, O. 1929. *Die differentialgleichung der ultrazentrifugierung,* Almqvist & Wiksell.

LAPASIN, R. & PRICL, S. 1995. *Rheology of Industrial Polysaccharides: Theory and Applications,* Boston, MA, Springer Science.

LARSEN, M. J., JENSEN, A. F., MADSEN, D. M. & PEARCE, E. I. F. 1999. Individual variations of pH, buffer capacity, and concentrations of calcium and phosphate in unstimulated whole saliva. *Archives of Oral Biology,* 44**,** 111-117.

LAUE, T. M. & STAFFORD, W. F. I. 1999. MODERN APPLICATIONS OF ANALYTICAL ULTRACENTRIFUGATION. *Annual Review of Biophysics and Biomolecular Structure,* 28**,** 75-100.

LECACHEUX, D., MUSTIERE, Y., PANARAS, R. & BRIGAND, G. 1986. Molecular weight of scleroglucan and other extracellular microbial polysaccharides by size-exclusion chromatography and low angle laser light scattering. *Carbohydrate Polymers,* 6**,** 477-492.

LECOURTIER, J., CHAUVETEAU, G. & MULLER, G. 1986. Salt-induced extension and dissociation of a native double-stranded xanthan. *International Journal of Biological Macromolecules,* 8**,** 306-310.

LEE, B.-B., CHAN, E.-S., RAVINDRA, P. & KHAN, T. A. 2012. Surface tension of viscous biopolymer solutions measured using the du Nouy ring method and the drop weight methods. *Polymer Bulletin,* 69**,** 471-489.

LEE, S.-K., LEE, S.-W., CHUNG, S.-C., KIM, Y.-K. & KHO, H.-S. 2002. Analysis of residual saliva and minor salivary gland secretions in patients with dry mouth. *Archives of Oral Biology,* 47**,** 637-641.

LI, X., LU, Y., ADAMS, G. G., ZOBEL, H., BALLANCE, S., WOLF, B. & HARDING, S. E. 2020. Characterisation of the molecular properties of scleroglucan as an alternative rigid rod molecule to xanthan gum for oropharyngeal dysphagia. *Food Hydrocolloids,* 101**,** 105446.

LINDH, L., GLANTZ, P. O., ISBERG, P. E. & ARNEBRANT, T. 2001. An in vitro study of initial adsorption from human parotid and submandibular/sublingual resting saliva at solid/liquid interfaces. *Biofouling,* 17**,** 227-239.

LLENA, C. 2006. *The Role of saliva in maintaining oral health and as an aid to diagnosis*.

LöFGREN, D. C., JOHANSSON, D., BOHLIN, L., SAHLSTRöM, A. & CHRISTERSSON, C. The Challenge of Measuring Viscoelastic Properties of Human Whole Saliva to Fit Clinical Purpose. 2016.

LOPES DA SILVA, J. A., GONçALVES, M. P. & RAO, M. A. 1993. Viscoelastic behaviour of mixtures of locust bean gum and pectin dispersions. *Journal of Food Engineering,* 18**,** 211-228.

LUNDIN, M., SANDBERG, T., CALDWELL, K. D. & BLOMBERG, E. 2009. Comparison of the adsorption kinetics and surface arrangement of “as received” and purified bovine submaxillary gland mucin (BSM) on hydrophilic surfaces. *Journal of Colloid and Interface Science*, 336**,** 30-39.

LYNGE PEDERSEN, A. M. & BELSTRøM, D. 2019. The role of natural salivary defences in maintaining a healthy oral microbiota. *Journal of Dentistry,* 80**,** S3-S12.

MACAKOVA, L., YAKUBOV, G. E., PLUNKETT, M. A. & STOKES, J. R. 2010. Influence of ionic strength changes on the structure of pre-adsorbed salivary films. A response of a natural multi-component layer. 77**,** 31-39.

MACAKOVA, L., YAKUBOV, G. E., PLUNKETT, M. A. & STOKES, J. R. 2011. Influence of ionic strength on the tribological properties of pre-adsorbed salivary films. 44**,** 956-962.

MäCHTLE, W. & BöRGER, L. 2006. Sedimentation Equilibrium. *Analytical Ultracentrifugation of Polymers and Nanoparticles.* Berlin, Heidelberg: Springer Berlin Heidelberg.

MADSEN, J. B., PAKKANEN, K. I. & LEE, S. 2014. Thermostability of bovine submaxillary mucin (BSM) in bulk solution and at a sliding interface. *Journal of Colloid and Interface Science,* 424**,** 113-119.

MADSEN, J. B., SOTRES, J., PAKKANEN, K. I., EFLER, P., SVENSSON, B., ABOU HACHEM, M., ARNEBRANT, T. & LEE, S. 2016. Structural and Mechanical Properties of Thin Films of Bovine Submaxillary Mucin versus Porcine Gastric Mucin on a Hydrophobic Surface in Aqueous Solutions. *Langmuir,* 32**,** 9687-9696.

MALKIN, A. Y. & ISAYEV, A. I. 2012a. 3 - LIQUIDS. *In:* MALKIN, A. Y. & ISAYEV, A. I. (eds.) *Rheology Concepts, Methods, and Applications (Second Edition).* Oxford: Elsevier.

MALKIN, A. Y. & ISAYEV, A. I. 2012b. 5 - RHEOMETRY EXPERIMENTAL METHODS. *In:* MALKIN, A. Y. & ISAYEV, A. I. (eds.) *Rheology Concepts, Methods, and Applications (Second Edition).* Oxford: Elsevier.

MALONE, M. E., APPELQVIST, I. A. M. & NORTON, I. T. 2003. Oral behaviour of food hydrocolloids and emulsions. Part 1. Lubrication and deposition considerations. *Food Hydrocolloids,* 17**,** 763-773.

MANRIQUE, Y. J., LEE, D. J., ISLAM, F., NISSEN, L. M., CICHERO, J. A., STOKES, J. R. & STEADMAN, K. J. 2014. Crushed tablets: does the administration of food vehicles and thickened fluids to aid medication swallowing alter drug release? *J Pharm Pharm Sci,* 17**,** 207-19.

MANRIQUE, Y. J., SPARKES, A. M., CICHERO, J. A., STOKES, J. R., NISSEN, L. M. & STEADMAN, K. J. 2016. Oral medication delivery in impaired swallowing: thickening liquid medications for safe swallowing alters dissolution characteristics. *Drug Dev Ind Pharm,* 42**,** 1537-44.

MARCOTTE, M., TAHERIAN HOSHAHILI, A. R. & RAMASWAMY, H. S. 2001. Rheological properties of selected hydrocolloids as a function of concentration and temperature. *Food Research International,* 34**,** 695-703.

MARTINO, R., PRON, G. & DIAMANT, N. 2000. Screening for Oropharyngeal Dysphagia in Stroke: Insufficient Evidence for Guidelines. *Dysphagia,* 15**,** 19-30.

MATSUO, R. & MORIMOTO, T. 1994. Role of Salivary Ions in Maintenance of Taste Sensitivity in the Chorda Tympani Nerve of Rats. *In:* KURIHARA, K., SUZUKI, N. & OGAWA, H. (eds.) *Olfaction and Taste XI: Proceedings of the 11th International Symposium on Olfaction and Taste and of the 27th Japanese Symposium on Taste and Smell. Joint Meeting held at Kosei-nenkin Kaikan, Sapporo, Japan, July 12–16, 1993.* Tokyo: Springer Japan.

MAZZUCA, C., BOCCHINFUSO, G., PALLESCHI, A., CONFLITTI, P., GRASSI, M., DI MEO, C., ALHAIQUE, F. & COVIELLO, T. 2017. The Influence of pH on the Scleroglucan and Scleroglucan/Borax Systems. *Molecules (Basel, Switzerland),* 22**,** 435.

MCCLEMENTS, D. J. 2007. *Understanding and Controlling the Microstructure of Complex Foods*, Woodhead Publishing.

MCKINLEY, G. H. 2005. Visco-Elasto-Capillary Thinning and Break-Up of Complex Fluids. *Annual Rheology Reviews*.

MCKINLEY, G. H. & SRIDHAR, T. 2002. FILAMENT-STRETCHING RHEOMETRY OF COMPLEX FLUIDS. *Annual Review of Fluid Mechanics,* 34**,** 375-415.

MCNEELY, W. H. & KANG, K. S. 1973. *Industrial gums,* Academic Press. New York.

MCNEIL, B. & HARVEY, L. M. 1993. Viscous Fermentation Products. *Critical Reviews in Biotechnology,* 13**,** 275-304.

MELDRUM, O. W., YAKUBOV, G. E., BONILLA, M. R., DESHMUKH, O., MCGUCKIN, M. A. & GIDLEY, M. J. 2018. Mucin gel assembly is controlled by a collective action of non-mucin proteins, disulfide bridges, Ca2+-mediated links, and hydrogen bonding. *Scientific Reports,* 8**,** 5802.

MEZGER, T. G. 2014. *The Rheology Handbook,* Hanover, Germany, Vincentz Network.

MILLANE, R. P. & NARASAIAH, T. V. 1990. X-ray fiber diffraction studies of a variant of xanthan gum in which the sidechain terminal mannose unit is absent. *Carbohydrate Polymers,* 12**,** 315-321.

MILLANE, R. P., NARASAIAH, T. V. & WANG, B. 1990. Molecular structures of variants of xanthan gum with truncated sidechains. *Gums and Stabilisers for the Food Industry 5***,** 365.

MILLER, E., CLASEN, C. & ROTHSTEIN, J. P. 2009. The effect of step-stretch parameters on capillary breakup extensional rheology (CaBER) measurements. *Rheologica Acta,* 48**,** 625-639.

MOFFAT, J., MORRIS, V. J., AL-ASSAF, S. & GUNNING, A. P. 2016. Visualisation of xanthan conformation by atomic force microscopy. *Carbohydrate Polymers,* 148**,** 380-389.

MOHAMED, R., CAMPBELL, J.-L., COOPER-WHITE, J., DIMESKI, G. & PUNYADEERA, C. 2012. The impact of saliva collection and processing methods on CRP, IgE, and Myoglobin immunoassays. *Clinical and Translational Medicine,* 1**,** 19.

MOORHOUSE, R., WALKINSHAW, M. D. & ARNOTT, S. 1977. Xanthan Gum—Molecular Conformation and Interactions. *Extracellular Microbial Polysaccharides.* AMERICAN CHEMICAL SOCIETY.

MORESI, M., LO PRESTI, S. & MANCINI, M. 2001. Rheology of scleroglucan dispersions. *Journal of Food Engineering,* 50**,** 235-245.

MORRIS, E. R. 1993. Rheological and Organoleptic Properties of Food Hydrocolloids. *In:* NISHINARI, K. & DOI, E. (eds.) *Food Hydrocolloids: Structures, Properties, and Functions.* Boston, MA: Springer US.

MORRIS, E. R. 2019. Ordered conformation of xanthan in solutions and “weak gels”: Single helix, double helix – or both? *Food Hydrocolloids,* 86**,** 18-25.

MORRIS, E. R., REES, D. A., YOUNG, G., WALKINSHAW, M. D. & DARKE, A. 1977. Order-disorder transition for a bacterial polysaccharide in solution. A role for polysaccharide conformation in recognition between Xanthomonas pathogen and its plant host. *Journal of Molecular Biology,* 110**,** 1-16.

MORRIS, G. A., ADAMS, G. G. & HARDING, S. E. 2014. On hydrodynamic methods for the analysis of the sizes and shapes of polysaccharides in dilute solution: A short review. *Food Hydrocolloids,* 42**,** 318-334.

MORRIS, G. A. & HARDING, S. E. 2009. Polysaccharides, Microbial. *Encyclopedia of Microbiology.* 3rd ed. Amsterdam: Elsevier Inc.

MORRIS, G. A. & HARDING, S. E. 2013. Hydrodynamic Modeling of Carbohydrate Polymers. *In:* ROBERTS, G. C. K. (ed.) *Encyclopedia of Biophysics.* Berlin, Heidelberg: Springer Berlin Heidelberg.

MORRISON, N. A., CLARK, R., TALASHEK, T. & YUAN, C. R. 2004. New forms of xanthan gum with enhanced properties. *Gums and Stabilisers for the Food Industry 12.* The Royal Society of Chemistry.

MULLER, G., AURHOURRACHE, M., LECOURTIER, J. & CHAUVETEAU, G. 1986. Salt dependence of the conformation of a single-stranded xanthan. *International Journal of Biological Macromolecules,* 8**,** 167-172.

MUTHAMIZHI, K., KALAICHELVI, P., POWAR, S. T. & JAISHREE, R. 2014. Investigation and modelling of surface tension of power-law fluids. *RSC Advances,* 4**,** 9771-9776.

MYSTKOWSKA, J., JAŁBRZYKOWSKI, M. & DĄBROWSKI, J. R. 2013. Tribological Properties of Selected Self-Made Solutions of Synthetic Saliva. *Solid State Phenomena,* 199**,** 567-572.

NAGLER, R. M. & HERSHKOVICH, O. 2005. Relationships between age, drugs, oral sensorial complaints and salivary profile. *Archives of Oral Biology,* 50**,** 7-16.

NAVAZESH, M. 1993. Methods for Collecting Saliva. *Annals of the New York*

Academy of Sciences, 694**,** 72-77.

NAVAZESH, M., MULLIGAN, R. A., KIPNIS, V., DENNY, P. A. & DENNY, P. C. 1992. Comparison of Whole Saliva Flow Rates and Mucin Concentrations in Healthy Caucasian Young and Aged Adults. *Journal of Dental Research,* 71**,** 1275-1278.

NEWMAN, R., VILARDELL, N., CLAVé, P. & SPEYER, R. 2016. Effect of Bolus Viscosity on the Safety and Efficacy of Swallowing and the Kinematics of the Swallow Response in Patients with Oropharyngeal Dysphagia: White Paper by the European Society for Swallowing Disorders (ESSD). *Dysphagia,* 31**,** 232-249.

NIKOLAJSKI, M., ADAMS, G. G., GILLIS, R. B., BESONG, D. T., ROWE, A. J., HEINZE, T. & HARDING, S. E. 2014. Protein–like fully reversible tetramerisation and super-association of an aminocellulose. 4.

NOïK, C. & LECOURTIER, J. 1993. Studies on scleroglucan conformation by rheological measurements versus temperature up to 150°C. *Polymer,* 34**,** 150-157.

NORTON, I. T., GOODALL, D. M., FRANGOU, S. A., MORRIS, E. R. & REES, D. A. 1984. Mechanism and dynamics of conformational ordering in xanthan polysaccharide. *Journal of Molecular Biology,* 175**,** 371-394.

OKOBIRA, T., MIYOSHI, K., UEZU, K., SAKURAI, K. & SHINKAI, S. 2008. Molecular Dynamics Studies of Side Chain Effect on the β-1,3-d-Glucan Triple Helix in Aqueous Solution. *Biomacromolecules,* 9**,** 783-788.

OKUYAMA, K., ARNOTT, S., MOORHOUSE, R., WALKINSHAW, M. D., ATKINS, E. D. T. & WOLF-ULLISH, C. H. 1980. Fiber Diffraction Studies of Bacterial Polysaccharides. *Fiber Diffraction Methods.* AMERICAN CHEMICAL SOCIETY.

PADOVAN, L., SEGAT, L., PONTILLO, A., ANTCHEVA, N., TOSSI, A. & CROVELLA, S. 2010. Histatins in non-human primates: gene variations and functional effects. *Protein Pept Lett,* 17**,** 909-18.

PARK, M.-S., CHUNG, J.-W., KIM, Y.-K., CHUNG, S.-C. & KHO, H.-S. 2007. Viscosity and wettability of animal mucin solutions and human saliva. *Oral Diseases,* 13**,** 181-186.

PARKER, A., GUNNING, P. A., NG, K. & ROBINS, M. M. 1995. How does xanthan stabilise salad dressing? *Food Hydrocolloids,* 9**,** 333-342.

PELLETIER, E., VIEBKE, C., MEADOWS, J. & WILLIAMS, P. A. 2001. A rheological study of the order–disorder conformational transition of xanthan gum. *Biopolymers,* 59**,** 339-346.

PEREIRA, L. J. 2012. Oral Anatomy and Physiology. *Food Oral Processing: fundamentals of eating and sensory perception.* Wiley-Blackwell.

PERRY, G. H., DOMINY, N. J., CLAW, K. G., LEE, A. S., FIEGLER, H., REDON, R., WERNER, J., VILLANEA, F. A., MOUNTAIN, J. L., MISRA, R., CARTER, N. P., LEE, C. & STONE, A. C. 2007. Diet and the evolution of human amylase gene copy number variation. *Nature Genetics,* 39**,** 1256-1260.

PETRI, D. F. S. 2015. Xanthan gum: A versatile biopolymer for biomedical and technological applications. *Journal of Applied Polymer Science,* 132.

PETRIE, C. J. S. 2006. Extensional viscosity: A critical discussion. *Journal of Non-Newtonian Fluid Mechanics,* 137**,** 15-23.

PHILLIPS, G. O. & WILLIAMS, P. A. 2009. *Handbook of Hydrocolloids,* Cambridge, UK, Woodhead Publishing Limited.

PRADAL, C. & STOKES, J. R. 2016. Oral tribology: bridging the gap between physical measurements and sensory experience. *Current Opinion in Food Science,* 9**,** 34-41.

PREININGER, M. 2016. Interactions of flavor components in foods. *In:* GAONKAR, A. G. & MCPHERSON, A. (eds.) *Ingredient interactions: effects on food quality.* 2 ed. Boca Raton: CRC press.

PROCTOR, G. B. 2016. The physiology of salivary secretion. *Periodontology 2000,* 70**,** 11-25.

PROCTOR, G. B., HAMDAN, S., CARPENTER, G. H. & WILDE, P. 2005. A statherin and calcium enriched layer at the air interface of human parotid saliva. *The Biochemical journal,* 389**,** 111-116.

QAZI, W. M., JOHAN, W., ANNIKA, A., OLLE, E. & MATS, S. 2017. Shear and extensional rheology of commercial thickeners used for dysphagia management. *Journal of Texture Studies,* 48**,** 507-517.

RADICIONI, G., CAO, R., CARPENTER, J., FORD, A. A., WANG, T., LI, L. & KESIMER, M. 2016. The innate immune properties of airway mucosal surfaces are regulated by dynamic interactions between mucins and interacting proteins: the mucin interactome. *Mucosal immunology,* 9**,** 1442-1454.

RALSTON, G. 1993. *Introduction to analytical ultracentrifugation,* Beckman California:.

RANTONEN, P. J. F. & MEURMAN, J. H. 1998. Viscosity of whole saliva. *Acta Odontologica Scandinavica,* 56**,** 210-214.

RAU, U., MüLLER, R. J., CORDES, K. & KLEIN, J. 1990. Process and molecular data of branched 1,3-β-D-glucans in comparison with Xanthan. *Bioprocess Engineering,* 5**,** 89-93.

RAYMENT, S. A., LIU, B., OFFNER, G. D., OPPENHEIM, F. G. & TROXLER, R. F. 2000. Immunoquantification of Human Salivary Mucins MG1 and MG2 in Stimulated whole Saliva: Factors Influencing Mucin levels. *Journal of Dental Research,* 79**,** 1765-1772.

RAYNAL, B. D. E., HARDINGHAM, T. E., SHEEHAN, J. K. & THORNTON, D. J. 2003. Calcium-dependent protein interactions in MUC5B provide reversible cross-links in salivary mucus. *J Biol Chem,* 278**,** 28703-10.

RAYNAL, B. D. E., HARDINGHAM, T. E., THORNTON, D. J. & SHEEHAN, J. K. 2002. Concentrated solutions of salivary MUC5B mucin do not replicate the gel-forming properties of saliva. *The Biochemical journal,* 362**,** 289-296.

REN, Y., YAKUBOV, G. E., LINTER, B. R., MACNAUGHTAN, W. & FOSTER, T. J. 2020. Temperature fractionation, physicochemical and rheological analysis of psyllium seed husk heteroxylan. *Food Hydrocolloids,* 104**,** 105737.

RICHARDSON, R. K. & ROSS-MURPHY, S. B. 1987. Non-linear viscoelasticity of polysaccharide solutions. 2: Xanthan polysaccharide solutions. *International Journal of Biological Macromolecules,* 9**,** 257-264.

RINAUDO, M. & VINCENDON, M. 1982. 13C NMR structural investigation of scleroglucan. *Carbohydrate Polymers,* 2**,** 135-144.

ROARK, D. E. & YPHANTIS, D. A. 1969. STUDIES OF SELF-ASSOCIATING SYSTEMS BY EQUILIBRIUM ULTRACENTRIFUGATION *. *Annals of the New York Academy of Sciences,* 164**,** 245-277.

ROCHEFORT, W. E. & MIDDLEMAN, S. 1987. Rheology of Xanthan Gum: Salt, Temperature, and Strain Effects in Oscillatory and Steady Shear Experiments. *Journal of Rheology,* 31**,** 337-369.

ROFES, L., ARREOLA, V., MUKHERJEE, R., SWANSON, J. & CLAVé, P. 2014. The effects of a xanthan gum-based thickener on the swallowing function of patients with dysphagia. *Alimentary Pharmacology & Therapeutics,* 39**,** 1169-1179.

ROSS-MURPHY, S. B., MORRIS, V. J. & MORRIS, E. R. 1983. Molecular viscoelasticity of xanthan polysaccharide. 18**,** 115.

ROSSETTI, D., BONGAERTS, J. H. H., WANTLING, E., STOKES, J. R. & WILLIAMSON, A. M. 2009. Astringency of tea catechins: More than an oral lubrication tactile percept. *Food Hydrocolloids,* 23**,** 1984-1992.

RUHL, S., RAYMENT, S. A., SCHMALZ, G., HILLER, K.-A. & TROXLER, R. F. 2005. Proteins in Whole Saliva during the First Year of Infancy. *Journal of Dental Research,* 84**,** 29-34.

SARKAR, A., GOH, K. & SINGH, H. 2009. *Colloidal stability and interactions of milk-protein-stabilized emulsions in an artificial saliva*.

SARKAR, A. & KROP, E. M. 2019. Marrying oral tribology to sensory perception: a systematic review. *Current Opinion in Food Science,* 27**,** 64-73.

SARKAR, A. & SINGH, H. 2012. Oral Behaviour of Food Emulsions. *In:* JIANSHE CHEN, L. E. (ed.) *Food Oral Processing: fundamentals of eating and sensory perception.* WILEY-BLACKWELL.

SARKAR, A., XU, F. & LEE, S. 2019. Human saliva and model saliva at bulk to adsorbed phases – similarities and differences. *Advances in Colloid and Interface Science*, 273**,** 102034.

SATO, T., NORISUYE, T. & FUJITA, H. 1984. Double-Stranded Helix of Xanthan in Dilute Solution: Evidence from Light Scattering. *Polymer Journal,* 16**,** 341-350.

SCHIPPER, R. G., SILLETTI, E. & VINGERHOEDS, M. H. 2007. Saliva as research material: Biochemical, physicochemical and practical aspects. *Archives of Oral Biology,* 52**,** 1114-1135.

SCHUCK, P., GILLIS, R. B., BESONG, T. M., ALMUTAIRI, F., ADAMS, G. G., ROWE, A. J. & HARDING, S. E. 2014. SEDFIT–MSTAR: molecular weight and molecular weight distribution analysis of polymers by sedimentation equilibrium in the ultracentrifuge. *Analyst,* 139**,** 79-92.

SCHUCK, P. & ROSSMANITH, P. 2000. Determination of the sedimentation coefficient distribution by least-squares boundary modeling. *Biopolymers,* 54**,** 328-341.

SCOTT, D. & SCHUCK, P. 2005. A Brief Introduction to the Analytical Ultracentrifugation of Proteins for Beginners. *Analytical Ultracentrifugation: Techniques and Methods*.

SELWAY, N., CHAN, V. & STOKES, J. R. 2017. Influence of fluid viscosity and wetting on multiscale viscoelastic lubrication in soft tribological contacts. *Soft Matter,* 13**,** 1702-1715.

SERDYUK, I. N., ZACCAI, J. & ZACCAI, N. R. 2007. Viscosity. *In:* SERDYUK, I. N., ZACCAI, J. & ZACCAI, N. R. (eds.) *Methods in Molecular Biophysics: Structure, Dynamics, Function.* Cambridge: Cambridge University Press.

SHATWELL, K. P., SUTHERLAND, I. W. & ROSS-MURPHY, S. B. 1990. Influence of acetyl and pyruvate substituents on the solution properties of xanthan polysaccharide. *International Journal of Biological Macromolecules,* 12**,** 71-78.

SHEWAN, H. M. & STOKES, J. R. 2020. Chapter 8 Food Structure Development for Rheological/Tribological Performance. *Handbook of Food Structure Development.* The Royal Society of Chemistry.

SHIMOMURA-KUROKI, J., NASHIDA, T., MIYAGAWA, Y., MORITA, T. & HAYASHI-SAKAI, S. 2020. Analysis of salivary factors related to the oral health status in children. *Journal of Oral Science,* 62**,** 226-230.

SHOMERS, J. P., TABAK, L. A., LEVINE, M. J., MANDEL, I. D. & HAY, D. I. 1982. Properties of cysteine-containing phosphoproteins from human submandibular-sublingual saliva. *J Dent Res,* 61**,** 397-9.

SILLETTI, E., VINGERHOEDS, M., VAN AKEN, G. & NORDE, W. 2008. Rheological Behavior of Food Emulsions Mixed with Saliva: Effect of Oil Content, Salivary Protein Content, and Saliva Type. 3**,** 318-328.

SINGH, P. P., WHISTLER, R. L., TOKUZEN, R. & NAKAHARA, W. 1974. Scleroglucan, an antitumor polysaccharide from Sclerotium glucanicum. *Carbohydr Res,* 37**,** 245-7.

SMIDSRøD, O. & ANDRESEN, I. 1979. Biopolymerkjemi, Tapir. *Trondheim, Norway*.

SOLOMON, O. F. & CIUTĂ, I. Z. 1962. Détermination de la viscosité intrinsèque de solutions de polymères par une simple détermination de la viscosité. *Journal of Applied Polymer Science,* 6**,** 683-686.

SONESSON, M., WICKSTRöM, C., KINNBY, B., ERICSON, D. & MATSSON, L. 2008. Mucins MUC5B and MUC7 in minor salivary gland secretion of

children and adults. *Archives of Oral Biology,* 53**,** 523-527.
SONG, K. W., KIM, Y. S. & CHANG, G. S. 2006a. Rheology of concentrated xanthan gum solutions: Steady shear flow behavior. *Fibers and Polymers,* 7**,** 129-138.
SONG, K. W., KUK, H. Y. & CHANG, G. S. 2006b. Rheology of concentrated xanthan gum solutions: Oscillatory shear flow behavior. *Korea-Australia Rheology Journal,* 18**,** 67-81.
SOUSA, P. C., PINHO, F. T., OLIVEIRA, M. S. N. & ALVES, M. A. 2011. Extensional flow of blood analog solutions in microfluidic devices. *Biomicrofluidics,* 5**,** 014108.
SREEBNY, L. M. & VISSINK, A. 2010. *Dry mouth, the malevolent symptom: a clinical guide*, John Wiley & Sons.
STACHOWIAK, G. W. & BATCHELOR, A. W. 2013. *Engineering tribology*, Butterworth-Heinemann.
STELTER, M., BRENN, G., YARIN, A. L., SINGH, R. P. & DURST, F. 2000. Validation and application of a novel elongational device for polymer solutions. *Journal of Rheology,* 44**,** 595-616.
STELTER, M., BRENN, G., YARIN, A. L., SINGH, R. P. & DURST, F. 2002. Investigation of the elongational behavior of polymer solutions by means of an elongational rheometer. *Journal of Rheology,* 46**,** 507-527.
STOKES, J. R. 2012a. 'Oral' Rheology. *In:* JIANSHE CHEN, L. E. (ed.) *Food Oral Processing: fundamentals of eating and sensory perception.* WILEY-BLACKWELL.
STOKES, J. R. 2012b. 'Oral' Tribology. *In:* JIANSHE CHEN, L. E. (ed.) *Food Oral Processing: fundamentals of eating and sensory perception.* WILEY-BLACKWELL.
STOKES, J. R., BOEHM, M. W. & BAIER, S. K. 2013. Oral processing, texture and mouthfeel: From rheology to tribology and beyond. *Current Opinion in Colloid & Interface Science,* 18**,** 349-359.
STOKES, J. R. & DAVIES, G. A. 2007a. Viscoelasticity of human whole saliva collected after acid and mechanical stimulation. *Biorheology,* 44**,** 141-160.
STOKES, J. R. & DAVIES, G. A. 2007b. Viscoelasticity of human whole saliva collected after acid and mechanical stimulation. *Biorheology,* 44**,** 141-160.
STOKES, J. R. & FRITH, W. J. 2008. Rheology of gelling and yielding soft matter systems. *Soft Matter,* 4**,** 1133-1140.
STOKES, J. R., GRAHAM, L. J. W., LAWSON, N. J. & BOGER, D. V. 2001. Swirling flow of viscoelastic fluids. Part 2. Elastic effects. *Journal of Fluid Mechanics,* 429**,** 117-153.
STOKES, J. R., MACAKOVA, L., CHOJNICKA-PASZUN, A., DE KRUIF, C. G. & DE JONGH, H. H. J. 2011. Lubrication, Adsorption, and Rheology of Aqueous Polysaccharide Solutions. *Langmuir,* 27**,** 3474-3484.
STOKKE, B. T., ELGSAETER, A., BJøRNESTAD, E. Ø. & LUND, T. 1992. Rheology of xanthan and scleroglucan in synthetic seawater. *Carbohydrate*

Polymers, 17**,** 209-220.
STOKKE, B. T., FALCH, B. H. & DENTINI, M. 2001. Macromolecular triplex zipping observed in derivatives of fungal (1 → 3)-β-D-glucan by electron and atomic force microscopy. *Biopolymers,* 58**,** 535-547.
STOKKE, B. T., SMIDSRøD, O. & ELGSAETER, A. 1989. Electron microscopy of native xanthan and xanthan exposed to low ionic strength. *Biopolymers,* 28**,** 617-637.
STRIBIŢCAIA, E., KROP, E. M., LEWIN, R., HOLMES, M. & SARKAR, A. 2020. Tribology and rheology of bead-layered hydrogels: Influence of bead size on sensory perception. *Food Hydrocolloids,* 104**,** 105692.
SURVASE, S. A. S., PARAG S.; BAJAJ, ISHWAR B.; SINGHAL, REKHA S. 2007. Scleroglucan: Fermentative Production, Downstream Processing and Applications. *Food Technology & Biotechnology,* 45**,** 107 - 118.
SWORN, G. 2009a. 8 - Xanthan gum. *Handbook of Hydrocolloids (Second edition).* Woodhead Publishing.
SWORN, G. 2009b. Xanthan Gum. *In:* IMESON, A. P. (ed.) *Food Stabilisers, Thickeners and Gelling Agents.*
TAM, K. C. & TIU, C. 1989. Steady and Dynamic Shear Properties of Aqueous Polymer Solutions. *Journal of Rheology,* 33**,** 257-280.
TANFORD, C. 1961. *Physical chemistry of macromolecules,* New York, J. Wiley and Sons.
TAYLOR, C., ALLEN, A., DETTMAR, P. W. & PEARSON, J. P. 2003. The Gel Matrix of Gastric Mucus Is Maintained by a Complex Interplay of Transient and Nontransient Associations. *Biomacromolecules,* 4**,** 922-927.
TE NIJENHUIS, K., MCKINLEY, G. H., SPIEGELBERG, S., BARNES, H. A., AKSEL, N., HEYMANN, L. & ODELL, J. A. 2007. *Springer Handbook of Experimental Fluid Mechanics*.
TECHATANAWAT, S., SURARIT, R., CHAIRATVIT, K., ROYTRAKUL, S., KHOVIDHUNKIT, W., THANAKUN, S., IZUMI, Y. & KHOVIDHUNKIT, S.-O. P. 2019. Salivary and serum cystatin SA levels in patients with type 2 diabetes mellitus or diabetic nephropathy. *Archives of Oral Biology,* 104**,** 67-75.
THERMOELECTRON 2009. *Instruction Manual-Haake CaBER 1 version 1.8,* germany, Thermo Electron GmbH.
THOMSSON, K. A., PRAKOBPHOL, A., LEFFLER, H., REDDY, M. S., LEVINE, M. J., FISHER, S. J. & HANSSON, G. C. 2002. The salivary mucin MG1 (MUC5B) carries a repertoire of unique oligosaccharides that is large and diverse. *Glycobiology,* 12**,** 1-14.
THORNTON, D. J., KHAN, N., MEHROTRA, R., HOWARD, M., SHEEHAN, J. K., VEERMAN, E. & PACKER, N. H. 1999. Salivary mucin MG1 is comprised almost entirely of different glycosylated forms of the MUC5B gene product. *Glycobiology,* 9**,** 293-302.

TSVETKOV, V. N., ESKIN, V. E. & FRENKEL, S. I. 1971. *Structure of macromolecules in solution*, National Lending Library for Science and Technology.

TURCANU, M., TASCON, L. F., BALAN, C. & GALLEGOS, C. Capillary breakup extensional properties of whole human saliva. 2015 9th International Symposium on Advanced Topics in Electrical Engineering (ATEE), 7-9 May 2015 2015. 269-274.

VALSTAR, M. H., DE BAKKER, B. S., STEENBAKKERS, R. J. H. M., DE JONG, K. H., SMIT, L. A., KLEIN NULENT, T. J. W., VAN ES, R. J. J., HOFLAND, I., DE KEIZER, B., JASPERSE, B., BALM, A. J. M., VAN DER SCHAAF, A., LANGENDIJK, J. A., SMEELE, L. E. & VOGEL, W. V. 2020. The tubarial salivary glands: A potential new organ at risk for radiotherapy. *Radiotherapy and Oncology*.

VAN DER REIJDEN, W. A., VEERMAN, E. C. & AMERONGEN, A. V. 1993. Shear rate dependent viscoelastic behavior of human glandular salivas. *Biorheology,* 30**,** 141-52.

VAN DER REIJDEN, W. A., VEERMAN, E. C. I. & NIEUW AMERONGEN, A. V. 1994. Rheological properties of commercially available polysaccharides with potential use in saliva substitutes. *Biorheology,* 31**,** 631-642.

VAN HOLDE, K. E. 1971. *Physical Biochemistry,* Englewood Cliffs, Prentice-Hall.

VAN HOLDE, K. E. 1985. *Physical Biochemistry,* New Jersy, Prentice-Hall.

VAN HOLDE, K. E. & BALDWIN, R. L. 1958. Rapid Attainment of Sedimentation Equilibrium. *The Journal of Physical Chemistry,* 62**,** 734-743.

VAN NIEUW AMERONGEN, A., BOLSCHER, J. G. M. & VEERMAN, E. C. I. 2004. Salivary Proteins: Protective and Diagnostic Value in Cariology? *Caries Research,* 38**,** 247-253.

VEEREGOWDA, D. H., BUSSCHER, H. J., VISSINK, A., JAGER, D.-J., SHARMA, P. K. & VAN DER MEI, H. C. 2012. Role of Structure and Glycosylation of Adsorbed Protein Films in Biolubrication. *PLoS ONE,* 7**,** e42600.

VEERMAN, E. C., VALENTIJN-BENZ, M. & NIEUW AMERONGEN, A. V. 1989. Viscosity of human salivary mucins: effect of pH and ionic strength and role of sialic acid. *J Biol Buccale,* 17**,** 297-306.

VIJAY, A., INUI, T., DODDS, M., PROCTOR, G. B. & CARPENTER, G. H. 2015. Factors That Influence the Extensional Rheological Property of Saliva. *PLOS ONE,* 10**,** e0135792.

VIñARTA, S. C., YOSSEN, M. M., VEGA, J. R., FIGUEROA, L. I. C. & FARIñA, J. I. 2013. Scleroglucan compatibility with thickeners, alcohols and polyalcohols and downstream processing implications. *Carbohydrate Polymers,* 92**,** 1107-1115.

VUPPU, A. K., GARCIA, A. A. & VERNIA, C. 1997. Tapping mode atomic force microscopy of scleroglucan networks. *Biopolymers,* 42**,** 89-100.

WATERMAN, H., BLOM, C., HOLTERMAN, H. & MELLEMA, J. 1988.

Rheological properties of human saliva. *Archives of oral biology,* 33**,** 589-596.

WEBMD UK LIMITED., B. U. L. 2017. *Salivary gland disorders - Salivary stones, blocked glands and more* [Online]. Available: https://www.webmd.boots.com/oral-health/guide/salivary-gland-problems [Accessed 9th Oct 2017].

WEI, B., ROMERO-ZERóN, L. & RODRIGUE, D. 2014. Mechanical Properties and Flow Behavior of Polymers for Enhanced Oil Recovery. *Journal of Macromolecular Science, Part B,* 53**,** 625-644.

WHITCOMB, P. J. & MACOSKO, C. W. 1978. Rheology of Xanthan Gum. *Journal of Rheology,* 22**,** 493-505.

WICKSTRöM, C., CHRISTERSSON, C., DAVIES, J. R. & CARLSTEDT, I. 2000. Macromolecular organization of saliva: identification of 'insoluble' MUC5B assemblies and non-mucin proteins in the gel phase. *Biochemical Journal,* 351**,** 421-428.

WICKSTRöM, C., DAVIES, J. R., ERIKSEN, G. V., VEERMAN, E. C. & CARLSTEDT, I. 1998. MUC5B is a major gel-forming, oligomeric mucin from human salivary gland, respiratory tract and endocervix: identification of glycoforms and C-terminal cleavage. *The Biochemical journal,* 334 (Pt 3)**,** 685-693.

WICKSTRöM, C., HAMILTON, I. R. & SVENSäTER, G. 2009. Differential metabolic activity by dental plaque bacteria in association with two preparations of MUC5B mucins in solution and in biofilms. *Microbiology (Reading),* 155**,** 53-60.

WITT, T. & STOKES, J. R. 2015. Physics of food structure breakdown and bolus formation during oral processing of hard and soft solids. *Current Opinion in Food Science,* 3**,** 110-117.

WOODARD, G., WOODARD, M. W., MCNEELY, W. H., KOVACS, P. & CRONIN, M. T. I. 1973. Xanthan gum: Safety evaluation by two-year feeding studies in rats and dogs and a three-generation reproduction study in rats. *Toxicology and Applied Pharmacology,* 24**,** 30-36.

WYATT, N. B. & LIBERATORE, M. W. 2009. Rheology and viscosity scaling of the polyelectrolyte xanthan gum. *Journal of Applied Polymer Science,* 114**,** 4076-4084.

XU, S., XU, X. & ZHANG, L. 2012. Branching Structure and Chain Conformation of Water-Soluble Glucan Extracted from Auricularia auricula-judae. *Journal of Agricultural and Food Chemistry,* 60**,** 3498-3506.

XU, Y. & STOKES, J. R. 2020. Soft lubrication of model shear-thinning fluids. *Tribology International,* 152**,** 106541.

YAKUBOV, G. E. 2014. Lubrication. *In:* LIGTENBERG, A. J. M. & VEERMAN, E. C. I. (eds.) *Saliva: Secretion and Functions.*

YAKUBOV, G. E., GIBBINS, H., PROCTOR, G. B. & CARPENTER, G. H. 2014. Oral Mucosa: Physiological and Physicochemical Aspects. *Mucoadhesive*

Materials and Drug Delivery Systems.
YAKUBOV, G. E., MACAKOVA, L., WILSON, S., WINDUST, J. H. C. & STOKES, J. R. 2015. Aqueous lubrication by fractionated salivary proteins: Synergistic interaction of mucin polymer brush with low molecular weight macromolecules. *Tribology International,* 89**,** 34-45.
YAKUBOV, G. E., MCCOLL, J., BONGAERTS, J. H. H. & RAMSDEN, J. J. 2009. Viscous Boundary Lubrication of Hydrophobic Surfaces by Mucin. *Langmuir,* 25**,** 2313-2321.
YAMAKAWA, H. & FUJII, M. 1974. Intrinsic viscosity of wormlike chains. Determination of the shift factor. *Macromolecules,* 7**,** 128-135.
YANAKI, T., KOJIMA, T. & NORISUYE, T. 1981. Triple Helix of Scleroglucan in Dilute Aqueous Sodium Hydroxide. 13**,** 1135-1143.
YANAKI, T. & NORISUYE, T. 1983. Triple Helix and Random Coil of Scleroglucan in Dilute Solution. *Polymer Journal,* 15**,** 389.
YANAKI, T., NORISUYE, T. & FUJITA, H. 1980. Triple Helix of Schizophyllum commune Polysaccharide in Dilute Solution. 3. Hydrodynamic Properties in Water. *Macromolecules,* 13**,** 1462-1466.
YASEEN, E. I., HERALD, T. J., ARAMOUNI, F. M. & ALAVI, S. 2005. Rheological properties of selected gum solutions. *Food Research International,* 38**,** 111-119.
ZACCAI, N. R., SERDYUK, I. N. & ZACCAI, J. 2017. *Methods in molecular biophysics,* Cambridge University Press.
ZATZ, J. L. & KNAPP, S. 1984. Viscosity of Xanthan Gum Solutions at Low Shear Rates. *Journal of Pharmaceutical Sciences,* 73**,** 468-471.
ZHANG, Y., KONG, H., FANG, Y., NISHINARI, K. & PHILLIPS, G. O. 2013. Schizophyllan: A review on its structure, properties, bioactivities and recent developments. *Bioactive Carbohydrates and Dietary Fibre,* 1**,** 53-71.
ZIRNSAK, M. A., BOGER, D. V. & TIRTAATMADJA, V. 1999. Steady shear and dynamic rheological properties of xanthan gum solutions in viscous solvents. *Journal of Rheology,* 43**,** 627-650.
ZUSSMAN, E., YARIN, A. L. & NAGLER, R. M. 2007. Age- and Flow-dependency of Salivary Viscoelasticity. *Journal of Dental Research,* 86**,** 281-285.

Appendix

Supplementary Table

Supplementary Table 1. Hydrodynamic properties of scleroglucan in aqueous solution (20.0°C, *water solvent)*

Parameter	
$s^{o}_{20,w}$ (component 1)	(13.0 ± 0.5) S
% (component 1) a	65.5 ± 2.5
$s^{o}_{20,w}$ (component 2)	(15.7 ± 1.3) S
%(component 2)b	34.5 ± 2.5
M_w (whole distribution weight average)	(2.8 ± 0.3) x 106 g/mol
[η]	(2190 ± 110) ml/g
MHKS a (lower molecular weights)	1.14 ± 0.03
MHKS a (higher molecular weights)	0.76 ± 0.01

a: mean value – decreases with increase in concentration; b: mean value – increases with increase in concentration

Supplementary Table 2. The filament break-up time, relaxation time and steady state apparent extensional viscosity of xanthan gum solution under different stir time (2 min, 5 min, 30 min, 60 min and 120 min) (The ANOVA test of data can be found in Supplementary table 4)

Control samples (0.5% XG solution + water)	Stir time	Filament break-up time (ms)		Relaxation time (ms)		Steady state apparent extensional viscosity (Pa·s)	
		Mean	Stdev	Mean	Stdev	Mean	Stdev
	2 min	58.9	0.6	10.7	0.5	26.6	1.7
	5 min	60.4	1.0	11.1	0.4	28.4	2.0
	30 min	60.2	1.1	11.1	0.5	28.4	3.3
	60 min	59.7	1.6	11.1	0.8	28.4	3.5
	90 min	59.6	0.8	11.4	0.4	27.2	3.6

	120 min	59.1	0.6	10.8	0.3	26.6	1.2
HWS samples (0.5% XG + HWS)							
	2 min	72.9	1.3	15.1	0.7	24.1	1.1
	5 min	70.6	1.7	14.0	0.5	25.8	1.0
	30 min	70.3	1.4	13.9	0.9	23.4	1.2
	60 min	69.7	3.0	14.0	1.2	24.4	0.8
	90 min	70.7	2.3	14.5	1.0	25.3	1.6
	120 min	68.3	3.1	13.5	1.0	23.1	1.0
RS samples (0.5% XG solution + RS-1.2 mg/ml BSM)							
	2 min	63.0	1.9	12.9	0.7	22.3	1.0
	5 min	63.2	1.2	13.0	0.5	21.3	1.7
	30 min	61.3	0.7	12.8	0.6	21.4	1.1
	60 min	61.2	3.3	12.6	1.2	21.5	1.7
	90 min	60.5	3.9	12.3	1.1	20.3	2.1
	120 min	61.3	1.3	12.4	0.8	22.3	0.6
RS samples (0.5% XG solution + RS-30 mg/ml BSM)							
	2 min	77.8	2.9	15.4	0.6	32.1	0.5
	5 min	78.3	2.3	15.6	0.1	31.3	1.1
	30 min	77.6	2.5	15.7	0.4	30.9	2.0
	60 min	77.8	1.8	15.9	0.3	31.1	2.2
	90 min	77.7	2.5	15.9	0.6	32.2	2.8
	120 min	77.2	1.7	15.7	0.9	31.0	0.9

Supplementary Table 3. The filament break-up time, relaxation time and steady state apparent extensional viscosity of scleroglucan solution under different stir time (2 min, 5 min, 30 min, 60 min and 120 min) (The ANOVA test of data can be found in Supplementary table 4)

Control samples (0.5% SG solution + water)	Stir time	Filament break-up time (ms)		Relaxation time (ms)		Steady state apparent extensional viscosity (Pas)	
		Mean	Stdev	Mean	Stdev	Mean	Stdev
	2 min	159.0	3.3	26.6	1.5	70.5	1.7
	5 min	159.2	5.1	27.0	3.5	68.2	3.1
	30 min	156.3	2.9	27.5	1.2	68.3	3.1
	60 min	162.7	3.9	24.9	1.2	72.7	1.4
	90 min	160.6	2.8	25.1	1.2	72.3	2.2
	120 min	160.1	5.1	25.8	1.2	70.4	1.8
HWS samples (0.5% SG solution + HWS)							
	2 min	195.4	6.9	30.1	1.9	81.4	2.0
	5 min	190.1	3.4	30.8	1.2	79.5	2.1
	30 min	188.8	8.0	30.0	1.4	78.6	1.8
	60 min	194.0	5.0	30.3	0.8	80.6	3.1
	90 min	186.4	3.1	31.7	1.6	76.0	3.0
	120 min	187.3	3.7	31.1	2.2	77.1	2.0
RS samples (0.5% SG solution + RS-1.2mg/ml BSM)							
	2 min	160.7	5.1	27.7	1.9	70.4	3.2
	5 min	162.0	2.6	26.8	1.8	70.7	2.5
	30 min	160.7	4.2	25.5	1.4	68.6	2.3
	60 min	158.9	3.4	27.4	2.1	68.3	2.3
	90 min	160.2	3.6	26.4	0.8	69.4	2.7
	120 min	159.8	2.6	25.9	1.3	69.3	2.0
RS samples (0.5% SG solution + RS-30 mg/ml BSM)							
	2 min	205.7	2.8	30.8	2.4	88.6	4.4

	5 min	203.3	7.0	31.1	1.7	84.0	4.0
	30 min	203.1	6.4	31.6	1.0	84.0	2.8
	60 min	205.5	5.0	30.7	2.6	85.7	3.2
	90 min	204.9	5.0	30.9	1.8	88.9	2.8
	120 min	203.8	6.0	30.8	2.7	88.5	2.5

Supplementary Table 4. ANOVA results of 0.5% XG and 0.5% SG solution

Samples		P value	Significant
0.5% xanthan gum solution + water (5:1)	Filament break-up time	0.078	No
	Relaxation time	0.170	No
	Steady state apparent extensional viscosity	0.572	No
0.5% xanthan gum solution + saliva (5:1)	Filament break-up time	0.019	Yes
	Relaxation time	0.029	Yes
	Steady state apparent extensional viscosity	0.000	Yes
0.5% xanthan gum solution + reconstituted saliva (5:1) (1.2 mg/mL BSM)	Filament break-up time	0.215	No
	Relaxation time	0.539	No
	Steady state apparent extensional viscosity	0.155	No
0.5% xanthan gum solution + reconstituted saliva (5:1) (30 mg/mL BSM)	Filament break-up time	0.972	No
	Relaxation time	0.810	No
	Steady state apparent extensional viscosity	0.574	No
0.5% scleroglucan solution + water (5:1)	Filament break-up time	0.618	No
	Relaxation time	0.128	No
	Steady state apparent extensional viscosity	0.193	No
0.5% scleroglucan solution + saliva (5:1)	Filament break-up time	0.005	Yes
	Relaxation time	0.204	No
	Steady state apparent extensional viscosity	0.000	Yes
0.5% scleroglucan solution + reconstituted saliva (5:1) (1.2 mg/mL BSM)	Filament break-up time	0.618	No
	Relaxation time	0.128	No
	Steady state apparent extensional viscosity	0.193	No
0.5% scleroglucan solution + reconstituted saliva (5:1) (30	Filament break-up time	0.865	No
	Relaxation time	0.968	No

mg/mL BSM)	Steady state apparent extensional viscosity	0.002	Yes

Supplementary Table 5. The filament break-up time, relaxation time and steady state apparent extensional viscosity of 20% dextrain solution under different stir time (2 min, 5 min, 30 min, 60 min and 120 min)

Control samples (20% dextran solution + water)	Stir time	Filament break-up time (ms)	
		Mean	Stdev
	2 min	43.1	1.9
	5 min	42.8	1.2
	30 min	43.3	1.2
	60 min	43.4	2.3
	90 min	43.8	2.9
	120 min	43.5	2.2
Saliva samples (20% dextran solution + saliva)			
	2 min	88.0	4.7
	5 min	82.9	6.0
	30 min	76.6	3.4
	60 min	73.9	1.9
	90 min	70.3	1.3
	120 min	67.2	1.5
Reconstituted saliva samples (20% dextran solution + reconstituted saliva)			
	2 min	71.9	3.6
	5 min	72.9	4.1
	30 min	71.0	4.4
	60 min	73.1	2.8
	90 min	73.5	4.5
	120 min	71.9	4.9

Supplementary Table 6. Viscosity parameters from Figure 5.1 and Figure 5.5

	$\eta_{0.01}$ (Pa·s)	η_{1000} (Pa·s)
water	/	0.0009
0.2% (w/v) XG solution	1	0.005
0.5% (w/v) XG solution	45	0.01
1% (w/v) XG solution	461	0.02
0.2% (w/v) SG solution	4	0.005
0.5% (w/v) SG solution	60	0.006
1% (w/v) SG solution	515	0.01
0.5% (w/v) XG solution (40%sucrose solution solvent)	142	0.03
0.5% (w/v) SG solution (40%sucrose solution solvent)	276	0.02

Supplementary Figures

(a)

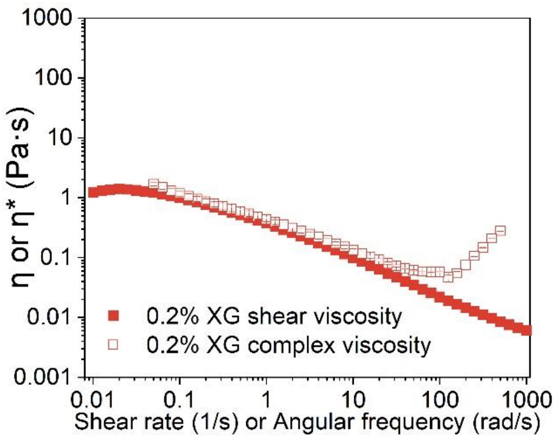

(b)

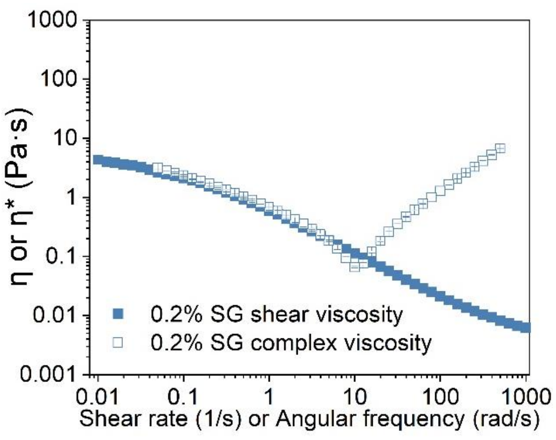

(c)

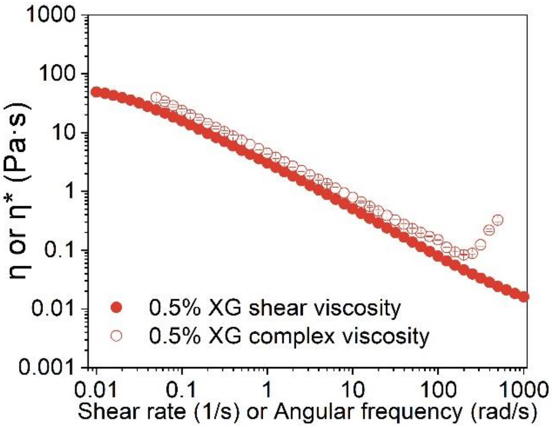

(d)

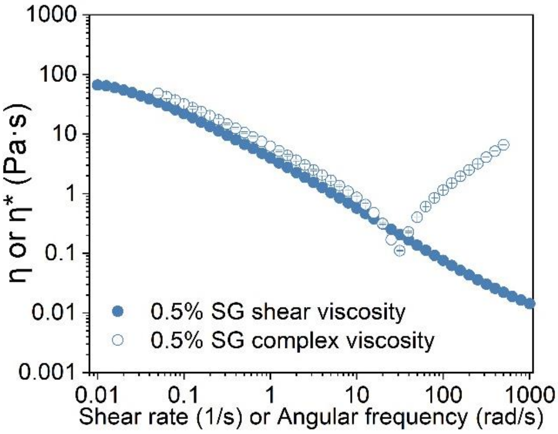

(e)

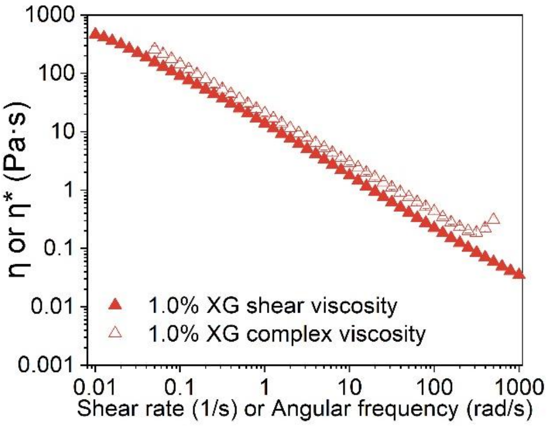

(f)

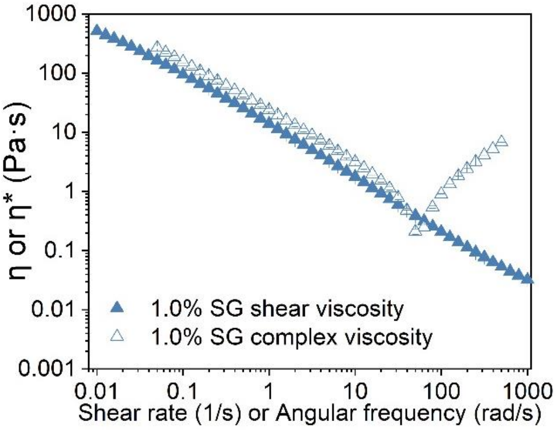

Supplementary figure 1. The shear rheological viscosity (full) and complex viscosity (void) of XG (red) and SG (blue) solution (water as the solvent) with different concentrations at 20°C : (a) 0.2% XG solution (red square), (b) 0.2% SG solution (blue square), (c) 0.5% XG solution (red circle), (d) 0.5% SG solution (blue circle), (e) 1.0% XG solution (red triangle), (f) 1.0% SG solution (blue triangle)

(a)

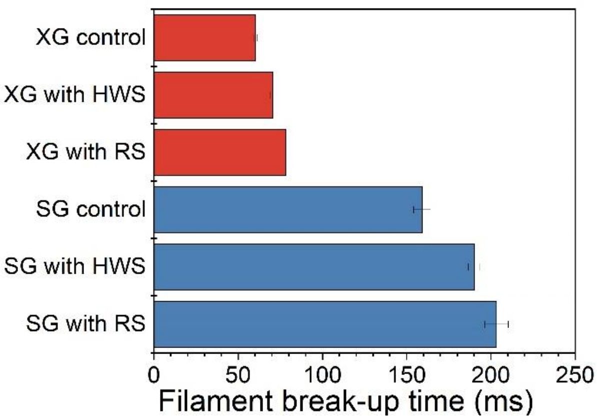

(b)

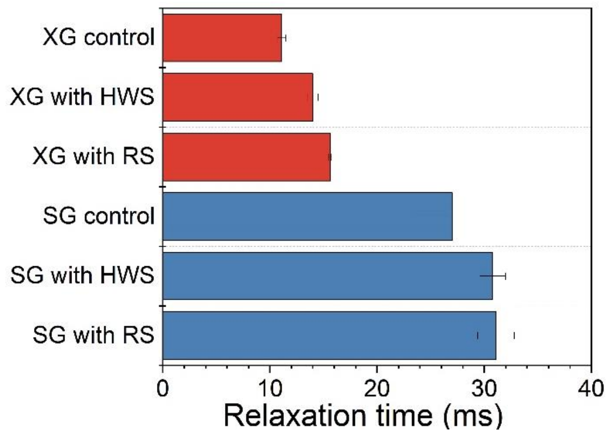

(c)

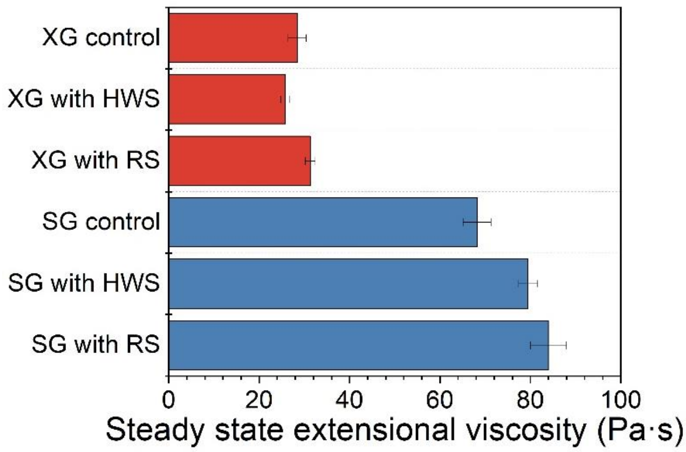

Supplementary figure 2. The (a) filament break-up time, (b) relaxation time, (c) steady state extensional viscosity of control, HWS samples and RS samples of XG and SG solution (40% sucrose solution as the solvent)